5-2021

# Synthetic Heterosynaptic Plasticity Enhances the Versatility of Memristive Systems Emulating Bio-synapse Structure and Function

William T. McClintic
*University of Tennessee, Knoxville*, wmcclint@vols.utk.edu

To the Graduate Council:

I am submitting herewith a dissertation written by William T. McClintic entitled "Synthetic Heterosynaptic Plasticity Enhances the Versatility of Memristive Systems Emulating Bio-synapse Structure and Function." I have examined the final electronic copy of this dissertation for form and content and recommend that it be accepted in partial fulfillment of the requirements for the degree of Doctor of Philosophy, with a major in Energy Science and Engineering.

Charles P. Collier, Major Professor

We have read this dissertation and recommend its acceptance:

Fred A. Heberle, Maxim O. Lavrentovich, Michael L. Simpson

Accepted for the Council:

Dixie L. Thompson

Vice Provost and Dean of the Graduate School

(Original signatures are on file with official student records.)

# Synthetic Heterosynaptic Plasticity Enhances the Versatility of Memristive Systems Emulating Bio-synapse Structure and Function

A Dissertation Presented for the

Doctor of Philosophy

Degree

The University of Tennessee, Knoxville

William Travers McClintic

May 2021

# Dedication

This work is dedicated to all those who navigate life with a family, you will figure out life and family, keep working at it and you will amaze yourself.

# Acknowledgments

I am very thankful for C. Patrick Collier's mentorship and guidance during my doctoral pursuit. Pat, you spent a lot of the most precious resource, time, on my development as a scientist and a person. You taught me about the importance of details, of being a detective, of getting things right, and teaching others. You showed a lot of patience and understanding with me; I will carry that forward. My favorite part of my PhD was at the end when everything you taught me came together in our heterosynaptic plasticity paper. I will take your teachings with me wherever life takes me and I will be better equipped because of that. Thanks Pat.

Michael L. Simpson deserves a very special thanks for extending me my opportunity to work with the Nanofabrication Research Laboratory and mentorship during my doctoral pursuit. Mike, you really pushed me to think more effectively. That is incredibly valuable not only in science but in life. Thanks Mike.

A special thank you to my committee members Fred A. Heberle and Maxim O. Lavrentovich for your guidance and support throughout my doctoral pursuit.

Thank you to the Nanofabricaiton Research Laboraotry and other Center for Nanophase Material Science staff, including Dale Hensley, Bernadeta Srijanto, Scott Retterer, Kevin Lester, and Daryl Briggs, Nick Lavrik, Jason Fowlkes, Lisa Goins, Liam Collins, Peter Bonnesen, Jan Micheal Carillo, Kevin Harman, Scott Hellenbeck, Ilia Ivanov, Brad Lokitz, Chris Rouleau, and Leslie Wilson.

More thanks to Andy Sarles, Paul Dalhaimer, John Katsaras, Larry Millet, Joseph Najem, Jonathan Boreyko, Fangjie Liu, Graham Taylor, Haden Scott, Dimitry Bolmatov, Carmen Foster, Milka Doktorova, Mikayla Maxwell, Nick Moore, Guru Venkatesan, Nima Tamaddoni, MaryAnne Nguyen, Eric Muckley, Patrick Caveney, Jayde Aufrecht, Liz Norred, and Jeff Beegle.

I would like to thank the Department of Energy and the Bredesen Center for Interdisciplinary Research and Graduate Education, University of Tennessee, Knoxville, for research funding and a graduate fellowship. A very special thank you to Lee Riedinger, Suresh Babu, Allie Burns, Rebecca Christ, and Shannon Brown. Suresh, thank you very much for your lesson on gratitude.

Most importantly, this dissertation would not be completed without the love of my life's time, clarity, and encouragement for me to succeed. Thank you so much Avery!

# Abstract

Memristive systems occur in nature and are hallmarked via pinched hysteresis, the difference in the forward and reverse pathways for a given phenomenon. For example, neurons of the human brain are composed of synapses which apply the properties of memristance for neuronal communication, learning, and memory consolidation. Modern technology has much to gain from the characteristics of memristive systems, including lower power operation, on-chip memory, and bio-inspired computing. What is more, a relationship between memristive systems and synaptic plasticity exists and can be investigated focusing on homosynaptic and heterosynaptic plasticity. Where homosynaptic plasticity applies to interactions between neurons at a synapse, heterosynaptic plasticity applies to an interneuron, a neuron that is not a part of the synapse, that modulates the neuronal interactions of synapses located elsewhere. Here, a synthetic synapse was used to study the heterosynaptic modulatory effects of osmotic stress via macromolecular crowding in the aqueous environment, membrane defects introduced from pH-sensitive secondary membrane species, and oxidative stress via oxidation of lipid species present in the membrane. Osmotic stress lowers the voltage threshold for alamethicin ion channels via depletion interactions and transmembrane water gradients. Secondary membrane species lowered the voltage threshold for alamethicin and lower pH environments enhanced the self-interaction between alamethicin monomers in a pore upon dissolution from the membrane. Oxidative stress created lipid species that compete for space in the polar-apolar interface of the lipid bilayer, leading to pore formation extending cell-free gene expression reactions. These findings help reveal how to environmentally modulate the synthetic synapse. Harnessing the power of memristive systems to create a biological computer enables the creation of new computers capable of adaptation, self-repair, and low-power operation while maintaining powerful computing and memory storage schemes.

# Table of Contents

# List of Tables

# List of Figures

# Chapter 1

# Introduction

The operating system of the brain hinges on plasticity, the adaptability in the structure and function of the nervous system in response to learning and memory. The conduit for expressing plasticity is the neuron and its connectivity, represented as neural networks. Implementing plasticity arises from two scenarios: conscious use of the neural network and emotional influence over the neural network. Consciously using the neural network includes repetition, practice, and intention. Emotionally influencing the neural network includes changes in the neural network due to how the organism feels. In the modern computational age, energy efficiency in computational hardware and computing schemes are paramount for next generation computers capable of adaptability, self-learning, and facile communication between memory and processing, all found in the brain. To harness the properties of the brain for use in computational hardware, computing schemes, and information processing, the search for the existence of synthetic conduits for expressing and implementing synaptic plasticity is underway. These are the motivating topics of this dissertation.

Neuronal circuits make up the brain, much like the electronic circuitry found in electronic devices. The connectivity of the neurons and synaptic plasticity provides functionality in neuronal circuits. Two general classes of synaptic plasticity include homosynaptic plasticity and heterosynaptic plasticity. Beyond these general classes of synaptic plasticity, the plasticity of neurons is modulated through metaplasticity.

### 1.1 Synaptic Plasticity: Homosynaptic and Heterosynaptic

Homosynaptic plasticity was inspired by the synaptic plasticity theory of Donald Hebb, also known as Hebbian plasticity, who theorized rules for forming synaptic connections in response to stimulation (Hebb, D. O., 1949). Hebb's theory applied to synapses, that is a presynaptic axon terminal connected to a postsynaptic axon terminal and had three components for the performance of neuronal plasticity: associative, homosynaptic, and input-specific. Associative refers to changes in neuronal strength due to coincident firing of the presynaptic and postsynaptic terminal. Homosynaptic refers to synaptic strength changes brought about by the synapse's own activity. Input-specific refers to postsynaptic neuronal targeting via stimulating the adjacent presynaptic neuron. Hebb's plasticity theory initially only included synaptic potentiation or facilitation, which

represented strengthening and forming new synaptic connections, but was later modified to include synaptic depression, the inverse of synaptic potentiation and defined to represent weakening and decreased synaptic connections. Homosynaptic plasticity rules were studied in the vertebrate and invertebrate brains (Bailey, C. H., Giustetto, M., Huang, Y. Y., Hawkins, R. D., and Kandel, E. R., 2000).

Heterosynaptic plasticity is the second rule proposed from studies conducted on the synaptic plasticity of marine mollusk *Aplysia*, proposed by Kandel and Tauc, after noticing certain neuronal strength changes occurred in the absence of homosynaptic stimulation. This form of synaptic plasticity was dependent on modulatory chemical inputs to either the presynaptic or postsynaptic terminal coming from a third neuron, termed an interneuron or modulator neuron. These chemical inputs resulted in stable long-term memories when repeatedly used alone, called non-associative heterosynaptic plasticity, or when used in combination with homosynaptic stimulation, called associative heterosynaptic plasticity (Bailey, C. H., Giustetto, M., Huang, Y. Y., Hawkins, R. D., and Kandel, E. R., 2000).

Neurons contain axons which extend from the cell body of the neuron and connect with other neurons, forming junctions called synapses, allowing the passage of chemical or electrical signals. The two types of synapses discussed here are the homosynapse and the heterosynapse. A homosynapse is the connection between the presynaptic axon terminal and a neuron resulting in a presynaptic and postsynaptic junction (Figure 1.1). Homosynapses are responsible for homosynaptic plasticity in which the energized presynapse coincidentally energizes the postsynapse leading to synaptic strength redistributions via non-transcriptional neurotransmission, for example via glutamatergic signaling. Here, existing proteins are covalently modified via activated protein kinases (PKA, PKC, or calcium/calmodulin-dependent protein kinase II – CaMKII) to increase the synaptic strength at energized synapses (Figure 1.2). A heterosynapse is the connection between an axon terminal and a pre- or postsynapse of a homosynapse. Heterosynapses are responsible for heterosynaptic plasticity in which an energized heterosynapse signals the pre- or postsynapse of the homosynapse via transcriptional neuromodulation, for example via hormonal signaling that recruits intracellular cyclic

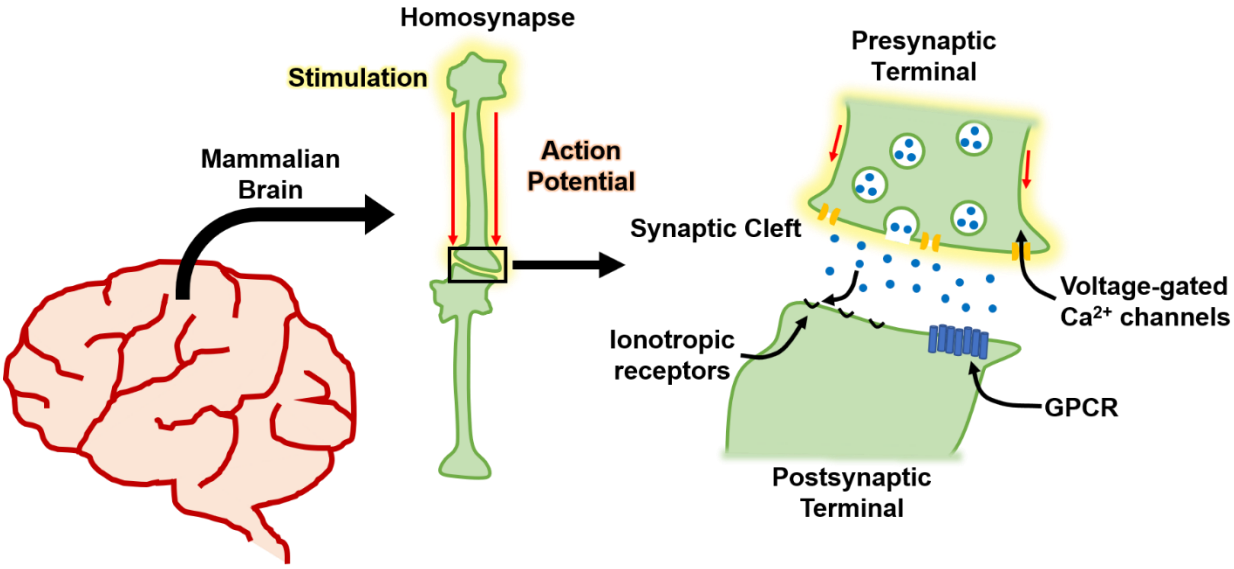


**Figure 1.1: Neurobiology of homosynaptic plasticity.** Homosynaptic plasticity results from firing between neurons through their junction, or synapse. An action potential from the presynaptic neuron stimulates voltage-sensitive ion channels leading to calcium ion influx, in turn leading to the release of neurotransmitter into and across the synaptic cleft. Once in the cleft, the neurotransmitter can interact with the ionotropic receptors. The more firing that happens between the neurons in a homosynaptic connection, the stronger the connection, or the synaptic weight, becomes.

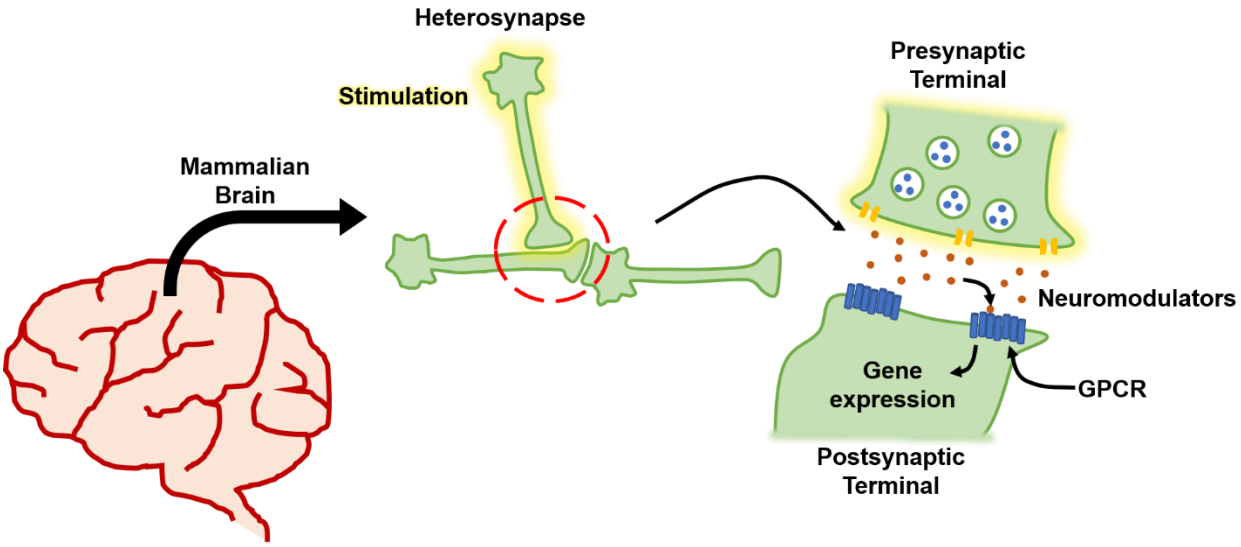


**Figure 1.2: Neurobiology of heterosynaptic plasticity.** Heterosynaptic plasticity results from a junction formed between a neuron not participating in a homosynapse, also called an interneuron, energizing a pre- or postsynapse in a homosynapse. This occurs when glutamatergic inputs **and** neuromodulatory inputs occur simultaneously or through **multiple** heterosynapse firing. Effects of heterosynaptic plasticity include enhanced gene expression of synaptic membrane receptors and overall size of the synapse, thus increasing the overall strength of the homosynapse.

adenosine monophosphate (cAMP), mitogen-activated protein kinase (MAPK), and PKA cascade signaling pathways leading to cAMP response element binding protein (CREB)-mediated transcription. Here, new proteins are created to modify the synaptic strength through formation of more glutamatergic signaling membrane proteins and overall size of the homosynapse (Figure 1.2) (Bailey, C. H., Giustetto, M., Huang, Y. Y., Hawkins, R. D., and Kandel, E. R., 2000).

The brain uses both forms of plasticity independently and combined. Both forms have the potential to elicit short-term memory independently, with homosynaptic plasticity lasting between one and two hours and heterosynaptic plasticity lasting ten minutes. Stable long-term memory, experimentally defined as synaptic plasticity changes lasting more than twenty-four hours is possible with both forms occurring simultaneously or with heterosynaptic plasticity alone. The result of long-term plasticity mechanisms is non-additive learning and memory formation, that is strength changes greater than the sum of the individual strength changes due to homosynaptic and heterosynaptic mechanisms, made possible because of plasticity triggered gene transcription and protein synthesis stabilizing the increased neuronal strength through changes in the number of glutamatergic membrane receptors. Homosynaptic long-term memory consolidation is believed to be more complex if possible (Bailey, C. H., Giustetto, M., Huang, Y. Y., Hawkins, R. D., and Kandel, E. R., 2000).

### 1.2 Synaptic Plasticity: Short-term and Long-term

Neuronal cell culture enabled model systems to be designed so that *in vitro* studies could reveal long and short-term memory mechanisms of the brain. Two types of stimulus could be executed: the homosynaptic electrical stimulus called a train or tetanus and the heterosynaptic pulse. The two types of stimulus differed in one type having electrical origins and the other having molecular origins, respectively. Microelectrodes enabled electrical stimulus as well as perfusion of heterosynaptic modulatory inputs. Electrical stimulation as a train or tetanus refers to the application of a frequency dependent electrical signal. Pulses refer to microinjections of modulatory chemicals to the bath of the cell culture or to the presynaptic or postsynaptic terminal.

These model systems enabled precise control over timing of applied stimulus and could replicate behavioral studies performed on model organisms using that model organism neurons via cell culture (Martin, K. C., Casadio, A., Zhu, H., Yaping, E., Rose, J. C., Chen, M., ... and Kandel, E. R., 1997).

Two main forms of short-term plasticity have been demonstrated in vertebrates and invertebrates. Short-term facilitation in Aplysia neuron culture, as well as in the mammalian hippocampus was shown to be triggered by repeated trains of electrical stimulus and last up to one hour. This type of synaptic plasticity is homosynaptic plasticity. However, in both vertebrates and invertebrates, a single heterosynaptic pulse of neuromodulator elicits short-term facilitation, shown to last roughly ten minutes. This includes 5-HT (serotonin) in Aplysia and, depending on the location of the neurons in the mammalian organism, a single pulse of dopamine, serotonin, or noradrenaline, among others (Bailey, C. H., Giustetto, M., Huang, Y. Y., Hawkins, R. D., and Kandel, E. R., 2000).

Three main forms of long-term plasticity have also been demonstrated in vertebrates and invertebrates. Long-term facilitation was proposed from studying marine mollusk Aplysia. Facilitation was the terminology introduced from the original Aplysia experimental investigations into synaptic plasticity, starting with short-term plasticity. However, an abrupt shift to experimental investigations into long-term plasticity in the mammalian hippocampus occurred, starting with long-term potentiation. Moreover, both forms of long-term plasticity required repeated pulses of neuromodulator and included protein kinase signal cascades which led to gene transcription and new protein synthesis, with neuronal changes shown to persist over twenty-four hours. This type of synaptic plasticity is called heterosynaptic plasticity. The final main form of long-term plasticity was shown to result from combining homosynaptic stimulation with heterosynaptic pulses. Here, a single train of homosynaptic stimulus combined with a single heterosynaptic pulse resulted in neuronal changes shown to persist over twenty-four hours (Bailey, C. H., Giustetto, M., Huang, Y. Y., Hawkins, R. D., and Kandel, E. R., 2000).

### 1.3 Metaplasticity

Metaplasticity refers to the plasticity of synaptic plasticity. Metaplastic changes enable long-lasting changes in the ability of a synapse to undergo synaptic plasticity changes in the future via modulation of the threshold dependence of synaptic plasticity. Said another way, metaplasticity refers in part to synaptic plasticity that depends on the history of synaptic plasticity of a given synapse. Modulating synaptic plasticity thresholds can build a network of connected neurons through synaptic tagging and capture, a hypothesis that certain molecular species are tagged to modulate future synaptic plasticity through phosphorylation and dephosphorylation, enabling synaptic modulation over a network of neurons (Abraham, W. C., 2008).

### 1.4 Plasticity Translates to Neuronal Circuitry

Interestingly, it seems nature has created new forms of plasticity using different combinations of homosynaptic plasticity and heterosynaptic plasticity. Different combinations of plasticity were observed in behavioral changes of an organism in response to different behavioral conditioning methods, including classical conditioning, sensitization, habituation, and addiction. These observations made clear that timing between stimulus was very important. One example already discussed is the long-term memory consolidation via a single homosynaptic electrical stimulus and a single heterosynaptic pulse, serving as a general mechanism of long-term memory storage in vertebrates and invertebrates. A second example is retrograde signaling induced from classical conditioning coincidentally combining a conditioned stimulus with a non-conditioned stimulus. Here, the general mechanism of homosynaptic and heterosynaptic plasticity occur in combination, however, following a postsynaptic neuron is stimulated from the unconditioned stimulus that generates a retrograde signal that facilitates its presynapse to release more neurotransmitter adding a homosynaptic plasticity mechanism as reinforcement (Bailey, C. H., Giustetto, M., Huang, Y. Y., Hawkins, R. D., and Kandel, E. R., 2000). New synthetic neuronal circuits are derived from the known plasticity mechanism of organisms just described and more.

## 1.5 Memristive Systems

Experimental evidence of memristance began in an early nineteenth century experiment with Sir Humphry Davy's arcing current experiment to fashion a new technology for generating light (Davy, H, 1801). However, the experiments were not characterized as memristive and more experimental evidence would appear over time, leading up to Chua's 1971 paper theorizing the existence of a fourth fundamental circuit element (Chua, L., 1971). Like the resistor, inductor, and capacitor, the fourth fundamental circuit element would be passive, that is unable to supply power to the circuit, and was hypothesized to exist due to the lacking sixth combination of the four fundamental circuit variables, current i, voltage v, charge q, and flux $\phi$. Namely the relationship between flux and charge. Memristor, a portmanteau of memory resistor, was the name given to the theorized fourth fundamental circuit element.

Chua reported four classes of memristors: ideal memristors, ideal generic memristors, generic memristors and extended memristors (Chua, L., 2014). The classes of memristor vary in complexity of the constitutive relationship driving the memristance, or memductance, of the system, with the ideal memristor representing the most basic relationship and the extended memristor representing the most complex relationship (Chua, L., 2015). Two categories of memristors exist depending on the input being current or voltage, resulting in a current-controlled, with charge dependence, or voltage-controlled, with flux dependence, memristor, respectively. Mathematically, the current controlled ideal memristor, with memristance R, current i, and voltage v, is defined by the following,

$$v = R(q)i \tag{1-1}$$

$$\frac{dq}{dt} = i \tag{1-2}$$

While conductance is the inverse and reciprocal relationship to resistance, memductance is the inverse and reciprocal relationship to memristance. A mathematical formulation exists for the voltage-controlled memristor with memductance G,

$$i = G(\phi)v \tag{1-3}$$

$$\frac{d\phi}{dt} = v \tag{1-4}$$

and magnetic flux $\phi$.

Because direct relationships between flux and charge are rare, the ideal memristor mathematics is axiomatic and pedagogical. Most memristors are considered generic memristors and operate on a set of state variables collected in the state vector $\boldsymbol{x} = (x_1, x_2, \ldots x_n)$ representing internal physical parameters such as temperature, pressure, impurity concentration, chemical moiety, etc. (Chua, L., 2013). Generally, generic memristors are referred to as memristors unless otherwise specified. A voltage-controlled generic memristor functions via state-dependent Ohm's law represented by a vector of state variables **x**,

$$v = R(\boldsymbol{x})i \tag{1-5}$$

$$\frac{d\boldsymbol{x}}{dt} = f(\boldsymbol{x}, i) \tag{1-6}$$

for the current-controlled memristor and,

$$i = G(\boldsymbol{x})v \tag{1-7}$$

$$\frac{d\boldsymbol{x}}{dt} = g(\boldsymbol{x}, v) \tag{1-8}$$

for the voltage-controlled memristor.

The first experimental demonstration of a physical memristor was reported by Hp labs (Strukov, D. B., Snider, G. S., Stewart, D. R., and Williams, R. S., 2008). Interestingly, the first memristor was a generic memristor, that is a memristor that did not directly depend on physical flux-charge relationship, rather depended on nanoscale hysteresis of coupled solid-state ionic and electronic transport. Surprisingly, the first memristor to depend on the physical flux-charge relationship, was reported in 2019 (Wang, F. Z., Li, L., Shi, L., Wu, H., and Chua, L. O., 2019). Practically, following the 2008 experimental demonstration of memristance the race to explore and produce a commercially viable memristor technology started.

While studying plasticity *in vivo* is a challenging task, synthetic memristive systems can reproduce plastic responses with more control and ease (Chua, L., 2014). Synthetic memristive systems can be further categorized as solid state, biomolecular, or bioarchitectural. Solid state uses the nanoscale properties of metals and semiconductors to emulate synaptic function (Strukov, D. B., Snider, G. S., Stewart, D. R., and Williams, R. S., 2008). Biomolecular systems emulate synaptic function using biomolecular materials but generally operate using the same architecture as the solid-state counterparts (Kim, M. K., and Lee, J. S., 2018). Bioarchitectural systems emulate the structure and function of both chemical synapses (Najem, J. S., Taylor, G. J., Weiss, R. J., Hasan, M. S., Rose, G., Schuman, C. D., ... and Sarles, S. A., 2018) and electrical synapses (Koner, S., Najem, J. S., Hasan, M. S., and Sarles, S. A., 2019) of the brain, using lipid based membranes and voltage-gated ion channels. Synaptic physical growth as synapse weight increases has been emulated in bioarchitectural systems via electrostriction of synthetic lipid bilayers (Najem, J. S., Hasan, M. S., Williams, R. S., Weiss, R. J., Rose, G. S., Taylor, G. J., ... and Collier, C. P., 2019) as well as the changes to the number of ion channels in the membrane (Najem, J. S., Taylor, G. J., Weiss, R. J., Hasan, M. S., Rose, G., Schuman, C. D., ... and Sarles, S. A., 2018).

## 1.6 Synthetic Heterosynaptic Toolbox

Before stating the specific research aims, a review of key concepts surrounding the synthetic heterosynaptic toolbox is warranted, including the droplet interface bilayer model membrane and how it models a synthetic synapse, homosynaptic DIB representations, and heterosynaptic DIB representations.

### *1.6.1 Emulating the Synapse with Droplet Interface Bilayers*

Emulating synaptic function can be achieved using synthetic lipid membrane platforms, such as the droplet interface bilayer (DIB) (Bayley, H., Cronin, B., Heron, A., Holden, M. A., Hwang, W. L., Syeda, R., ... and Wallace, M., 2008). Here, two aqueous droplets are incubated under oil at room temperature. While incubating, a lipid monolayer spontaneously assembles at the interface of the aqueous drops and oil, due to the amphiphilic nature of phospholipids and interfacial energy. Once coated in a lipid monolayer, the droplets can be connected to spontaneously form a lipid bilayer. Droplets are suspended from electrodes capped in a hydrogel coating, enabling the droplets to be mobile in three dimensions when installed on a micromanipulator. Electrodes apply potential and record currents. DIB stability can be maintained up to days.

DIBs are important to the study of synthetic synaptic plasticity because of the similarity with synaptic structure and function. Synapses make use of a cell membrane to separate and propagate charge, for example during action potentials. Membranes house the required proteinaceous machinery, such as voltage-gated ionotropic channels and GPCR complexes, responsible for neurotransmission as embedded pieces in a lipid sea. Synthetic DIBs can reproduce the lipid nature, the charge separation, housing of gateable voltage-sensitive ion channels in the bilayer membrane, and the housing of aqueous biochemical compositions found in cells, including modulatory conditions and agents, such as local molecules that adhere to the membrane phase or reside in the aqueous phase and global conditions such as pH affecting the aqueous and membrane regions coincidentally.

### *1.6.2 Emulating Homosynaptic Plasticity with Membrane Active Peptides – Alamethicin*

Homosynaptic plasticity in a bioarchitectural memristor is achieved using DIBs housing the voltage-gateable membrane peptide alamethicin (Najem, J. S., Taylor, G. J., Weiss, R. J., Hasan, M. S., Rose, G., Schuman, C. D., ... and Sarles, S. A., 2018). Alamethicin is a peptide known to self-organize to form pores in cell membranes and synthetic lipid membranes in a voltage and concentration dependent fashion (reviewed in Leitgeb, B., Szekeres, A., Manczinger, L., Vágvölgyi, C., and Kredics, L., 2007). Monomers of Alamethicin are composed of nineteen amino acids, including non-proteinogenic aminoisobutryic acid, synthesized via post-translational modifications, and one amino alcohol at the C-terminus. While the mechanism for pore formation with alamethicin is still being investigated, the barrel stave model (Baumann, G., and Mueller, P., 1974) is accepted as the most probable pore structure, in which alamethicin monomers connect parallel to each other and perpendicular to the membrane to line the circular perimeter of the pore lumen. Alamethicin contains a structural dipole of approximately 80D, composed of the lone negative charge of the glutamate residue at physiological pH, located at the 18th residue towards the C-terminus, and the alpha-helical secondary structure of the peptide. A proline residue introduces a kink in the helical structure. The dipole nature of alamethicin is broadly accepted as the voltage sensing mechanism. Alamethicin interacts with lipid membranes in a two-state model: surface bound and inserted (Duclohier, H., and Wroblewski, H., 2001). While surface bound, alamethicin lies parallel to the membrane and interacts with the polar/apolar interface, laterally stretching and deforming lipids locally. Membrane binding is driven by the amphiphilic nature of alamethicin, with the polar peptide backbone hydrogen bonding with the polar region of the membrane and the hydrophobic side groups residing in the hydrophobic membrane interior. Upon the application of an electric potential, alamethicin adopts the inserted state, perpendicular to the plane of the membrane. The angle of insertion depends on the applied potential (Ye, S., Li, H., Wei, F., Jasensky, J., Boughton, A. P., Yang, P., and Chen, Z., 2012). Beyond a voltage threshold, full insertion occurs, and other inserted state monomers bind to each other to form pores. Pores become conductive upon reaching four monomers or more in a pore. Lipid type also modulates

the number of monomers per pore, due to differences in lipid thickness, lipid packing, and lipid headgroup properties. Alamethicin provides a synthetic model of synaptic plasticity via the memristive nature alamethicin including the voltage responsiveness, conductive pore formation, and the capacity for environmental modulation.

### *1.6.3 Emulating Heterosynaptic Plasticity with Membrane Active Peptides - ATRAM2*

Heterosynaptic modulation can occur through membrane competition between pH sensitive membrane peptide ATRAM2. Acidity-triggered rational membrane (ATRAM) peptide is a pH responsive, membrane-active molecule designed to target the low pH environment of cancer cells (Nguyen, V. P., Alves, D. S., Scott, H. L., Davis, F. L., and Barrera, F. N., 2015). ATRAM primary structure contains 34 amino acids, is composed of 4 glutamate residues for pH sensing, and many hydrophobic residues such as leucine and glycine. In solution, ATRAM is unstructured and remains unstructured upon binding to the membrane at physiological pH. In the unstructured form, ATRAM has hydrophobic residues embedded in the hydrophobic core of the membrane while the charged glutamates and tryptophan reside at the polar interface. A lone glutamate is predicted to remain accessible to the aqueous environment for pH sensing (Nguyen, V. P., Dixson, A. C., and Barrera, F. N., 2019). Upon transitioning to pH5, below the insertion pK midpoint of 6.5 (Nguyen, V. P., Alves, D. S., Scott, H. L., Davis, F. L., and Barrera, F. N., 2015), ATRAM adopts more alpha-helical structure as it inserts into the membrane with the C-terminus traversing the lipid membrane (Nguyen, V. P., Palanikumar, L., Kennel, S. J., Alves, D. S., Ye, Y., Wall, J. S., ... and Barrera, F. N., 2019). ATRAM2 is a variant of ATRAM substituting a glutamate residue for a leucine residue at the nineteenth position but has very similar biophysical properties, including pH-induced conformational changes. ATRAM2 serves as a unique synthetic heterosynaptic modulator via competition with homosynaptic alamethicin in three ways: local modulation via secondary binding of unstructured ATRAM2 to the membrane, local modulation via structured and inserted ATRAM2 in the membrane, and global modulation via environmental pH drop from physiological pH required for switching from bound to inserted states.

### *1.6.4 Emulating Heterosynaptic Plasticity with Macromolecular Crowding – PEG and DEX*

Heterosynaptic modulation can be achieved via loading the aqueous phase of the DIB model synapse with macromolecular crowders. Macromolecular crowding results from an abundance of macromolecules in the cytosol of cells such as ribosomes, proteins, and cytoskeletal filaments. In synthetic systems, polymeric macromolecules, such as polyethylene glycol (PEG), a polymer of ethylene glycol, dextran (DEX), a polymer of glucose, and ficoll, a polymer of sucrose, mimic macromolecular crowding in cells and are used to investigate biophysical processes, such as peptide binding to lipid membranes (McClintic, W. T., Taylor, G. J., Simpson, M. L., and Collier, C. P., 2020), gene expression rates (Norred, S. E., Caveney, P. M., Chauhan, G., Collier, L. K., Collier, C. P., Abel, S. M., and Simpson, M. L., 2018), and lipid membrane mechanical properties (Parsegian, V. A., Fuller, N., and Rand, R. P., 1979) under crowding conditions. Macromolecular crowding is typically mimicked using nonelectrolyte polymers of sizes ranging from a few hundred Daltons (g/mol) to thousands of kilodaltons. Global effects of macromolecular molecular crowding include modulating the environment via colligative effects as well as depletion interactions, solvent gradients, and aqueous-aqueous phase separation. Crowding an aqueous solution increases the osmotic pressure of the solution, creating an osmotic potential capable of initiating osmosis when compartments of different osmotic pressure are contacted through a solvent permeable membrane, such as the lipid membrane. Although miscible in water, these macromolecular polymers can undergo phase-separations as functions of solution conditions such as concentration and temperature due to entropic effects (Helfrich, M. R., Mangeney-Slavin, L. K., Long, M. S., Djoko, K. Y., and Keating, C. D., 2002). Macromolecular crowding serves as a global heterosynaptic modulator via induction of solvent gradients, redistribution of molecules in the system, and modified reaction rates.

### *1.6.5 Emulating Heterosynaptic Plasticity with Oxidative Stress – POPC Oxidation Derivatives*

One final heterosynaptic modulator includes oxidative stress. Oxidative stress in biological systems refers to uncontrolled redox reactions between reactive oxygen species (ROS) and biomolecules of the system. Interaction between biomolecules of a certain type and ROS lead to irreversible chemical modifications of the biomolecules, such as formation of aldehydes, ketones, and carboxylic acids. These can result in metastable structures but invariably lead to eventual breakdown of the system when uncontrolled. Biomolecular targets include proteins, DNA, and lipids. For lipids, unsaturated bonds on the hydrophobic acyl chains are susceptible to oxidation from ROS, resulting in a variety of oxidized lipid species. These reactions are confined to the hydrophobic center of the lipid membrane, which can lead to amplified local concentrations of oxidative reaction products sufficient to trigger autocatalytic lipid peroxidation. In other words, once initiation occurs via ROS reactions with unsaturated bonds on lipid acyl chains, propagation to other lipids with unsaturated bonds occurs via free radical byproducts of the reaction and continue propagating until a termination step occurs. Antioxidant molecules such as vitamin C and sodium azide are known to quench radical species produced via oxidative stress. Synthetic lipid membranes have been extensively studied by ROS generation *in situ,* or systematically via titration of oxidized lipid species in the membrane. Lipid oxidation by either mechanism modifies the mechanical properties of the lipid membranes (Tsubone, T. M., Baptista, M. S., and Itri, R., 2019), enhances phase separation and the formation of microdomains (Tsubone, T. M., Junqueira, H. C., Baptista, M. S., and Itri, R., 2019), and increases membrane permeability through pore formation (Corvalán, N. A., Caviglia, A. F., Felsztyna, I., Itri, R., and Lascano, R., 2020). Oxidative stress serves as a global heterosynaptic modulator via modification to the mechanical properties of lipid membranes and conductive pore formation.

## 1.7 Research Aims

Model membranes have been used to study active and passive transport, channel formation, membrane species diffusion and dynamics, and now with the recent acknowledgement that neurons operate on principles of memristance, model membranes are advancing our understanding of the memristor. The general knowledge gap is to identify candidates for the information storage mechanism of neurons and elucidate their principles of operation through synaptic plasticity in model membranes, specifically incorporating heterosynaptic plasticity to the current state-of-the-art bioarchitectural memristor. This dissertation addresses the knowledge gap by studying three cases: aqueous-based macromolecular crowding, membrane-based peptide crowding, and membrane oxidative stress.

Chapter 2 presents heterosynaptic modulation via aqueous-based macromolecular crowding with high molecular weight polymers, such as PEG8kDa and DEX500kDa. Here, the aspiration is to modulate the memristive properties of the bioarchitectural memristor using aqueous macromolecular crowders. Voltage-sensitive alamethicin ion channels and voltage-sensitive membrane geometry are responsible for memristive behavior. Crowders with two distinct sets of properties provide unique modulatory effects. Specifically, the shape, solvent affinity, and number of species explores the modulatory effects on the memristive dynamics. Apart from offering distinct sets of properties, asymmetric membrane solutions elucidate additional candidate mechanisms for modulating memristive dynamics. Cyclic voltammetry (CV) monitors the affects of modulatory macromolecular crowding on the homosynaptic model of the DIB housing alamethicin, via changes in membrane conductance measured as alamethicin voltage threshold for insertion, V*.

Chapter 3 presents heterosynaptic modulation via membrane-associated pH-sensitive peptide ATRAM2. Here, the aspiration is to show how the addition of a secondary membrane peptide species modulates membrane conductance through interaction with the membrane and alamethicin. Two states of the peptide crowder explore the dependence of memristive dynamics on crowder orientation in the membrane. Because

memristive dynamics depend on the number of ion-channels and membrane area, crowder specific orientation effects on alamethicin channel dynamics, including the transition from bound to inserted (B-I) and inserted to bound (I-B), and membrane electrowetting properties elucidate the corresponding modulatory potential of ATRAM2 on memristor dynamics. Beyond peptide orientation, pH illuminates an additional candidate mechanism for heterosynaptic modulation of memristor dynamics. Again, CV monitors the changes in membrane conductance.

Chapter 4 will present heterosynaptic modulation via lipid membrane composition, such as oxidized lipids including POPC oxidation products. Here, the aspiration is to use lipid oxidation to model pure heterosynaptic plasticity, for example in the absence of the homosynaptic conditions requiring alamethicin described previously. The modulatory effects of the lipid composition on the memristive behavior are explored. As the light interacts with photosensitizers (PS), photosensitive molecules in solution, lipid oxidation results modifying the lipid membrane constituents to now harbor lipid variants containing oxygen. These oxidative modifications modulate the membrane conductance via change the polarity of the lipid species. Modulatory effects can be delivered in multiple ways: light induced oxidation, oxidized lipid titration in the membrane, and leaflet asymmetry in oxidative lipid composition. The latter scenario can be further broken down to single-sided lipid oxidation. For example, PS can be incorporated on one side of the membrane, the membrane can be asymmetric including oxidation prone POPC in one leaflet, and oxidized POPC can be added to one side. All cases explore potential conduits for heterosynaptic functionality of memristors as an electrochemical circuit element in a biological computer. Biologically, adding PS to one side mimics one-sided oxidative stress effects as seen in cellular compartments containing high oxidative stress, mitochondria and chloroplast, or in cells under higher quantities of oxidative stress, for example cancer cells. Single-sided oxidized lipid titration investigates with chemical precision the exact threshold of modulation on memristive dynamics. Oxidative stress serves as a purely heterosynaptic form of plasticity capable of long-term modulation in learning and memory formation via permanent changes to the lipid constituents of the membrane when exposed to ROS.

# Chapter 2

# Macromolecular Crowding Affects Voltage-Dependent Alamethicin Pore Formation in Lipid Bilayer Membranes

A version of this chapter was originally published by William T. McClintic, Graham J. Taylor, Michael L. Simpson, and C. Patrick Collier: McClintic, W. T., Taylor, G. J., Simpson, M. L., and Collier, C. P. (2020). Macromolecular Crowding Affects Voltage-Dependent Alamethicin Pore Formation in Lipid Bilayer Membranes. The Journal of Physical Chemistry B.

## 2.1 Abstract

Macromolecular crowding is known to modulate chemical equilibria, reaction rates, and molecular binding events, both in aqueous solutions and at lipid bilayer membranes, natural barriers that enclose the crowded environments of cells and their subcellular compartments. Previous studies on the effects of macromolecular crowding in aqueous compartments on conduction through membranes have focused on single-channel ionic conduction through previously formed pores at thermodynamic equilibrium. Here, the effects of macromolecular crowding on the mechanism of pore formation itself were studied using the droplet interface bilayer (DIB) technique with the voltage-dependent pore-forming peptide alamethicin (alm). Macromolecular crowding was varied using 8 kDa molecular weight polyethylene glycol (PEG8k) or 500 kDa dextran (DEX500k) in two aqueous droplets on both sides of the bilayer membrane. In general, voltage thresholds for pore formation in the presence of crowders in the droplets decreased compared to their values in the absence of crowders, due to excluded volume effects, water binding by PEG, and changes in the ordering of water molecules and hydrogen-bonding interactions involving the polar lipid headgroups. In addition, asymmetric crowder loading (e.g., PEG8k−DEX500k on either side of the membrane) resulted in transmembrane osmotic pressure gradients that either enhanced or degraded the ionic conduction through the pores.

## 2.2 Introduction

Studies on excitable cellular systems have indicated that much of the nonlinear dynamical behavior exhibited by these cells comes from their membranes (Mueller, P., 1958; Blinks, L. R., 1936; Mueller, P., Rudin, D. O., Tien, H. T., and Wescott, W. C., 1962). The use of synthetic membrane models have resulted in the reduction of the

complexity of experimental protocols, better control of chemical composition, and facile transverse electrical interrogation capability (Mueller, P., Rudin, D. O., Tien, H. T., and Wescott, W. C., 1962), all in the absence of confounding crowded and complex cellular environments. Simplifying the cellular environment enables quantitative interpretation of the specific effects that macromolecular crowders of varying size and concentration have on the system. To date, electrical investigations of cell membrane physiology using synthetic lipid membranes in the presence of macromolecular crowding have primarily focused on crowding effects on ionic transport properties (Bezrukov, S. M., and Vodyanoy, I., 1993; Vodyanoy, I., and Bezrukov, S. M., 1992) and partitioning and transport of biomolecules in intracellular environments (Bezrukov, S. M., and Vodyanoy, I., 1993; Larimi, M. G., Mayse, L. A., and Movileanu, L., 2019; Bashford, C. L., Alder, G. M., Fulford, L. G., Korchev, Y. E., Kovacs, E., MacKinnon, A., ... and Pasternak, C. A., 1996; Bezrukov, S. M., Vodyanoy, I., Brutyan, R. A., and Kasianowicz, J. J., 1996; Korchev, Y. E., Bashford, C. L., Alder, G. M., Kasianowicz, J. J., and Pasternak, C. A., 1995; Bezrukov, S. M., Vodyanoy, I., and Parsegian, V. A., 1994; Vodyanoy, I., Bezrukov, S. M., and Parsegian, V. A., 1993), while crowding induced changes in binding equilibria between pore-forming biomolecules and membranes have been studied using SDS-PAGE with fluorescent staining (Bashford, C. L., Alder, G. M., Fulford, L. G., Korchev, Y. E., Kovacs, E., MacKinnon, A., ... and Pasternak, C. A., 1996; Ye, C., Chai, Q., Zhong, M., and Wei, Y., 2013) or through coupling conductance data with SDS-PAGE fluorescence (Bashford, C. L., Alder, G. M., Fulford, L. G., Korchev, Y. E., Kovacs, E., MacKinnon, A., ... and Pasternak, C. A., 1996).

Macromolecular crowding levels found in cellular organisms range from 5 to 40% of the volume of the cell (Mourão, M. A., Hakim, J. B., and Schnell, S., 2014), introducing osmotic stresses (Parsegian, V. A., Rand, R. P., and Rau, D. C., 2000), excluded volumes (Rivas, G., and Minton, A. P., 2016), and altered behavior of the biological water solvent (Ferreira, L. A., Uversky, V. N., and Zaslavsky, B. Y., 2017; Zaslavsky, B. Y., and Uversky, V. N., 2018). In cellular membranes, high aqueous crowding fractions of macromolecules dehydrate lipid headgroups and osmotically stress channel pores, which increases packing densities of membrane-specific molecules (Boni, L. T., and Hui, S. W., 1987) and increases the relative probability of closed versus open states in

membrane pores (Zimmerberg, J., Bezanilla, F., and Parsegian, V. A., 1990). In synthetic lipid membrane systems, crowders of different molecular weights have been used to estimate the membrane pore size (Bezrukov, S. M., and Vodyanoy, I., 1993; Korchev, Y. E., Bashford, C. L., Alder, G. M., Kasianowicz, J. J., and Pasternak, C. A., 1995) and to track partitioning into pores as functions of molecular size and affinity for the pore lumen in conjunction with electrochemical methods (Bezrukov, S. M., and Vodyanoy, I., 1993; Larimi, M. G., Mayse, L. A., and Movileanu, L., 2019; Bezrukov, S. M., Vodyanoy, I., Brutyan, R. A., and Kasianowicz, J. J., 1996). Additional studies have focused on the effects of crowding-induced osmotic gradients between the lumen of a pore and the bulk aqueous solution on pore dynamics (Korchev, Y. E., Bashford, C. L., Alder, G. M., Kasianowicz, J. J., and Pasternak, C. A., 1995; Vodyanoy, I., Bezrukov, S. M., and Parsegian, V. A., 1993; Zimmerberg, J., and Parsegian, V. A., 1986). Recently, macromolecular crowding effects on Syn B2 cationic polypeptide-binding kinetics with the transmembrane α-hemolysin pore were investigated in the presence of the crowder polyethylene glycol (PEG). It was found that the binding energy decreased with increasing crowder concentration and decreasing crowder molecular weight, highlighting the importance of colligative properties in solutions on the properties of the interface (Larimi, M. G., Mayse, L. A., and Movileanu, L., 2019).

Membrane-active antimicrobial peptides such as alamethicin (alm) form conductive pores in lipid bilayer membranes above specific concentration and voltage thresholds (Huang, H. W., 2006; Stankowski, S., Schwarz, U. D., and Schwarz, G., 1988; Hall, J. E., 1981; Vodyanoy, I., Hall, J. E., and Balasubramanian, T. M., 1983; Vodyanoy, I., Hall, J. E., and Vodyanoy, V. I. T. A. L. Y., 1988; Eisenberg, M., Hall, J. E., and Mead, C. A., 1973). In this paper, we explored how the inclusion of large polymeric macromolecules that are water-soluble like PEG8k (molecular weight of 8000 Da) and DEX500k (molecular weight of 500000 Da) at identical (w/w) concentrations in the aqueous phases of droplet interface bilayers (DIBs) affected the insertion and pore formation of alm peptides in model cell membranes. Alm pore formation has been shown to be sensitive to changes in the chemical potential of water induced by high molecular weight PEG8k and DEX500k polymers (Vodyanoy, I., Bezrukov, S. M., and Parsegian, V. A., 1993), and to changes in the extent of bilayer hydration associated

with changes in the chemical potential of water (Huang, H. W., 2006; Huang, H. W., and Wu, Y., 1991). In electrophysiological experiments carried out by Bezrukov and Voydyanoy (Bezrukov, S. M., and Vodyanoy, I., 1993) and by Parsegian (Vodyanoy, I., Bezrukov, S. M., and Parsegian, V. A., 1993), macromolecular crowding molecules in aqueous solutions were perfused into the system after the membrane-bound protein or peptide had sufficient time to form pores in the membrane, and the system had achieved thermodynamic equilibrium. There are fewer studies examining the effects of macromolecular crowding on pore formation itself in the membrane (Bashford, C. L., Alder, G. M., Fulford, L. G., Korchev, Y. E., Kovacs, E., MacKinnon, A., ... and Pasternak, C. A., 1996; Ye, C., Chai, Q., Zhong, M., and Wei, Y., 2013). The mechanisms governing protein and peptide insertion in membranes to form conductive pores are complex, consisting of a series of dynamic steps such as adsorption, insertion or translocation, and oligomerization, each of which is sensitive to interactions with other molecules in the confined and the crowded micro- and nanoenvironments of the membrane and the compartmentalized aqueous solvent (Figure 1.1).

Here, we show that macromolecular crowding using PEG8k and DEX500k polymers alter voltage-dependent alamethicin pore formation, using droplet interface bilayers as models for cell membranes. Cyclic voltammetry was used with DIBs to extract thresholds for voltage-dependent alamethicin insertion in the presence and absence of macromolecular crowding. The two crowders used to simulate the crowded, cellular environment were PEG8k, representing a relatively compact water-ordering macromolecule, and DEX500k, a significantly larger, multibranched polymer that was solvent inert. Alm pore formation was studied for both symmetric and asymmetric crowder loading in DIBs at the lower end of the crowding fraction found in cells (10 wt % of solution, upper limit at 40 wt %) (Mourão, M. A., Hakim, J. B., and Schnell, S., 2014).

We found that macromolecular crowding in PEG8k-only or DEX500k-only aqueous solutions in DIBs increased the activities of the alm monomers, which were assumed to be present in solution as peptide-decorated 100 nm diameter liposomes residing in the surface bound (S-state) but not inserted state. Additional alm monomers bound to vesicles in solution interacted with the main membrane of the DIB due to depletion

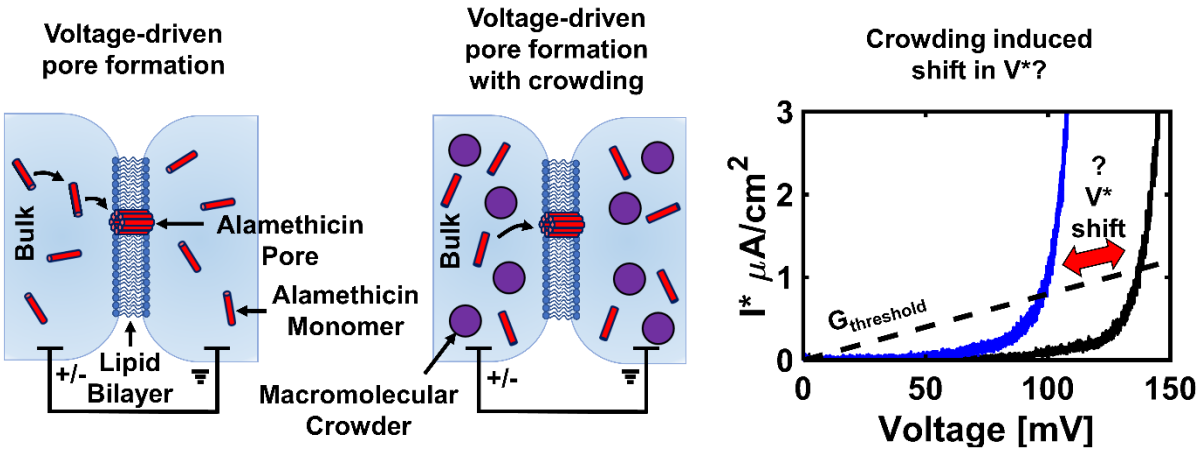


**Figure 2.1.** Pore formation in membranes is likely influenced by macromolecular crowding in aqueous solutions. Step 1 demonstrates the formation of a pore from aqueous peptide monomers in the absence of macromolecular crowders. Step 2 demonstrates pore formation in the presence of macromolecular crowding.

energies from macromolecular crowding. This lowered the voltage-dependent activation thresholds for pore formation by amounts that depended on the specific composition at the interface (no polymer, PEG8k−PEG8k, DEX500k−DEX500k, or PEG8k−DEX500k). For asymmetric droplets containing PEG8k−DEX500k, activation thresholds were also influenced by transmembrane gradients in the chemical potential of the water solvent itself, resulting in a decrease in the voltage threshold for pore formation from DEX500k to PEG8k across the interface compared to symmetric DEX500k−DEX500k, and an increase in the voltage threshold of PEG8k to DEX500k compared to PEG8k−PEG8k. These results help to elucidate how interactions between macromolecular crowding in aqueous solutions and peptide channel formation promote molecular binding events and pore formation in the interfacial membrane, for both synthetic systems and for living cells.

## 2.3 Materials and Methods

### *2.3.1 Materials*

Sodium chloride (NaCl), 3-(N-morpholino)- propanesulfonic acid (MOPS) buffer, sodium hydroxide, dextran (DEX500k, 450−650-kDa, p/n 31392), agarose powder (p/n A9539), and ethanol were obtained from Sigma-Aldrich. Polyethylene glycol (PEG8k, 8-kDa, p/n 43443) was obtained from Alfa Aesar, and alamethicin peptides (p/n/A-1286) were purchased from A.G. Scientific. Alamethicin was dissolved in ethanol to a concentration of 5 mg/mL to create a stock solution used for further sample preparation, and the stock solution was stored at −20 °C when not in use. Liposome solutions were prepared by dispersing 1,2-diphytanoyl-sn-glycero-3-phosphocholine (DPhPC) lipids (Avanti, Alabaster, AL) at 2.5 mg/mL in buffer (10 mM MOPS, 125 mM NaCl, NaOH to achieve pH 7.0) and extruding the resulting multilamellar vesicles 11 times through a 100 nm NanoSizer extruder containing a track-etched polycarbonate membrane (TandT Scientific, Knoxville, TN). Osmolarities of aqueous solutions containing PEG8k or DEX500k with NaCl, MOPS buffer, and DPhPC lipids were measured with a Wescor Vapro Model 5520 vapor pressure osmometer (Logan, UT). Alamethicin stocks were in ethanol, precluding osmometry measurements.

### *2.3.2 Droplet Interface Bilayer Formation*

Device assembly was based on the droplet interface bilayer (DIB) method, which has been used extensively in recent years to study the biophysics of model membranes (Taylor, G. J., Heberle, F. A., Seinfeld, J. S., Katsaras, J., Collier, C. P., and Sarles, S. A., 2017) and membrane-bound ion channels (Najem, J. S., Dunlap, M. D., Rowe, I. D., Freeman, E. C., Grant, J. W., Sukharev, S., and Leo, D. J., 2015; Taylor, G. J., Venkatesan, G. A., Collier, C. P., and Sarles, S. A., 2015; Taylor, G., Nguyen, M. A., Koner, S., Freeman, E., Collier, C. P., and Sarles, S. A., 2019) and has been used as building blocks for the development of stimuli-responsive materials (Sarles, S. A., and Leo, D. J., 2011). The liposome solution was diluted 1:1 with either salt-free buffer (MOPS, NaOH only), salt-free buffer with 20 wt % PEG8k, or salt-free buffer with 20 wt % DEX500k. 300 nL droplets of the final liposome or liposome/crowder solution (1.25 mg/mL DPhPC, 1.48 mM) were pipetted manually onto agarose-coated ball-ended electrodes submerged in hexadecane oil (10 % residual oil by volume in the membrane [Taylor, G. J., Venkatesan, G. A., Collier, C. P., and Sarles, S. A., 2015; Gross, L. C., Heron, A. J., Baca, S. C., and Wallace, M. I., 2011). Alamethicin was incorporated by first diluting the 5 mg/mL stock ethanol solution 200x with the final liposome or liposome/crowder solution, followed by another 12.5x dilution to achieve a final concentration of 2 μg/mL alm (1 μM).

### *2.3.3 Electrical Measurements and Imaging*

Electrical measurements were made using the suspended droplet DIB approach, with Ag/AgCl electrodes and a patch clamp amplifier, shown in Figure 2.2 (Axopatch 200B, Molecular Devices, San Jose, CA) (Taylor, G. J., Venkatesan, G. A., Collier, C. P., and Sarles, S. A., 2015). Bilayer membrane formation was detected as an increase in membrane capacitance by supplying a 10 Hz, 10 mV triangular waveform from a function generator clamped at zero bias voltage (Agilent). Due to the highly resistive and capacitive nature of the bilayer membrane, the resulting current response was square-like. The capacitance of the lipid interface was extracted from sections of the square wave current response using a MATLAB script (available upon request). In

parallel, changes in the minor axis of an elliptical membrane geometry, R, were acquired from bright field images of the droplets viewed from below through a 4x objective lens on a Nikon TE-300 inverted optical microscope. The images were postprocessed using custom scripts in MATLAB to extract values of R. The bilayer areas from these measurements were then used to calculate the specific capacitance, cm, from which the membrane thickness was obtained. Single-channel alamethicin activity in DIBs, measured by us (Boreyko, J. B., Polizos, G., Datskos, P. G., Sarles, S. A., and Collier, C. P., 2014) and others (Taylor, G. J., and Sarles, S. A., 2015; Sarles, S. A., Stiltner, L. J., Williams, C. B., and Leo, D. J., 2010; Harriss, L. M., Cronin, B., Thompson, J. R., and Wallace, M. I., 2011), gave very similar results compared to the more commonly used traditional black lipid membrane technique (BLM), as long as the conditions (choice of oil, lipids, bathing solution, etc.) were the same (Sansom, M. S., 1991). Alamethicin insertion was characterized at the bulk, ensemble level by a voltage threshold, V*, defined as the voltage at which the conductance of the lipid bilayer surpasses a conductance threshold roughly 1 order of magnitude higher than the bare membrane conductance. The conductance threshold was set to 8 $\mu S/cm^2$ for the current experiments (Figure 2.2F). Cyclic voltammetry measurements to obtain V* values were carried out with a voltage scan rate of 10 mV/s, through the specific conductance threshold of 8 $\mu S/cm^2$ (Taylor, G. J., Heberle, F. A., Seinfeld, J. S., Katsaras, J., Collier, C. P., and Sarles, S. A., 2017; Taylor, G. J., and Sarles, S. A., 2015; Najem, J. S., Taylor, G. J., Weiss, R. J., Hasan, M. S., Rose, G., Schuman, C. D., ... and Sarles, S. A., 2018). The amplitude of each CV scan was adjusted for each measurement to avoid excessive current levels and the risk of membrane rupture. A typical target range for the maximum current at peak voltages was ca. 1−5 nA. Bipolar scans (consisting of both positive and negative voltage sweeps) were performed, and the V* values from both polarities were averaged to obtain a single V* value per scan. Table S1 (Supporting Information) shows the V* means and standard deviations for all scenarios.

### 2.4 Results and Discussion

Alm activation in membranes can be described in terms of a threshold relating the concentration of peptide to available membrane lipids as the ratio (P/L) ((Taylor, G. J.,

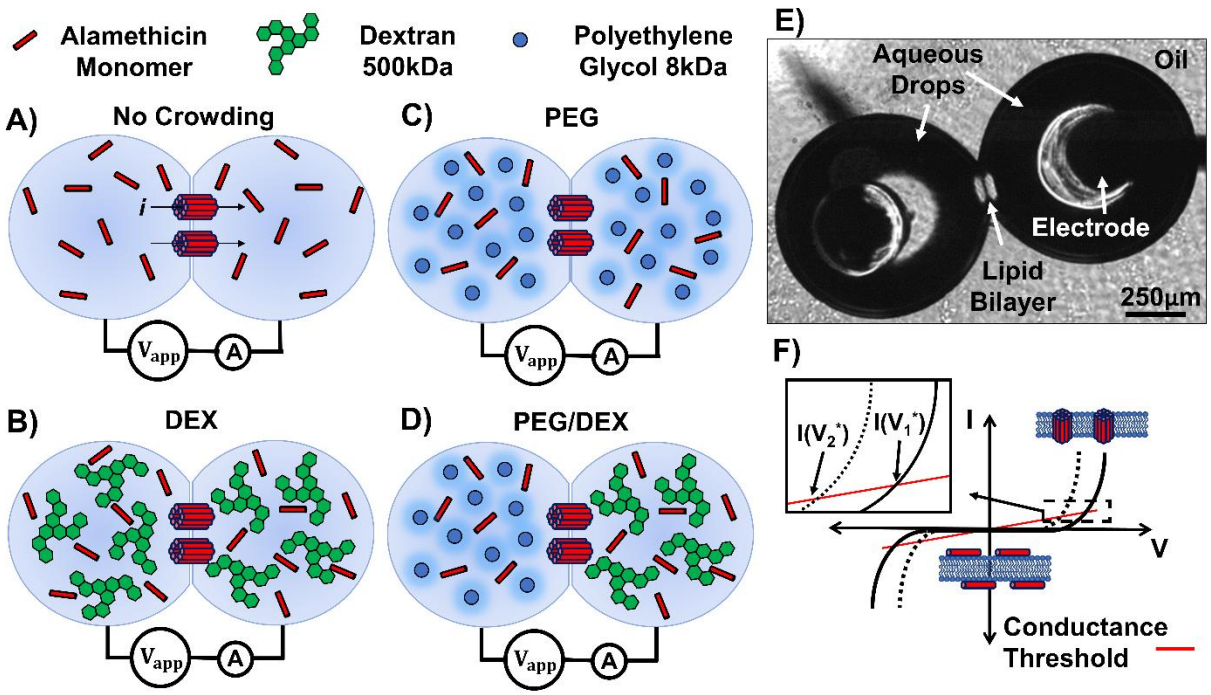


**Figure 2.2.** Experimental methods and data interpretation: (A) no crowding, (B) crowding with 10 wt % DEX500k, (C) crowding with 10 wt % PEG8k, and (D) crowding with a 10 wt % PEG8k droplet in contact with a 10 wt % DEX500k droplet. Alamethicin monomers oligomerize in the bilayer to form a pore with the application of an electrical potential above a threshold, and the current response is recorded. (E) A representative picture of the experimental setup. (F) schematic to aid interpretation of the current response to an increasing voltage ramp. The red line is the specific conductance threshold, meant to represent the conductance ten times that of a bare membrane, indicating the onset of alm insertion. The value of the voltage when the current crossed the conductance threshold, 8 µS/cm$^2$ , is the voltage threshold, V*.

and Sarles, S. A., 2015). In our DIB experiments, alm peptides became incorporated in the lipid bilayer membrane between aqueous droplets due to the binding and fusion of 100 nm liposomes decorated with about 26 peptide molecules (per liposome) residing in the S-state, which corresponds to the peptide being embedded in the headgroup region (determined with fluorescence and solid-state NMR) and aligned parallel to the membrane (Huang, H. W., 2006). The disruption of the headgroup region upon peptide binding expanded the membrane area near the embedded peptide, resulting in local changes in bilayer tension. Each peptide-binding event released water molecules from the headgroups, and the area expansion was accompanied by local thinning in the hydrocarbon region of the bilayer as lipid tails became distorted and deformed to fill in the void created by the embedded peptide (determined with X-ray diffraction) (Huang, H. W., 2006).

Alm peptides can be driven into a membrane-inserted I-state by either increasing the peptide concentration, applying a transmembrane potential, or both. Below peptide-to-lipid ratio thresholds for pore formation, (P/L)*, the membrane thickness decreases linearly with increasing (P/L). At these concentrations in the membrane, only peptide monomers exist, and there is no aggregation or oligomerization to form pores. X-ray diffraction studies have indicated the concentration threshold corresponds to an average distance between S-state peptides in the membrane of about 3.5 nm, which is roughly the persistence length of the dimple distortion caused by membrane thinning, based on elastic energy considerations. Above the threshold, the bilayer thickness remains constant, corresponding to excess peptides forming stable pores after the threshold, (P/L)*, had been reached. The nonlinear concentration dependence of the S-state to the I-state transition results in cooperativity in the peptide binding and a sigmoidal dependence of pore activity in the bilayer as a function of the (P/L) ratio (Huang, H. W., 2006; Chen, F. Y., Lee, M. T., and Huang, H. W., 2002). There is a very strong voltage dependence to the conductance of alm and other ion channels in both artificial and biological membranes. The application of voltage and the resulting transmembrane electrical potential difference significantly lowers the threshold for peptide insertion in the membrane compared to thresholds based only on the peptide concentration. The α-helix of alm has been reported to possess a dipole moment as

high as 70−80 D (Yantorno, R., Takashima, S., and Mueller, P. A. U. L., 1982; Schwarz, G., and Savko, P., 1982); the interaction of this large dipole moment with the electric field rotates peptide molecules from the S-state into inserted peptide states, followed by oligomerization to form open, conductive channels for ion transport. At a given potential, the conductance is strongly dependent on the concentrations of alm and salt activity, scaling to the ninth power for the alm concentrations and to the fourth power for electrolytes. When either of these two concentrations increases, the threshold shifts to lower voltages (Stankowski, S., Schwarz, U. D., and Schwarz, G., 1988).

### *2.4.1 Symmetric Macromolecular Crowding Effect on Alamethicin Voltage Threshold*

CV measurements were performed with DIBs incorporating alm to determine whether membrane-active peptide insertion was affected by the presence of crowding macromolecules. In a typical crowder-free DIB experiment, two aqueous droplets containing 1 μM alm peptide each (incorporated in 100 nm diameter unilamellar vesicles) were placed under hexadecane oil, allowed several minutes to form monolayers, and then brought into contact to promote spontaneous formation of a lipid bilayer between the two droplets (Taylor, G. J., and Sarles, S. A., 2015). Aqueous crowding effects on alm pore formation in the lipid bilayer were analyzed for the following cases: no crowding (Figure 2.2A), symmetric crowding (Figure 2.2B−C), and asymmetric crowding (Figure 2.2D).

While all the specific current−voltage (I*−V) curves in Figure 2.3A show an exponential dependence of alm pore formation-induced specific current on the voltage, the I*−V curves obtained with symmetric PEG8k−PEG8k droplets (blue trace) and symmetric DEX500k−DEX500k droplets (green) were shifted toward lower voltages compared to the noncrowded case (black). The bar graph in Figure 2.3B shows the average V* threshold value for each case, with error bars representing one standard deviation from the mean. The addition of 10 wt % of either type of crowding molecule resulted in decreased values of V* compared to the noncrowded solution case, with PEG8k crowders exerting a stronger effect then DEX500k when present at equal wt % values.

Table S1 in the Supporting Information contains the mean V* values and standard deviations for all cases.

### *2.4.2 Asymmetric Macromolecular Crowding Effect on Alamethicin Voltage Threshold*

CV measurements were also carried out on asymmetric DIBs containing PEG8k in one droplet and DEX500k in the other droplet. Two asymmetric cases were examined: one with PEG8k on the positive (cis) electrode and DEX500k on the grounded (trans) electrode (yellow trace in Figure 2.3A) and one with DEX500k on the positive electrode with PEG8k grounded (red). Average V* values obtained for the PEG8k− DEX500k and DEX500k−PEG8k cases are shown in Figure 2.3B. It is interesting to note that, in the presence of PEG8k− DEX500k or DEX500k−PEG8k asymmetry, the voltage required to drive alm insertion from the PEG8k phase was higher than what was observed with symmetric PEG8k− PEG8k droplets. Conversely, the voltage required to drive alm insertion from the DEX500k phase was lower in both asymmetric cases compared to the symmetric DEX500k− DEX500k case. Because the differences in the mean V* values for the PEG8k−DEX500k and DEX500k−PEG8k asymmetric cases were found not to be statistically significant (Table S3), the average value of the two voltage thresholds was used.

### *2.4.3 Depletion Energies and Osmotic Pressure Effect on Alm Voltage Thresholds*

Macromolecular crowding in symmetric PEG8k-only or DEX500k-only aqueous solutions in DIBs increased the thermodynamic activities of alm monomers, present in solution as peptide-decorated 100 nm diameter liposomes, compared to the simplest case without crowders. Table S1 contains physical data from PEG8k and DEX500k needed for understanding how crowding with these polymers affected peptide binding to the bilayer membrane, leading to ion channel activation. Entropic, excluded volume contributions resulted in higher activities for PEG8k than DEX500k. An overlap between the polymer exclusion zones around the peptide−liposomes and the bilayer membrane resulted in the depletion energies given by the following (Israelachvili, J. N., 2015):

$$W_D = -\rho R_g kT \quad 2.1$$

where ρ is the number density of the macromolecules and $R_g$ is the measured gyration radius for the two polymers (3.2 nm for PEG8k (Ling, K., Jiang, H., and Zhang, Q., 2013) and 8.3 nm for DEX500k (Granath, K. A., and Kvist, B. E., 1967). These resulted in entropic, attractive forces that "pushed" the liposomes to the bilayer, in a similar manner to the polystyrene nanoparticle hard spheres that were forced to the bilayer membrane of lipid vesicles in the presence of crowders (Dinsmore, A. D., Wong, D. T., Nelson, P., and Yodh, A. G., 1998). These depletion energies were almost an order of magnitude higher for PEG8k (about −0.9 mJ/$m^2$) than for DEX500k (−0.1 mJ/ $m^2$).

In addition to these entropic effects, PEG8k also specifically binds water molecules (an enthalpic effect), assumed to dehydrate the membrane by lowering the chemical potential of the water solvent, while raising the $Na^+$ activity, as seen elsewhere (Bezrukov, S. M., and Vodyanoy, I., 1993; Vodyanoy, I., Bezrukov, S. M., and Parsegian, V. A., 1993). There are three consequences of this increased salt activity due to PEG8k− water binding. First, the elevated salt activity resulted in higher ionic currents and lower apparent V* thresholds since the iR voltage drop from the electrodes to the membrane was less. Second, an additional access resistance near the ion channel opening based on electrodiffusion-limited ion transport at the mouth of the pore that added to the actual resistance of the pore itself decreased with increased salt activity. Third, the ionic conductance through the pore lumen increased (Bezrukov, S. M., and Vodyanoy, I., 1993).

For asymmetric PEG8k−DEX500k DIBs, activation thresholds were also likely influenced by transmembrane gradients in the chemical potential of the water solvent itself. The impact of PEG8k on the water chemical potential was greater than that of DEX500k because of the greater number of PEG8k molecules compared to DEX500k molecules at the same weight fraction and because PEG binds water molecules while DEX does not (Boni, L. T., and Hui, S. W., 1987).

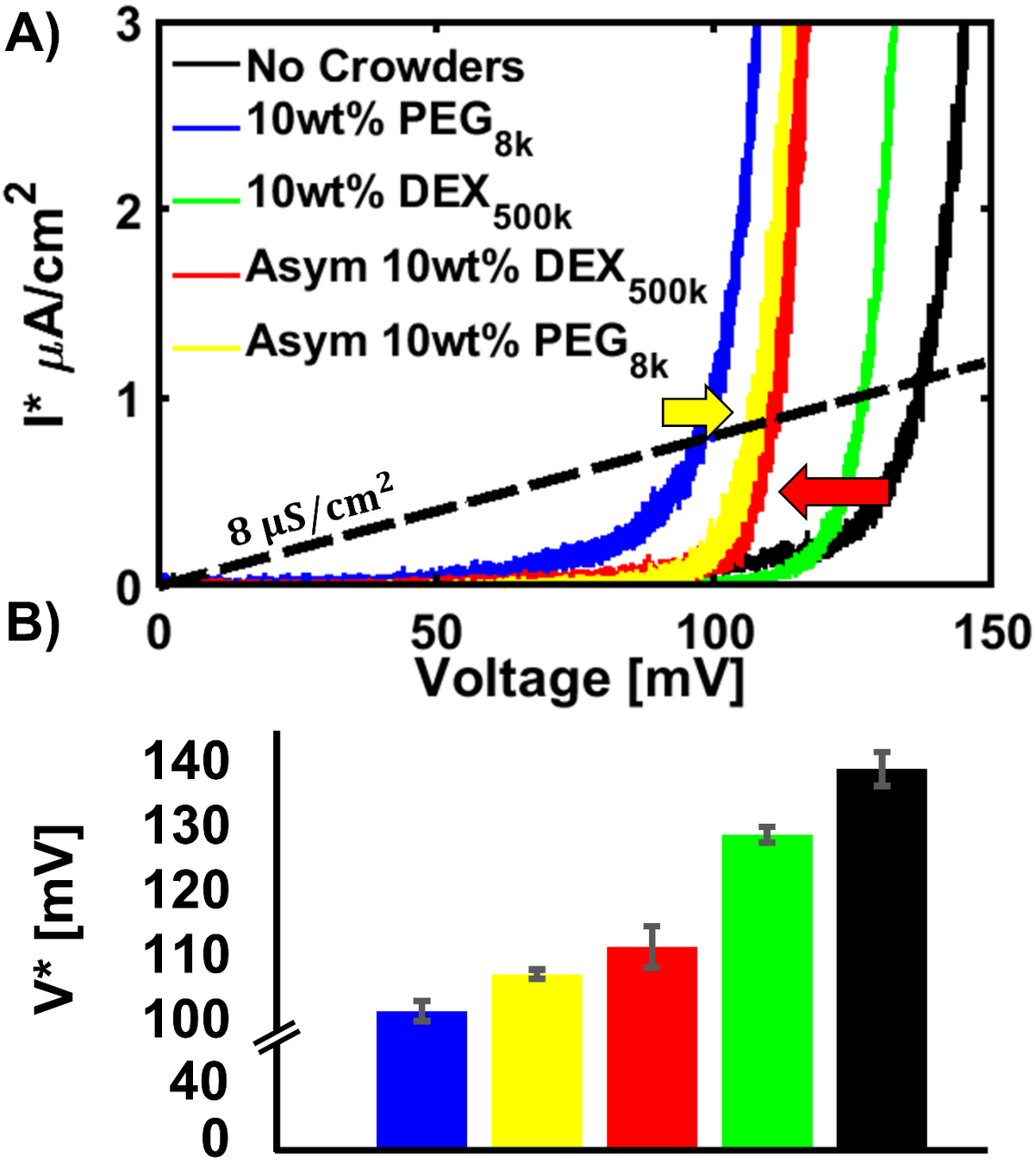


**Figure 2.3.** Specific current versus voltage curves revealed the V* voltage thresholds for symmetric and asymmetric crowder loading conditions. (A) Raw specific current−voltage curves in the presence of macromolecular crowding for the four cases shown in Figure 2.2A− D. (B) Bar graph of V* values for the four cases, with error bars representing one standard deviation from the mean. Statistical testing shows statistically significant differences (*) and not statistically different (**) differences.

The effects of the polymeric crowders in an aqueous solution can be described by the following form of the virial expansion of the excess water solvent chemical potential:

$$\Delta\mu_w = \mu_w^P - \mu_w^0 \quad (2.2)$$

$$= -\frac{RTM_1}{1000}\left[m_2 + m_3 + \left(\frac{a_{22}}{2}\right)m_2^2 + \left(\frac{a_{33}}{2}\right)m_3^2 + a_{23}m_2m_3\right] \quad (2.3)$$

Here, $\mu_w^P$ represents the chemical potential of water in the presence of crowders, $\mu_w^0$ represents the chemical potential of water in the ideal solution reference state, R is the gas constant, T is the absolute temperature, and $M_1$ is the solvent molecular weight. $m_2$ is the polymer molality (moles solute/kg water), while $m_3$ represents the sum of the molalities of the other solutes in the solution, which include NaCl, MOPS, the alm peptide, and the DPhPC lipid. We followed the convention of McGann and co-workers by grouping together all the solutes except the polymer macromolecules (PEG8k or DEX500k), which were the only species in the solution whose concentrations were varied (Prickett, R. C., Elliott, J. A., and McGann, L. E., 2011). Here, m3 is a constant and is given by

$$m_3 = k_{diss}m_{NaCl} + m_{MOPS} + m_{liposome} \quad (2.4)$$

where $k_{diss}$ is a nonstoichiometric, empirically determined “dissociation constant” that accounts for the additional nonideality in the solution behavior due to the electrolyte (Prickett, R. C., Elliott, J. A., and McGann, L. E., 2011). The liposome molality was estimated from the circumference of the 100 nm diameter unilamellar vesicle, the solution concentration of the DPhPC lipids (7.6 μmolal), and the equilibrium molecular areas of the lipid molecules in the bilayer (81.2 $Å^2$; Yasmann, A., and Sukharev, S., 2015). $a_{22}$ and $a_{33}$ are second virial coefficients specifically for the PEG8k−DEX500k polymer (Haynes, C. A., Beynon, R. A., King, R. S., Blanch, H. W., and Prausnitz, J. M., 1989) and NaCl (Prickett, R. C., Elliott, J. A., and McGann, L. E., 2011), respectively, and $a_{23}$ is a mixing term accounting for the nonideality of the solution due to polymer−electrolyte interactions.

The excess water chemical potentials from the virial expansion were validated experimentally with the osmotic coefficients of the polymer solutions, $\phi = \pi_{real}/\pi_{ideal}$, which can be found experimentally as the ratios of the true osmolarity of the polymer solution measured with a vapor pressure osmometer to the osmolarity of an ideal solution with the same composition (results presented in Table S2.1). The osmotic coefficients were related to the excess water chemical potential by the following (Levine, I. N., 1995):

$$\phi = -\frac{\Delta\mu_w}{RTM_1(m_2 + m_3)0.001} \qquad 2.5$$

The experimental values of $\phi$ at 10 wt % and those determined from the virial expansion were within a few percent of each other for both polymers, validating the use of the virial expansion (Table S2).

Changes in the chemical potential of water as a function of increasing polymer concentration led to increasing osmotic pressures in the droplets of different magnitudes on either side of the membrane for asymmetric DIBs:

$$\Pi = -\frac{\Delta\mu_w}{\bar{V}_w} \qquad 2.6$$

where $\bar{V}_w$ is the molar volume of water (18 mL/mol) (Parsegian, V. A., Rand, R. P., and Rau, D. C., 2000). The relationship between the crowder concentration and water chemical potentials and the corresponding osmotic pressures are shown in Figure S1A and B. For the asymmetric crowding cases, the resulting transmembrane osmotic stress gradients resulted in water flow from the DEX500k side to the PEG8k side of the membrane, leaving the state of membrane hydration, specifically at the lipid headgroups and alm monomers, unclear.

The transmembrane osmotic stress for the asymmetric crowding case also created an additional work term, $\Pi\Delta v$, one on either side of the bilayer, acting on the alm pores due to the impermeant polymers in the solution (Vodyanoy, I., Bezrukov, S. M., and Parsegian, V. A., 1993; Zimmerberg, J., and Parsegian, V. A., 1986). Here, $\Delta v$ involved

changes in the water volume associated with an alm channel opening and were in the 103 Å$^3$ range per transition per pore between conductance states. This extra work term increased the energy required for channel opening:

$$\Delta E(V, \Pi) = \Delta E(V, 0) + \Pi \Delta v \qquad 2.7$$

At room temperature and with 10 wt % PEG8k, Π = 4.6 × 10$^5$ Pa, corresponding to an energy cost of 277 J/mol. On the other hand, the osmotic pressure change for the channel opening from the 10 wt % DEX500k solution side of the membrane was less, 3.0 × 10$^5$ Pa, corresponding to an energy cost of 181 J/mol. For symmetric crowding, this energy difference did not exist, but for asymmetric crowding, the alm pores experienced an osmotic pressure difference ΔΠ = 1.6 × 10$^5$ Pa. While these additional work terms exist per alamethicin channel opening event in the asymmetric case only a channel gating molecular hinge would be affected after 10 or so alm channels had opening due competition with thermal energy (2500 J/mol).

The effects of these differences on the voltage thresholds for pore formation are represented schematically in Figure 2.4. The circuit convention used here includes the following: a positive voltage was applied to the left-hand (cis) droplet of the DIB pair, while the right-hand (trans) droplet was grounded. Since V* was defined relative to a specific conductance value (8 μS/ cm$^2$), it is reasonable that a decrease in the pore conductance would result in a higher apparent voltage threshold. A slight increase in V* was seen for the asymmetric PEG8k−DEX500k DIB (V*$_{avg}$ = 109 mV) case compared to the symmetric PEG8k−PEG8k (V* = 101 mV) case. This trend was reversed for DEX500k−DEX500k, which had a significantly higher voltage threshold (V* = 129 mV) than the asymmetrically crowded DIB (V*$_{avg}$ = 109 mV).

Figure 2.4 shows that the average voltage threshold for the asymmetric crowding case (V*$_{avg}$ = 109 mV) was much closer to the PEG8k−PEG8k symmetric crowding case (V* = 101 mV) than to the symmetric DEX500k−DEX500k case (V*=129 mV). The difference in the water chemical potentials in the asymmetric droplets created a chemical potential difference in the water solvent across the membrane, which either acted against the ionic current, as was the case for PEG8k−DEX500k, or with the ionic

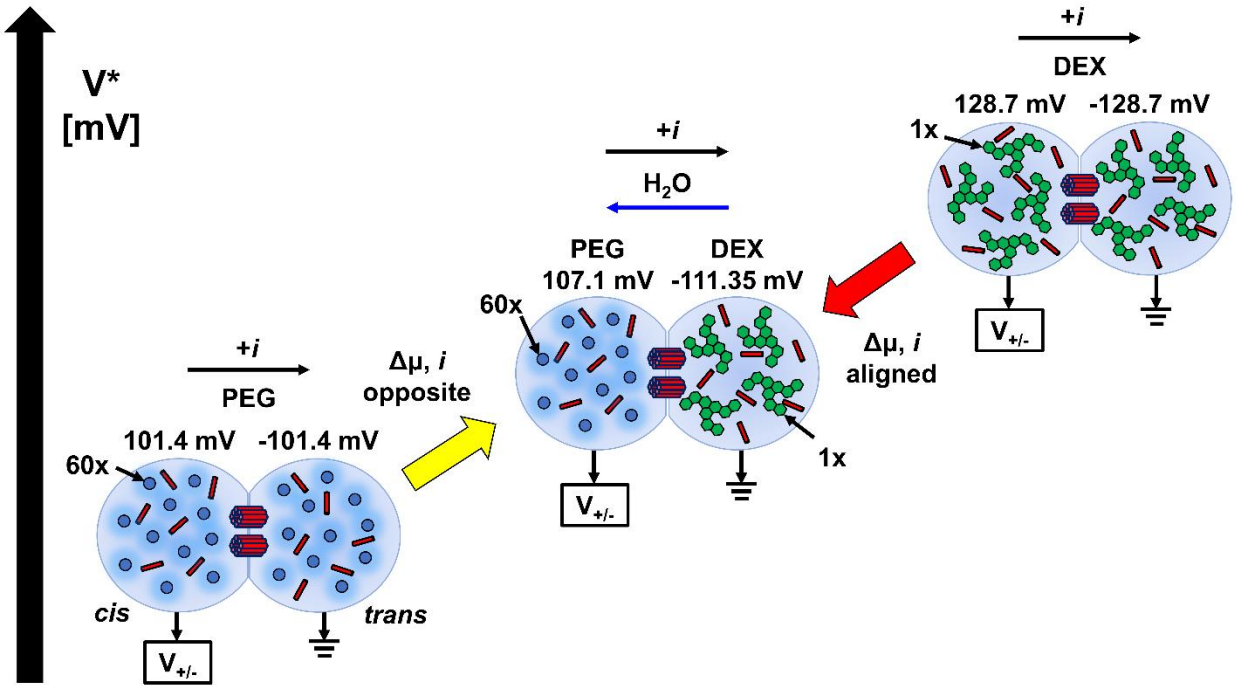


**Figure 2.4.** Voltage threshold comparisons for symmetric crowding versus asymmetric crowding conditions. For asymmetric crowding, osmotic pressure gradients existed due to differences in the excess water chemical potential between the two droplets, which created diffusional water currents, predicted in the preceding calculations, that either opposed the ionic currents through the pore (PEG8k−DEX500k) or were aligned with them (DEX500k−PEG8k). However, increased alm activity in PEG8k droplets due to colligative effects appeared to be the predominant factor in determining V* thresholds. The red and yellow arrows correspond to the voltage threshold changes in Figure 2.3. $\Delta\mu$ corresponds to the excess water chemical potential.

current, as was the case for DEX500k−PEG8k. These differences resulted in the diffusional transport of water molecules that modulated the voltage thresholds for alm pore conduction compared to the symmetric cases. However, the fact that the voltage threshold for the asymmetrically crowded DIBs was closer to the symmetric PEG8k−PEG8k DIB suggests colligative effects and/or changes to the water structuring near the headgroup region of the bilayer may have had a more prominent role in determining the V* shift. The enthalpic effects of PEG8k, consisting of water binding and changes to the structuring of water molecules in solution, can have an effect on the solubility of the solutes. While the second virial osmotic coefficient of PEG8k represents repulsive macromolecular interactions ($a_{22} > 0$), the increase in the second virial osmotic coefficient is related to the increased protein solubility in the solution (Wilson, W. W., and DeLucas, L. J., 2014). For example, PEG at a number of different molecular weights has been shown to order the solvent molecules in aqueous solutions above a threshold concentration, allowing hydrophobic amino acids such as tryptophan to become more soluble in solution and hydrophilic amino acids to become less soluble in solution (Boni, L. T., and Hui, S. W., 1987). While the solubility of alm peptide may increase in aqueous solutions containing PEG, the peptides are not present in the solution here as individual monomers but are sequestered onto 100 nm diameter liposome carriers that are driven to the DIB membrane by depletion forces. Each liposome carrier can deliver on average 26 alm monomers per fusion event at the DIB membrane.

### 2.5 Conclusion

The effect of macromolecular crowding on pore formation was investigated using the voltage-dependent, pore-forming peptide alamethicin by measuring shifts in the voltage thresholds for pore formation and conduction in the presence of crowding. A crowding fraction of 10 wt % shifts the voltage threshold to lower values for both DEX500k and PEG8k, indicating that crowding increases the propensity for pore formation, primarily through increases in local alm and electrolyte activities at the membrane. These results differ from the previous findings of Vodyanoy, Bezrukov, and Parsegian (Bezrukov, S. M., and Vodyanoy, I., 1993; Vodyanoy, I., Bezrukov, S. M., and Parsegian, V. A., 1993),

who reported decreases in alm conductance with crowding at both the ensemble and single-channel levels. These were due to increased osmotic stresses acting on polymer-inaccessible pores, which lowered conductance level populations and decreased the average channel conductance level lifetimes. The main difference with the results presented in this study is that, here, the crowder molecules were introduced in the aqueous phase of the droplets at the same time as the lipids and peptides, instead of first waiting for the pores to form in the membrane and to come to thermodynamic equilibrium or a steady-state. An important consequence of this difference is that our experiments monitored how macromolecular crowders affected pore formation itself by increasing the alm peptide activity in the solution and decreasing water activity.

Asymmetric crowding, consisting of PEG8k−DEX500k or DEX500k−PEG8k DIBs, had additional effects related to changes in the excess water chemical potential across the membrane and associated osmotic pressure gradients across the membrane. The consequences of this include the fact that an alm pore, inserted in the positive-voltage cis side of the membrane, would experience very different stresses on it if the trans droplet contained DEX500k instead of PEG8k. In addition to the possibility of diffusional water currents that could affect net measured ionic currents, colligative effects, and the unique water-binding and water-structuring properties of PEG8k, modulate the voltage thresholds for pore conduction.

At the single channel level, alm conductance, a reflection of the number of peptide monomers participating in oligomerization reactions to form the pore, is lowered when this osmotic stress is present across the membrane due to exclusion of polymers from the pore (Bezrukov, S. M., and Vodyanoy, I., 1993; Vodyanoy, I., Bezrukov, S. M., and Parsegian, V. A., 1993). This corroborates our hypothesis that the shifts in V* values to lower voltages with crowding are due to the increased binding of peptide monomers to the DIB membrane in the S-state and not to the oligomerization of I-state-inserted monomers in the membrane to form the pore.

The formation and stability of conductive pores in a biomimetic model membrane in the presence of macromolecular crowding will aid in understanding how the crowded and

confined in situ microenvironments found in cells and subcellular structures affect the membrane excitability. For example, neuronal excitability leading to both short-term and long-term memory consolidation involve covalent modifications and, for long-term mechanisms, gene expression of more membrane channels, receptors, and synaptic connections. This cargo resides at or is trafficked to the membrane while neuronal stimulation is ongoing. How is function maintained while the neuronal membrane is growing, maintained, or entirely new synaptic connecntions being formed? Future studies should examine the kinetics of pore formation in the presence of macromolecular crowding, temperature-dependent pore formation to dissect entropic and enthalpic contributions to changes in V* voltage thresholds, and the effect of macromolecular crowders on interfacial membrane dynamics, including alm pore-forming oligomerization dynamics. These studies can be used to optimize the functionality in soft material systems based on excitable membranes, including neuromorphic applications (Najem, J. S., Taylor, G. J., Weiss, R. J., Hasan, M. S., Rose, G., Schuman, C. D., ... and Sarles, S. A., 2018; Najem, J. S., Hasan, M. S., Williams, R. S., Weiss, R. J., Rose, G. S., Taylor, G. J., ... and Collier, C. P., 2019) by constitution in more realistic architectures that are closer to those found in biology.

# Appendix

## 2.6 Supporting Information

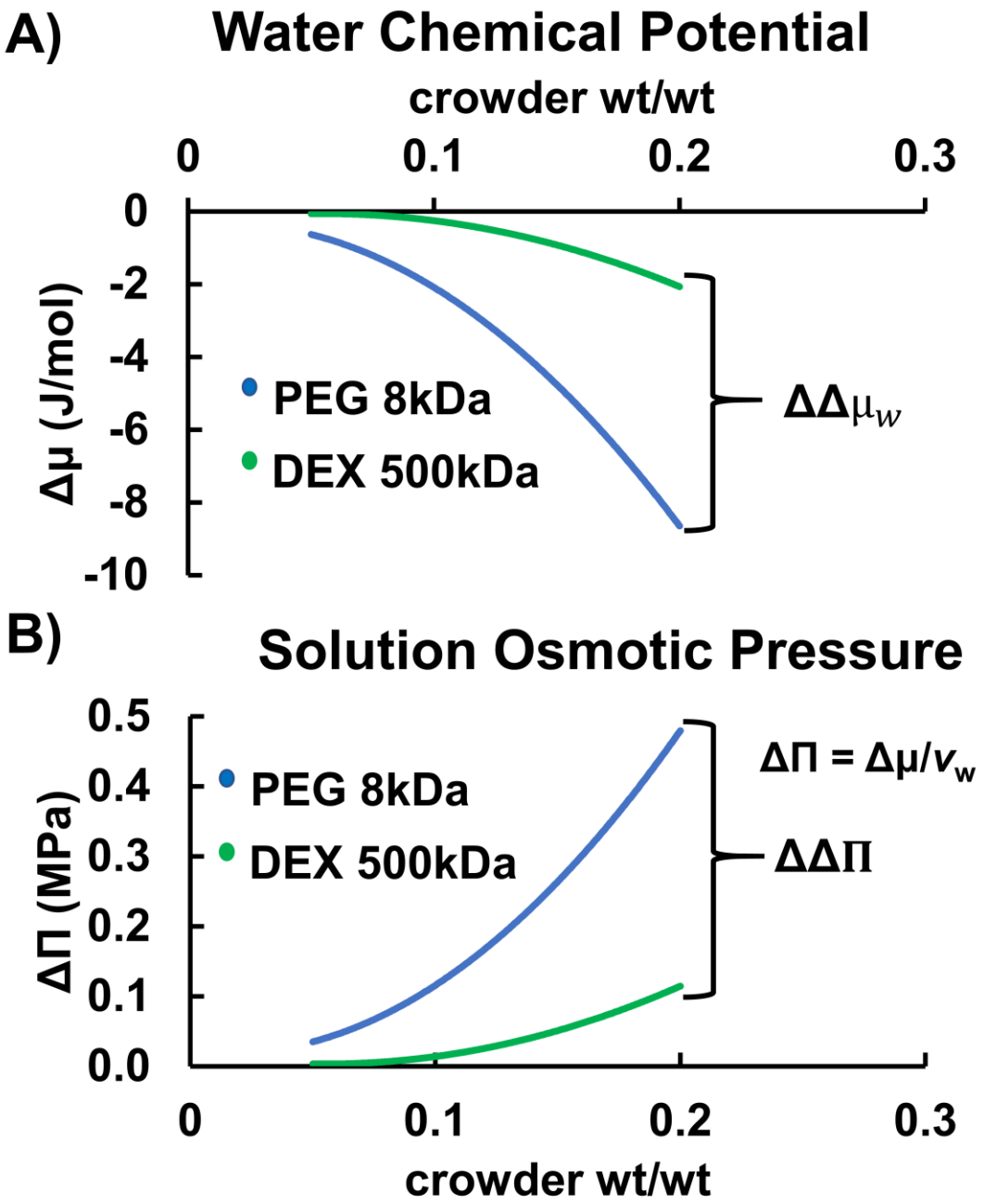


**Figure 2.5.** (A) Excess water chemical potentials as functions of crowder concentrations (wt/wt). (B) Corresponding osmotic pressures.

## Table 2.1: Table of Solution Osmotic Properties

| **PEG8k Solution Properties[a]** | | | | | |
|---|---|---|---|---|---|
| $a_{22}$ (kg/mol) | $6.82 * 10^2$ | - | - | - | - |
| $a_{33}$ (kg/mol) | $5.08 * 10^2$ | - | - | - | - |
| $a_{23}$ (kg/mol) | 5.88 | - | - | - | - |
| $V_w$ ($m^3$/mol) | $1.80 * 10^{-5}$ | - | - | - | - |
| $osmolal_{buffer}$ (mol/kg) | $1.15 * 10^{-1}$ | - | - | - | - |
| wt/wt (g/g) | 0 | 0.05 | 0.10 | 0.15 | 0.20 |
| $osmolal_{PEG}$ (mol/kg) | 0 | $5.82 * 10^{-3}$ | $1.23 * 10^{-2}$ | $1.95 * 10^{-2}$ | $2.77 * 10^{-2}$ |
| total osmolal (mol/kg) | $1.15 * 10^{-1}$ | $1.21 * 10^{-1}$ | $1.28 * 10^{-1}$ | $1.35 * 10^{-1}$ | $1.43 * 10^{-1}$ |
| $\Delta\mu_w$ (J/mol) | −5.16 | −6.11 | −8.38 | −12.41 | −18.86 |
| $\Pi$ (Pa) | $2.87 * 10^5$ | $3.40 * 10^5$ | $4.65 * 10^5$ | $6.90 * 10^5$ | $1.05 * 10^6$ |
| $\phi(m_i)$ | 1.00 | 1.13 | 1.47 (1.44) | 2.06 | 2.96 |
| **DEX500k Solution Properties[a]** | | | | | |
| $a_{22}$ (kg/mol) | $1.78 * 10^4$ | | | | |
| $a_{33}$ (kg/mol) | $5.08 * 10^2$ | | | | |
| $a_{23}$ (kg/mol) | $3.01 * 10^1$ | | | | |
| $V_w$ ($m^3$/mol) | $1.80 * 10^{-5}$ | | | | |
| $osmolal_{buffer}$ (mol/kg) | $1.15 * 10^{-1}$ | | | | |
| wt/wt (g/g) | 0 | 0.05 | 0.10 | 0.15 | 0.20 |
| $osmolal_{PEG}$ (mol/kg) | 0 | $3.15 * 10^{-4}$ | $6.65 * 10^{-4}$ | $1.06 * 10^{-3}$ | $1.50 * 10^{-3}$ |
| total osmolal (mol/kg) | $1.15 * 10^{-1}$ | $1.16 * 10^{-1}$ | $1.16 * 10^{-1}$ | $1.16 * 10^{-1}$ | $1.17 * 10^{-1}$ |
| $\Delta\mu_w$ (J/mol) | −5.16 | −5.26 | −5.47 | −5.82 | −6.35 |
| $\Pi$ (Pa) | $2.87 * 10^5$ | $2.92 * 10^5$ | $3.04 * 10^5$ | $3.23 * 10^5$ | $3.53 * 10^5$ |
| $\phi(m_i)$ | 1.00 | 1.02 | 1.06 (1.09) | 1.12 | 1.22 |

[a] $a_{22}$ is the self-interaction coefficient for crowder; $a_{33}$ is the self-interaction coefficient for the salt, NaCl; $a_{23}$ is the cross-interaction coefficient for salt and crowder; wt/wt is calculated from the ratio of masses of crowder to solution in grams (g); osmolal is the osmolality of crowder or buffer (NaCl, MOPS, DPhPC), as labeled; total osmolal is the solution osmolality; $\Delta\mu_w$ represents the excess chemical potential for the solvent, water; Π represents the solution osmotic pressure, related to water excess chemical potential b $\Pi = \Delta\mu_w/V_w$; $\phi$(mi) is the calculated solution osmotic coefficient, where mi is the total osmolality, and the parenthetical value is the experimentally measured solution osmotic coefficient.

**Table 2.2: Table of Voltage Thresholds for all Experimental Configurations**

| Scenario | $V^*$ [mV] | $\sigma$ [mV] |
|---|---|---|
| No Crowding | 138.7 | 2.87 |
| PEG/PEG | 101.4 | 1.55 |
| DEX/DEX | 128.7 | 1.20 |
| PEG/DEX[a] | 107.1/111.35 | 0.707/3.18 |

[a] Each droplet from an experimental orientation had a unique V* value from the presence of different crowder-containing solutions on each side of the membrane. PEG in PEG/DEX was averaged with PEG in DEX/PEG and the standard deviation, $\sigma$, was calculated the same way. Means from all other scenarios are calculated as described in the main text in the Methods and Materials section.

**Table 2.3: Table of Statistical Significance of Voltage Thresholds between Experimental Configurations**

| Group[a] | t-stat | DOF | Significance |
|---|---|---|---|
| No Crowding-PEG/PEG | 31.1339 | 16 | $p<0.05$ |
| No Crowding-DEX/DEX | 9.4724 | 16 | $p<0.05$ |
| No Crowding-DEX/PEG | 8.3380 | 14 | $p<0.05$ |
| No Crowding-PEG/DEX | 29.6679 | 14 | $p<0.05$ |
| PEG/DEX-DEX/PEG | 1.3038 | 2 | $p>0.05$ |
| DEX/DEX-DEX/PEG | 5.3278 | 4 | $p<0.05$ |
| PEG/PEG-PEG/DEX | 4.9976 | 4 | $p<0.05$ |
| DEX/DEX-PEG/PEG | 24.1221 | 6 | $p<0.05$ |

[a] Each statistical significance test is made between the conditions separated by the dash, -. A statistical difference is inferred for $p<0.05$ and no statistical significance is inferred for $p>0.05$.

# Chapter 3

# Heterosynaptic Plasticity in a DIB-Alamethicin memristor using pH-sensitive peptide ATRAM2

## 3.1 Abstract

Heterosynaptic plasticity drives efficient learning and maintains learned neural pathways behind behavior and memories using an effective “third neuron” to modulate a synapse between two neurons. Solid state systems have emulated heterosynaptic plasticity in function, however, emulation of structure is difficult in solid state systems, specifically in emulating lipid membranes for charge separation, protein channels for charge transport, and gene expression for synaptic changes related to memory consolidation. Here, we demonstrated heterosynaptic plasticity in a system mimicking the biomolecular structure of synapses in the brain. Specifically, we showed the synergistic effect of heterosynaptic and homosynaptic components in lowering the weight of the synaptic mimic. We used the droplet interface bilayer with voltage-sensitive alamethicin to elicit the homosynaptic response and pH-sensitive ATRAM2 peptide to elicit the heterosynaptic response. The implications of the results expand the versatility of soft matter neuromorphic computing hardware.

## 3.2 Introduction

The story revealing the molecular basis for information storage and processing in the brain is unraveling (Okuda, K., Højgaard, K., Privitera, L., Bayraktar, G., and Takeuchi, T., 2020). Inspired by the human brain’s ability to perform computationally demanding tasks, brain-inspired technology has advanced brain-science as well as showcased novel technologies that leverage computational sophistication, all while consuming less power. Scientists better understand the molecules at play in and orchestrating synaptic plasticity, the brain’s ability to learn and store memory via neuronal stimulation. Nevertheless, most brain-inspired technologies are fabricated with a solid-state platform (Strukov, D. B., Snider, G. S., Stewart, D. R., and Williams, R. S., 2008), exploiting mature nanofabrication methodology for creating devices exhibiting memristance, a property of systems that results in pinched hysteresis in response to any periodic voltage or current input signal (Chua, L., 2014). Others developed hybrid memristive devices using biomimetic materials layered with inorganic metals, resulting in the growth and rupture of filaments, including protein (Chen, Y. C., Yu, H. C., Huang, C. Y., Chung,

W. L., Wu, S. L., and Su, Y. K., 2015; Wang, H., Du, Y., Li, Y., Zhu, B., Leow, W. R., Li, Y., ... and Chen, X., 2015; Chang, Y. C., and Wang, Y. H., 2014; Wang, H., Meng, F., Cai, Y., Zheng, L., Li, Y., Liu, Y., ... and Chen, X., 2013; Meng, F., Jiang, L., Zheng, K., Goh, C. F., Lim, S., Hng, H. H., ... and Chen, X., 2011), nucleic acids (Lee, T., Yagati, A. K., Pi, F., Sharma, A., Choi, J. W., and Guo, P., 2015; Qin, S., Dong, R., Yan, X., and Du, Q., 2015), polysaccharide matrices (Kim, M. K., and Lee, J. S., 2018; Chiu, Y. C., Sun, H. S., Lee, W. Y., Halila, S., Borsali, R., and Chen, W. C., 2015), and others reviewed elsewhere (Sun, B., Zhou, G., Guo, T., Zhou, Y. N., and Wu, Y. A., 2020; Lv, Z., Zhou, Y., Han, S. T., and Roy, V. A. L., 2018). A final class of memristive systems uses biological architectures such as lipid bilayers and ion channels. This class of memristive systems, using the molecules and principles of synaptic plasticity, so far has demonstrated homosynaptic plasticity using lipid bilayers and the voltage sensitive ion channel alamethicin; voltage sensitivity is a signature of a “chemical synapse” (Najem, J. S., Taylor, G. J., Weiss, R. J., Hasan, M. S., Rose, G., Schuman, C. D., ... and Sarles, S. A., 2018). Alternatively, another study has described a different homosynaptically plastic system using lipid bilayers and the voltage insensitive ion channel, gramicidin. Gramicidin ion channels mimic proteinaceous gap junctions between neurons, components of “electrical synapses” (Koner, S., Najem, J. S., Hasan, M. S., and Sarles, S. A., 2019).

Here we describe a biological architecture responsible for another form of plasticity that enhanced information storage and processing in the brain called heterosynaptic plasticity. In heterosynaptic plasticity, no longer are we focused only on specific neurons firing together, and thus, wiring together (Lowel, S., and Singer, W., 1992). We are now concerned about a modulator neuron, termed an interneuron, that elicits synaptic growth via recruitment of additional cellular machinery to globally strengthen synapses involved in homosynaptic plasticity (Bailey, C. H., Giustetto, M., Huang, Y. Y., Hawkins, R. D., and Kandel, E. R., 2000; Okuda, K., Højgaard, K., Privitera, L., Bayraktar, G., and Takeuchi, T., 2020). Here, we aim to address how to demonstrate heterosynaptic plasticity using the bioarchitectural memristive system shown in Figure 3.1.

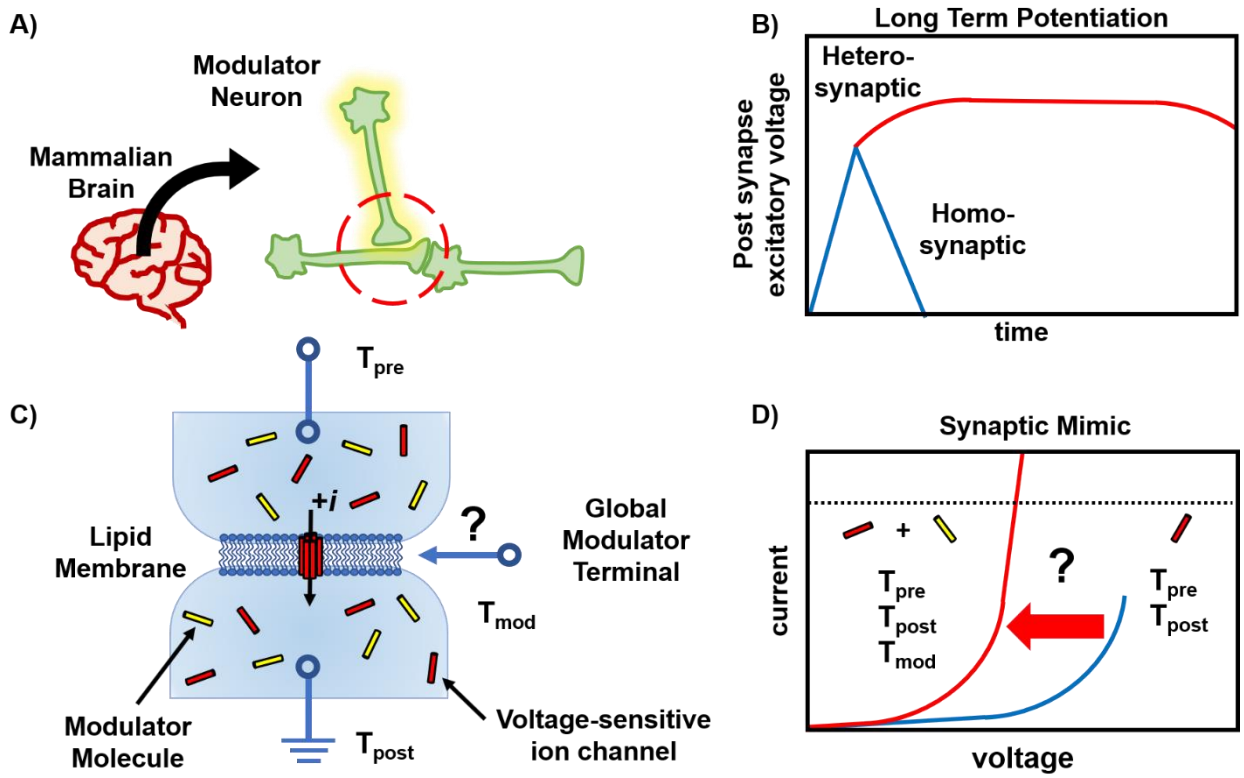


**Figure 3.1: Can heterosynaptic plasticity be modeled in a DIB memristor containing two membrane associated peptides?** A) Biological heterosynaptic plasticity is plasticity occurring through a modulator neuron, also called an "interneuron" that modulates the synapse involved in homosynaptic plasticity. B) Using the example of long-term potentiation (LTP), heterosynaptic plasticity allows the homosynaptic connection to achieve stable long-term changes resulting from gene expression and protein synthesis, while the homosynaptic connection alone would not have done so. Postsynapse excitatory voltage is the voltage required to cause an action potential in the postsynapse and is used to measure the effects of LTP. While electrical stimulation elicits a homosynaptic response (blue) a quick decline is followed relative to the heterosynaptic response (red) to neuromodulatory pulses. C) The droplet interface bilayer has successfully demonstrated homosynaptic plasticity via memristive dynamics, due to appropriate electrical stimulation of a lipid membrane housing a voltage-sensitive peptide (red). Now we have added a pH-sensitive peptide serving as a modulatory neuron (yellow). D) The voltammogram displays a shift in the I-V curve, revealing higher currents at equivalent voltages representative of modified synaptic weight in the biological synapse.

Memristive systems are believed to be the future of electronics and computation (Vera-Tasama, A., Gomez-Cano, M., and Marin-Hurtado, J. I., 2019, February). While solid state memristive systems have the industrial foundation to be incorporated into technology, memristive systems with bioarchitectures reveal how bio-computers can exist and connect brain-science to molecules via painting a simplified picture of synaptic function in the brain with simplified molecular components having identical function found in synapses. Memristive systems with bioarchitectures have demonstrated neuromorphic computing using fewer synapses to solve real-world problems (Hasan, M. S., Najem, J. S., Weiss, R., Schuman, C. D., Belianinov, A., Collier, C. P., ... and Rose, G. S., 2018, October). This was achieved using circuits of electronic neurons configured with the biomemristor architecture which functioned as a synapse to create a neuron-synapse capable of spike-rate-dependent plasticity (Weiss, R., Najem, J. S., Hasan, M. S., Schuman, C. D., Belianinov, A., Collier, C. P., ... and Rose, G. S., 2018, October). The system combines an artificial lipid membrane with voltage-controlled ion channels. Droplets containing aqueous solutions of lipid, peptide ion channel, and salts create the synthetic membrane. When the droplets are immersed in oil, lipid monolayers spontaneously assemble, forming a coating around the droplets. After lipid monolayers assemble, contacting the droplets creates the synthetic bilayer at their interface termed a droplet interface bilayer (DIB) (Bayley, H., Cronin, B., Heron, A., Holden, M. A., Hwang, W. L., Syeda, R., ... and Wallace, M., 2008).

Biological neurons harness incredibly complex cell membranes doped with many membrane protein species cooperating to fulfill the requirements of cognition in the brain. Bioarchitectural memristive systems composed of more than one membrane species have not yet been considered. However, studies incorporating additional membrane species in combination with alamethicin have revealed potential pathways to achieving heterosynaptic plasticity in a bioarchitectural system using multiple membrane species. Specifically, additional polycationic membrane protein species, including protamine, polylysine, and spermine, exhibit delayed rectification, negative differential resistance, and bistable membrane potentials capable of producing rhythmic action potentials when combined with alamethicin (Mueller, P., and Rudin, D. O., 1968). Ion selectivity leads to another form of oscillations using the combination of alamethicin and

nonactin, the former an ion channel, allowing the passage of ions through an opening in the membrane, and the latter an ion carrier, allowing the passage of ions through complex formation between the carrier and the ion followed by diffusion across the membrane (Boheim, G., and Hall, J. E., 1975). The molecular mechanism for the strongly nonlinear dynamical behavior likely involves a change in the membrane potential due to membrane binding from basic proteins like protamine, which are rich in charged arginine, and from charge imbalances created from ion selectivity, respectively. The difference arises from non-transporting, charged molecules docked on the membrane and charged ions selectively transporting across the membrane to create a charge gradient.

Recently, pH-responsive peptides have been synthesized modeling the C-helix of the membrane protein bacteriorhodopsin responsible for generating proton gradients across membranes (Hunt, J. F., Rath, P., Rothschild, K. J., and Engelman, D. M., 1997; Reshetnyak, Y. K., Andreev, O. A., Lehnert, U., and Engelman, D. M., 2006; Nguyen, V. P., Alves, D. S., Scott, H. L., Davis, F. L., and Barrera, F. N., 2015). Specifically, the acidity-triggered rational membrane peptide, or ATRAM peptide, was designed to enhance the targeting of tumor cell microenvironments, which are more acidic than healthy tissue. It was shown that four negatively charged glutamate residues could function as biochemical pH-sensors and lead to peptide conformational changes at or below pH 6.5 in POPC vesicles *in vitro*, and in the presence of tumor microenvironments *in vivo*. ATRAM's remaining residues were designed to enable aqueous solubility while remaining unstructured in solution, membrane binding in an unstructured conformation while above the pH-insertion threshold, and alpha-helical structure upon decreasing the pH below the pH-insertion threshold. Liposome binding assays revealed ATRAM oligomerizes to a dimer or trimer (Nguyen, V. P., Alves, D. S., Scott, H. L., Davis, F. L., and Barrera, F. N., 2015). ATRAM2 is a variant of ATRAM with an additional glutamate residue replacing the leucine residue at the nineteenth position, developed to enhance pH-sensing.

Here, we present ATRAM2 as a mimic of a modulator interneuron in brain heterosynaptic plasticity. Using the currently well-defined DIB memristor, we incorporate

a pH-sensitive, secondary membrane species, ATRAM2, and use pH as an environmental control variable capable of eliciting heterosynaptic plasticity. Alamethicin hysteresis and shifts in insertional voltage thresholds, ΔV*, due to inclusion of ATRAM2 reveal modulations to the memristive system using changes in pH. The distribution of alamethicin V* values, particularly V* values for membrane dissolution at low pH, reveal increased alamethicin pore lifetime. These findings increase the level of complexity in the synaptic mimic while enhancing the applicability of biomemristor architecture.

## 3.3 Methods

### *3.3.1 Materials*

Sodium chloride (NaCl), 3-(*N*-morpholino)propanesulfonic acid (MOPS) buffer, sodium hydroxide, agarose powder (p/n A9539), and ethanol were obtained from Sigma-Aldrich. Alamethicin peptides (p/n/A-1286) were purchased from A.G. Scientific. ATRAM2 peptide was synthesized by FMOC chemistry and are >95% pure, assessed by HPLC and MALDI-MS (Nguyen, V. P., Alves, D. S., Scott, H. L., Davis, F. L., and Barrera, F. N., 2015; Nguyen, V. P., Palanikumar, L., Kennel, S. J., Alves, D. S., Ye, Y., Wall, J. S., ... and Barrera, F. N., 2019; Nguyen, V. P., Dixson, A. C., and Barrera, F. N., 2019). Alamethicin was dissolved in ethanol to a concentration of 5 mg/mL to create a stock solution used for further sample preparation, and the stock solution was stored at −20 °C when not in use. ATRAM2 was dissolved in 10mM sodium phosphate, pH8 buffer at a concentration of 167.9 mg/mL (50μM) and stored at -20 °C. Peptide amino acid sequences can be found in Table 3.1. Liposome solutions were prepared by dissolving 1,2-diphytanoyl-*sn*-glycero-3-phosphocholine (DPhPC) lipids (Avanti, Alabaster, AL) at 2.5 mg/mL in buffer (unless otherwise stated, 10 mM MOPS, 420.0 mM NaCl, NaOH to achieve pH 7.45 or pH 5.00) and extruding the resulting multilamellar vesicles 21 times through a miniextruder (Avanti) containing a track-etched 100 nm polycarbonate membrane creating large unilamellar vesicles (LUVs).

**Table 3.1: Peptides with sequences, molecular weight, and charge at pH5.00 and pH7.45.**

| Peptide | Sequence | MW, Da | pH7.45 charge | pH5.00 charge |
|---|---|---|---|---|
| Alamethicin | Ac-Aib-Pro-Aib-Ala-Aib-Ala-Gln-Aib-Val-Aib-<br>Gly-Leu-Aib-Pro-Val-Aib-Aib-Glu-Gln-Pheol | 1964.4 | -1 | 0 |
| ATRAM2 | Gly-Leu-Ala-Gly-Leu-Ala-Gly-Leu-Leu-Gly-Leu-<br>Glu-Gly-Leu-Leu-Gly-Lue-Pro-Glu-Gly-Leu-Leu-<br>Glu-Leu-Trp-Leu-Gly-Leu-Glu-Leu-Glu-Gly-Asn | 3357.9 | -5 | 0 |

Aib is amino acid aminoisobutyric acid, a non-proteinogenic amino acid, expressed in fungal antibiotics.

### *3.3.2 Assembly*

Synaptic mimic assembly was based on the droplet interface bilayer (DIB) method, which has been used extensively in recent years to study the biophysics of bioarchitectural memristive systems (Najem et al., 2018; Najem et al. 2019) and membrane-bound ion channel in the presence of aqueous macromolecular crowding (McClintic et al. 2020). Concentrations for peptides were assigned using the molar ratio of available lipid to peptide and were $L/P_{alamethicin}$ = 1951 (2.0 μM) and $L/P_{ATRAM2}$ = 500 (8 μM). Peptides were suspended in aqueous buffer at 420.2mM NaCl and 4.0mM DPhPC (present as 100nm extruded vesicles) unless mentioned otherwise. Aqueous droplets of 400nL volume were manually pipetted to agarose coated silver/silver-chloride electrodes. Data was recorded using a patch clamp amplifier (Axopatch 200B, Molecular Devices, San Jose, CA). Capacitive current response to 10Hz, 10mV triangular voltage (Agilent) was used to monitor bilayer formation and thickness (Taylor, G. J., Venkatesan, G. A., Collier, C. P., and Sarles, S. A., 2015). Bright field images were acquired using the 4x objective of an inverted Nikon TE-300 optical microscope.

### *3.3.3 Recording and Analysis*

Alamethicin activity was assessed from macroscopic (multi-channel) insertion of the peptide in response to a cyclic triangular waveform, using bipolar cyclic voltammetry (CV) scans. Scan rates were held constant at 10 mV/s, however, during the pH 7.45 trials a Stanford Research Systems waveform generator was used that output an effective scan rate of 9.7-9.8 mV/s for and input of 10 mV/s. This difference is 2-3 % different from the 10 mV/s effective output from the Agilent waveform generator used in the pH 5.00 trials. Amplitudes were chosen to elicit current responses greater than 1nA. Additionally, 5 of 14 trials had DC bias voltages to help reduce asymmetry in the current response due to alamethicin cation selectivity and uncorrected electrode voltages. For pH 7.45 trials, this DC bias voltage had no affect on the voltage threshold magnitudes. However, voltage threshold magnitudes for pH 5.00 trials had higher variance, a characteristic seen only in the pH 5.00 trials. For this reason, we assume the DC offset had no affect on the voltage threshold magnitudes in the pH 5.00 trials, and changes in

magnitude were due to increased variance from pH. Quantitatively, macroscopic insertion was achieved once the membrane conductance in the presence of alamethicin increased beyond a conductance threshold of 8μS/cm$^2$ (Figure 3.2). The voltage at this conductance is called the voltage threshold, V*. Alamethicin and ATRAM2 were always added to both sides. Aqueous buffer and electrolyte were identically added to each side of the DIB.

### *3.3.4 Circular Dichroism*

Solutions of ATRAM2 peptide and DPhPC LUVs, extruded through 100 nm polycarbonate filters using an Avanti miniextruder, were prepared at an L/P of 150. Ellipticity was measured using Jasco J-815 spectropolarimeter at 25℃. A cuvette with 2mm pathlength was used. Solution buffers were prepared as described above.

## 3.4 Results and Discussion

### *3.4.1 Decreased Threshold Voltages for Alamethicin Conductance with ATRAM2*

Alamethicin responds to a characteristic voltage, called the voltage threshold, at which point the current response becomes nonlinear, a trademark of ion channel insertion (McClintic, W. T., Taylor, G. J., Simpson, M. L., and Collier, C. P., 2020; Taylor, G. J., and Sarles, S. A., 2015; Eisenberg, M., Hall, J. E., and Mead, C. A., 1973). Alamethicin forms channels following the barrel-stave model. The model involves a rotation and oligomerization among alamethicin monomers (Baumann, G., and Mueller, P., 1974). To interact and oligomerize with one another, alamethicin monomers need to first be bound and oriented at the membrane in a structurally specific manner. In the barrel-stave model, the alamethicin monomers first bind parallel to the membrane at the headgroup-acyl chain interface region, in what is known as the “S-state” (Huang, H. W., and Wu, Y., 1991). Upon application of a voltage threshold, V*, alamethicin monomers collectively rotate and insert into the membrane into the conducting “I-state”, aligning with the lipid tails in what can be characterized as a first-order phase transition (Huang, H. W., and Wu, Y., 1991). Only in the I-state can peptide monomers migrate in the

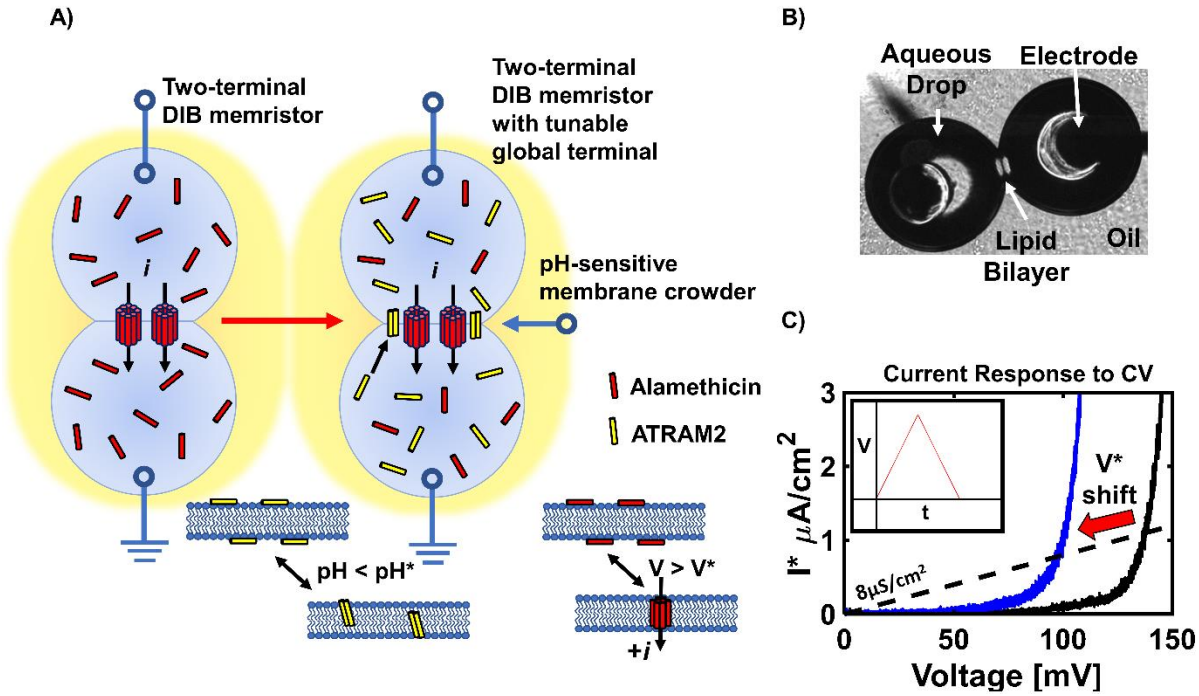


**Figure 3.2: Heterosynaptic plasticity emulation experimental setup and analysis.** A) The droplet interface bilayer has been well established as a two-terminal memristor. Here, we added a third terminal capable of reproducing heterosynaptic plasticity. This is achieved using pH-sensitive peptide ATRAM2 (yellow) in combination with voltage-sensitive peptide alamethicin (red). ATRAM2 has a conformational change from lying flat on the membrane when pH > pH* to inserting perpendicular to the membrane when pH < pH*. B) Representative bright-field image of the DIB captured on an inverted microscope. C) Representative I-V curve for alamethicin. Black and blue traces are independent trials. The red arrow indicates a shift in the trace due to the presence of a heterosynaptic molecular-based modulator. The dotted line is the conductance threshold signifying the macroscopic alamethicin insertion. V* is the voltage threshold, signifying the voltage at which the conductance threshold is surpassed. Alamethicin has a conformational change from lying parallel to the membrane when V < V* to inserting perpendicular to the membrane when V > V*. The inset represents the periodic voltage scans applied to the membrane during the CV sweeps. Scan rates were held constant at 10mV/s.

membrane and form oligomeric conductive pores, dependent on lipid composition, peptide concentration, and electric potential.

We found that adding a secondary peptide like ATRAM2, with a similar mechanism for binding to the membrane as alamethicin, resulted in a decrease in the voltage threshold V* for alamethicin pore conductance. Possible reasons for this decrease include enhanced membrane deformation due to ATRAM2 binding to the headgroup region, which would lower the threshold for peptide insertion, and increased total concentration of I-state peptide monomers in the membrane, which could affect the steady-state assembly and disassembly of monomers that reversibly form conductive pores as functions of voltage.

Figure 3.3A and B show histograms of V* threshold values for alamethicin pore conductance taken with alamethicin alone, and with ATRAM2, at two pH values, 7.45 and 5.00. They illustrate a shift in the voltage threshold for conductance for alamethicin, V* with the addition of ATRAM2, for the same L/P = 1951 when in the presence of ATRAM2. Values of mean V* values and changes in mean V* are presented in Table 3.2.

pH-low insertion peptide (pHLIP), a pH-sensitive peptide of which the ATRAM peptide family is a variant, was shown to enhance lipid flip-flop rates in its S-state and I-state in extruded 100nm diameter LUVs due to the creation of defects in the lipid headgroups (Nguyen, M. H., DiPasquale, M., Rickeard, B. W., Doktorova, M., Heberle, F. A., Scott, H. L., ... and Katsaras, J., 2019). In fact, alamethicin was shown to achieve the same enhanced lipid flip-flop rates in its S-state and suggested that when peptides with two-states, namely the S-state and I-state, are coincidentally present in the same membrane, as demonstrated here with alamethicin and ATRAM2, an enhanced effect occurred, resulting from both peptides generating defects in the lipid headgroup region synergistically. Interestingly, gramicidin, a membrane spanning peptide formed from a monomer of the inner and outer leaflets that coincided in space, had slower lipid flip-flop rates and further supported peptide monomers that span the membrane deform the

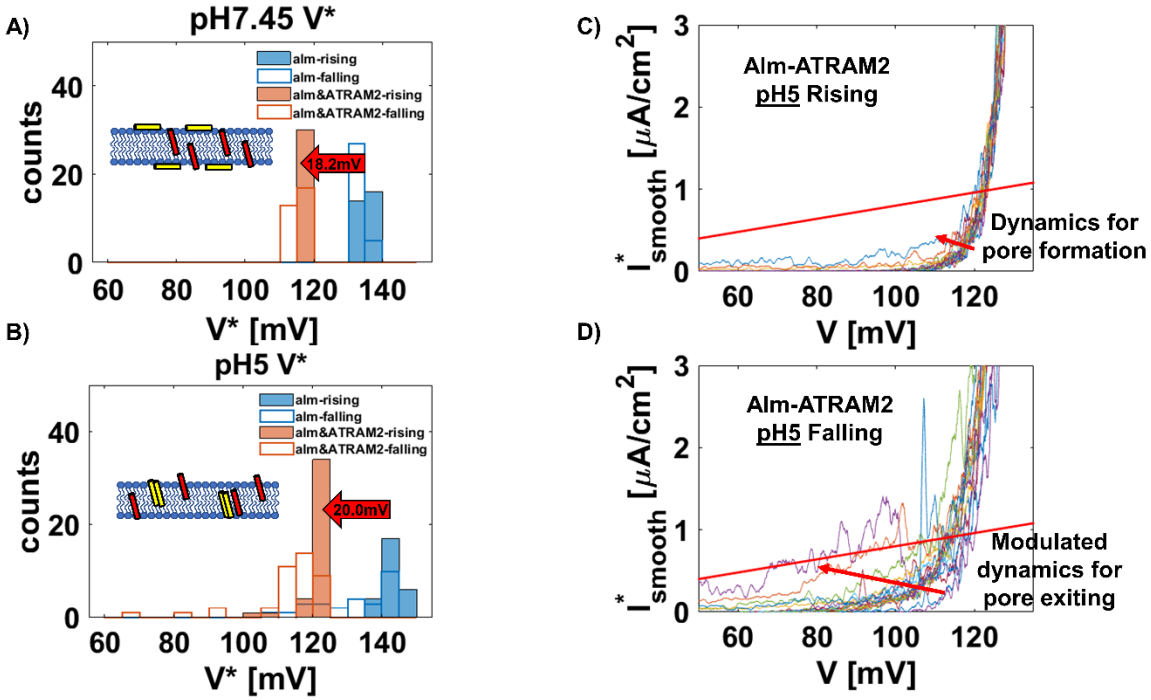


**Figure 3.3: Synaptic modulation from the heterosynaptic modulators ATRAM2 and pH.** The DIB-alamethicin system was tested under two pH conditions with and without ATRAM2. A) pH 7.45 shows a shift in the V* values in the presence of ATRAM2. B) pH 5.00 shows a shift in the V* values in the presence of ATRAM2, but also shows increased variability in the V* values independent of the presence of ATRAM2. The variability can occur for rising V* values during the increasing voltage scans but is found predominantly in the V* values during the decreasing voltage scans. C) and D) compare the pH 5.00 rising and falling V* values for identical CV sweeps. Enhanced variability and delayed pore dynamics for alamethicin leaving the membrane are shown in D) compared to more subtle variation in pore dynamics for peptide insertion in C) (see red arrows). The red line is the conductance threshold marking the voltage at which alamethicin pores insert macroscopically, defined as one order of magnitude higher than bare membrane conductance. The value of the conductance threshold is 8μS/cm$^2$.

**Table 3.2: Averages and Standard Deviations for all V* values with and without ATRAM2**

| | Alamethicin | | Alamethicin-ATRAM2 | | |
|---|---|---|---|---|---|
| **pH** | $V^*_{avg}$, mV | $V^*_{stdev}$, mV | $V^*_{avg}$, mV | $V^*_{stdev}$, mV | $\Delta V^*$, mV |
| **7.45** | 134.4 | 1.297 | 116.2 | 1.502 | -18.18 |
| **5** | 137.0 | 9.467 | 117.1 | 9.188 | -19.98 |

To understand the changes in V*, we need to revisit the molecular mechanism of pore formation for alamethicin. While alamethicin transitions from a bound to inserted state in response to voltage, alamethicin also transitions from a bound to inserted state in response to its own concentration (Huang, H. W., 2006). A critical component of the alamethicin transition from single-channel activity to ensemble-averaged channel activity in concentration-induced studies is the overlap of local defect areas in the membrane between neighboring monomeric peptides while in the surface-adsorbed state. Here, it appears ATRAM2 peptide monomers introduce additional local defects in the membrane that can overlap with monomer defects due to alamethicin. While this helps understand the impact of a secondary, two-state peptide on the average V*, a deeper look at the rising and falling V* of Figure 3.3C, D values reveal other changes related to variability and hysteresis in the voltage thresholds.

### *3.4.2 Alamethicin Voltage Threshold Variability and Hysteresis with Changes in pH*

Charge plays a major role in how biological membranes interact with molecular species. The choline lipid headgroups in phosphatidylcholine (PC) lipids are zwitterionic, consisting of a positively charged quaternary amine near a negatively charged phosphate group. These charges dictate the surface potential of the membrane from the lipid leaflet interface to the headgroups. The ATRAM2 peptide also has charged regions. At neutral pH, ATRAM2 is negative in charge in its deprotonated state (pH 7.45), due to its 5 glutamate residues. Under more acidic conditions (pH 5.00) these residues become protonated, which neutralizes the charge. It is this property that is responsible for its pH-sensing ability (Nguyen, V. P., Palanikumar, L., Kennel, S. J., Alves, D. S., Ye, Y., Wall, J. S., ... and Barrera, F. N., 2019). The alamethicin peptide also has negatively charged glutamate residues at neutral pH, which are thought to help anchor the molecule to the inserting side of the membrane, allowing the positively charged C-terminus to traverse the membrane during insertion. These charges can interact with the membrane and with each other, according to ionic strength, peptide concentration, and pH. Excess negative charge from the addition of ATRAM2 at neutral pH may lead one to expect electrostatic repulsion between the negatively charged

glutamate anchors of alamethicin and ATRAM2's five negatively charged glutamate residues. But this would be true only if ATRAM2 monomers could be positioned closer to alamethicin monomers in the membrane than the Debye screening length, which was 0.4 nm at the ionic strength of the aqueous solution used in the droplets, 500 mM (Huang, H. W., 2006). The only way this could occur would be if charged residues of ATRAM2 were at or very close to the pore entrance, which seems unlikely.

Tables 3.2-3.4 help isolate the effects of adding ATRAM2 to alamethicin from changes in pH. One can see from the tables that the addition ATRAM2 shifted the average V* values lower for both pH values, while lowering the pH resulted in slight increases in both the variance and the mean of voltage distributions in Table 3.2, with and without ATRAM2. This was likely related to the modest cation selectivity reported for alamethicin (Hall, J. E., Vodyanoy, I., Balasubramanian, T. M., and Marshall, G. R., 1984), in this case due to the neutralization of the negatively charged glutamate residues at the entrance to the alamethicin pore lumen under acidic conditions, which decreased the attractive electrostatic interactions with $Na^+$ ions, raising V* values for applied voltages having positive polarity (Boheim, G., W. Hanke, and G. Jung 1983). On closer inspection, the rising and falling current-voltage plots in Figure 3.3 C and D, and presented in Tables 3.3 and 3.4 that make up the averaged values in Table 3.2, show statistically significant increases in the mean threshold values at lower pH, but only for the rising leg, not the falling leg, due to long tails in their distribution trending to smaller V* values. The cause(s) of these long tails are not known definitively yet, but they are probably related at least in part to the introduction of a time lag between changes in the membrane area due to electrowetting of the membrane at the oil-aqueous interface, which changed the number of conductive pores in the membrane due to changes in membrane area, and the decay time of alamethicin conductive states

**Table 3.3: Averages and Standard Deviations for Rising and Falling Alamethicin V* Values and their Hysteresis**

| Alamethicin | | | | | |
|---|---|---|---|---|---|
| **pH** | $V^*_{avg,\ r}$, mV | $V^*_{stdev,\ r}$, mV | $V^*_{avg,\ f}$, mV | $V^*_{stdev,\ f}$, mV | $\Delta V^*_{hys}$, mV |
| **7.45** | 135.0* | 1.106 | 133.9* | 1.184 | 1.100 |
| **5** | 142.3 | 2.435 | 131.7 | 10.86 | 10.64 |

*Conducted at 500 mM NaCl.

**Table 3.4: Averages and Standard Deviations for Rising and Falling Alamethicin-ATRAM2 V* Values and their Hysteresis**

| Alamethicin-ATRAM2 | | | | | |
|---|---|---|---|---|---|
| **pH** | $V^*_{avg,\ r}$, mV | $V^*_{stdev,\ r}$, mV | $V^*_{avg,\ f}$, mV | $V^*_{stdev,\ f}$, mV | $\Delta V^*_{hys}$, mV |
| **7.45** | 117.5 | 0.4316 | 115.0 | 1.079 | 2.542 |
| **5** | 120.9 | 4.107 | 113.2 | 11.120 | 7.710 |

as a function of decreasing voltage, which resulted in pinched hysteresis in current-voltage plots that were qualitatively like the memristive behavior reported for DIBs containing alamethicin and DPhPC at neutral pH (Najem, J. S., Taylor, G. J., Weiss, R. J., Hasan, M. S., Rose, G., Schuman, C. D., ... & Sarles, S. A., 2018). The modification of the charge on the pore at low pH observed here likely modified this behavior, which may offer opportunities for tuning short-term synaptic plasticity simply by changing pH.

### *3.4.3 No Apparent ATRAM2 Insertion in DPhPC Membranes at Acidic pH*

However, an order of magnitude change in the $V^*_{stdev,r}$ was observed in the presence of ATRAM2 upon dropping the pH from 7.45 to 5 (Table 3.4). It appears insertion mechanisms become more consistent in the presence of ATRAM2 at neutral pH (7.45) but become more inconsistent at lower pH (5.00). Adjusting the pH below that reported for transitioning ATRAM2 from surface-bound random coil to a membrane-inserted alpha-helix had little effect on the alamethicin average V* values in this study (Figure 3.3 A and B and Table 3.2). However, here, DPhPC lipids were used, while 1-palmitoyl-2-oleoyl-glycero-3-phosphocholine (POPC) lipids had been used in the previous work (Nguyen, V. P., Alves, D. S., Scott, H. L., Davis, F. L., and Barrera, F. N., 2015). The structural differences between these two lipids are profound, and likely are the cause of the lack of ATRAM2 insertion under acidic conditions seen here. DPhPC lipids feature saturated and highly branched acyl chains, which result in lipid bilayers with exceptional stability, which makes them popular for forming model lipid bilayers, including DIBs. However, the tails are also sterically crowded, which likely results in an increased energy barrier for inserting ATRAM2 peptides. POPC lipids on the other hand contain unsaturated double bonds and are less sterically repulsive than DPhPC lipids (Huang, H. W., 2006). This is consistent with the fact that eleven alamethicin monomers are needed to form conductive pores in DPhPC membranes (He, K., Ludtke, S. J., Worcester, D. L., and Huang, H. W., 1996) while only five are needed in POPC lipids (Pan, J., Tristram-Nagle, S., and Nagle, J. F., 2009).

Circular dichroism routinely reveals shifts in molar ellipticity related to increases in alpha-helical content. pH-sensitive peptides show changes in molar ellipticity upon

adjusting the pH beyond the pH required for conformational changes in two-state, pH-sensitive peptides. To confirm anabsence in conformational change in ATRAM2 upon lowering the pH below pH6.5, the pH at which a conformational change occurs in ATRAM2 from surface bound to inserted, circular dichroism was performed on ATRAM2-decorated 100nm extruded DPhPC vesicles in buffer containing 500mM NaCl and 10mM MOPS (Figure 3.4). Indeed, circular dichroism revealed a negligible change in ATRAM2 conformation at pH5. Typical conformational changes adding alpha-helical content occur at wavelength 204nm and 222nm, which were negligible here. This was likely due to the steric nature of DPhPC lipids, as the acyl chains were decorated with bulky methyl groups making access to the hydrophobic region limited.

### 3.5 Conclusion

The homosynaptic plasticity model included a DIB with alamethicin and the framework of plasticity was described under memristive dynamics (Najem, J. S., Taylor, G. J., Weiss, R. J., Hasan, M. S., Rose, G., Schuman, C. D., ... and Sarles, S. A., 2018). Here, we evaluate the secondary, pH-sensitive peptide ATRAM2 on the voltage threshold of alamethicin and discuss the implications of our results for developing a heterosynaptic plasticity model in DIBs. The ability to assign an effective third terminal to emulate heterosynaptic plasticity represents an additional layer of complexity and nonlinear dynamical control needed for helping synthetic neuromorphic applications better emulate natural “brain-like” behaviors found in the biological central nervous system (CNS) and peripheral nervous systems (PNS). We have demonstrated the ability of a secondary adsorbate, in this case hydronium ions, to modify the synaptic weight of a synthetic synapse in a DIB memristive-system. We have also demonstrated enhanced current fluctuations under acidic conditions, indicative of increased sensitivity to stimuli.

Moving forward, future experiments should systematically look at the concentration dependence of the ATRAM2 induced voltage shift in alamethicin, at both pH conditions. ATRAM is known to have a concentration dependence on the rate constant for membrane insertion as well as binding to the membrane in POPC vesicles (Nguyen, V.

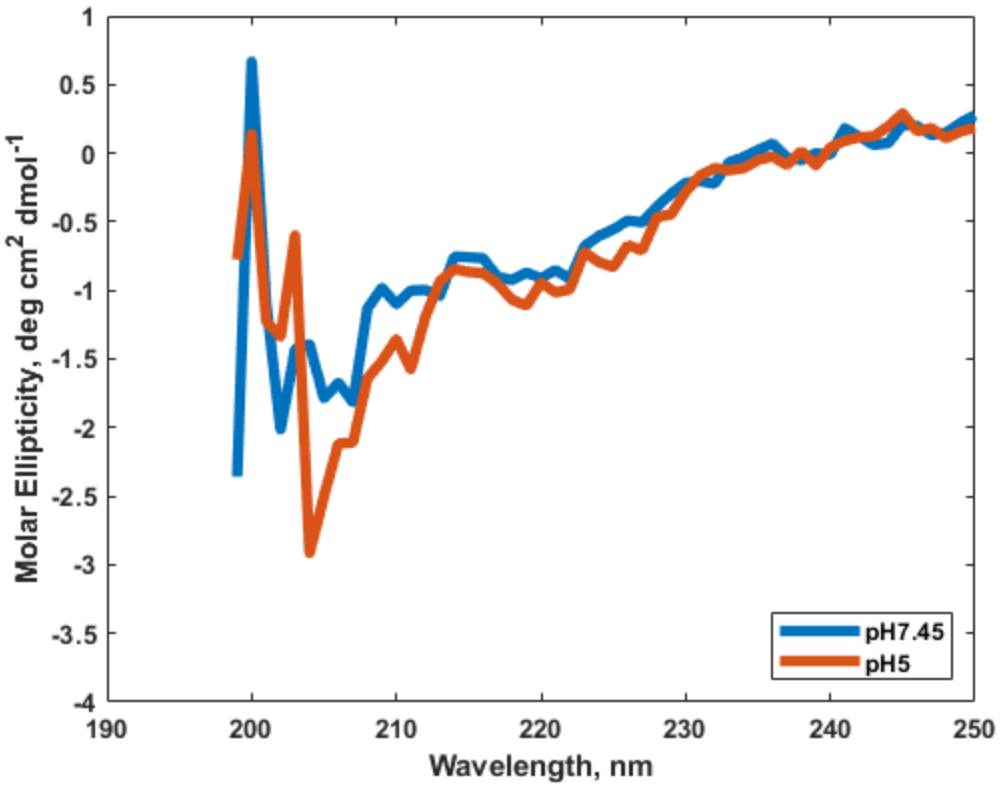


**Figure 3.4**: **CD data reveals reduced conformational change of ATRAM2 in upon dropping the pH.** ATRAM2 is designed to have a pH induced conformational change when the pH changes from 7.5 to below 6.5. This is seen by the shifts in the molar ellipticity at 204nm and 222nm. As seen in the CD spectrogram, the magnitude of the shifts corresponding to alpha helical content are negligible. ATRAM2, 10μM, was added to 100nm DPhPC extruded vesicles, 1.5mM, solution with NaCl, (420mM), for a ratio L/P of 150. Solutions are buffered with 10mM MOPS.

P., Palanikumar, L., Kennel, S. J., Alves, D. S., Ye, Y., Wall, J. S., ... and Barrera, F. N., 2019). Reportedly, lower ATRAM concentrations resulted in increased rate constant due to the peptide's oligomerization state while lower ATRAM concentration resulted in enhanced binding on the membrane due to repulsion effects at higher concentrations. Secondly, pH conditions should be considered as low as pH2 for the memristive device, as seen elsewhere (Gordon, L. G. M., and Haydon, D. A., 1975). The ionic strength and the interplay between positive hydronium ions and ions from NaCl have not been determined for the system presented here. However, NaCl at a concentration of 150mM does lower the insertion pH for ATRAM in POPC and POPC/POPS (9/1) lipid vesicles (Nguyen, V. P., Dixson, A. C., and Barrera, F. N., 2019). While pH2 may be unrealistic for cellular studies, the development of a biocomputer and other bio-based neuromorphic hardware can operate at such acidic pH. Finally, one-sided experiments more accurately represent the synapse model and should be pursued using any heterosynaptic plasticity modulator, here ATRAM2 and pH. Full investigations of the hysteresis through systematically varying CV scan rates, paired-pulse facilitation and paired-pulse depression should be conducted to explore the functionality of memristive systems emulating heterosynaptic plasticity.

# Chapter 4

# Lipid Oxidation as a Heterosynaptic Modulator

## 4.1 Abstract

Cell membrane permeabilization enables the transport of molecules into and out of lipid-encased compartments. Cell membrane permeability has been implicated in drug delivery, cell death, and osmotic balance. Recently, we demonstrated how reactive oxygen species (ROS) enhanced permeability of gene expression resources and led to enhanced gene expression across a population of giant unilamellar vesicles (GUVs) (Caveney, P. M., Dabbs, R. M., McClintic, W. T., Norred, S. E., Collier, C. P., and Simpson, M. L., 2019). We corroborated ROS as the source of the permeability by adding a known photosensitizer, methylene blue, along with sodium azide as a single oxygen quencher. So far, this dissertation has treated heterosynaptic plasticity occurring coincidentally with homosynaptic plasticity, without a direct causal connection. With this chapter, we investigate heterosynaptic plasticity acting without homosynaptic plasticity.

## 4.2 Introduction

Synthetic memristive systems emulate a variety of synaptic properties, including low power consumption, colocalization of memory and processing, and massively parallel information processing (Zhu, J., Zhang, T., Yang, Y., and Huang, R., 2020). Solid state memristive systems have shown drastically reduced power consumption and demonstrated methods of learning and computing mimicking synaptic plasticity (Strukov, D. B., Snider, G. S., Stewart, D. R., and Williams, R. S., 2008; Yang, Y., Chen, B., and Lu, W. D., 2015), the adaptability in structure and function due to the history of applied stimulus. Memristive systems have been built from equivalent classes of biomolecular species found in biological neurons and synapses and were shown to operate using nearly identical architectures found in chemical (Najem, J. S., Taylor, G. J., Weiss, R. J., Hasan, M. S., Rose, G., Schuman, C. D., ... and Sarles, S. A., 2018) and electrical synapses of the brain (Koner, S., Najem, J. S., Hasan, M. S., and Sarles, S. A., 2019). While solid state memristors comprised of metals, semiconductors, and insulators can simulate much of the functionality of biological synapses in the nervous system, memristors comprised of biological materials like proteins, peptides, and lipids

emulate their natural biological counterparts, even if they are not structurally and compositionally the same.

The voltage dependence of neurotransmission *in vivo* can be emulated *in vitro* with model biomembranes consisting of phospholipids and voltage-activated peptides that function as ion channels, like alamethicin (Taylor, G., Nguyen, M. A., Koner, S., Freeman, E., Collier, C. P., and Sarles, S. A., 2019; Taylor, G. J., and Sarles, S. A., 2015). Electrical stimulus applied in the form of pulses that leads to synaptic enhancement on the order of hundreds of milliseconds, and hence short-term plasticity, are referred to as paired-pulse facilitation (PPF). Pulses that lead to synaptic decline are called paired-pulse depression (PPD). PPF and PPD are two examples of short-term synaptic plasticity demonstrated in biomembranes consisting of lipid bilayers and alamethicin, that mimic synaptic connections between specific pre- and postsynaptic neurons. In biology, a common method for achieving longer-term synaptic plasticity is by using relevant molecular species capable of modulating the synthetic system via interaction with the membrane, with the crowded aqueous solution of the cytoplasm, or with ion channels such that the number of ion channels is modulated. Such routes of heterosynaptic plasticity are termed *molecular-based modulators*. They are commonly generated via genetic expression of effector proteins that act as universal neuromodulators of synaptic activity, such as dopamine and serotonin. A second path to achieve such plasticity is through fundamental environmental parameters, termed *global modulators*, including electric field, temperature, ionic strength, and environmental stresses, including osmotic, thermal, and oxidative stresses, just to name a few.

Of these, oxidative stress is an important example of a heterosynaptic modulator with versatile cell signaling potential. When controlled by the cell, oxidative stress provides healthy cell signaling compared to uncontrolled oxidative stress which leads to unhealthy cell signaling and loss of function (Pena-Bautista, C., Vento, M., Baquero, M., and Chafer-Pericas, C., 2019: Montine, T. J., Neely, M. D., Quinn, J. F., Beal, M. F., Markesbery, W. R., Roberts II, L. J., and Morrow, J. D., 2002). Oxidative stress occurs when a biological system becomes overexposed to ROS. ROS consists of molecular oxygen in its lowest electronic excited state (singlet oxygen), which is generated ground

state oxygen physically interacts with other molecules in excited electronic states, usually photosensitive molecules or redox-active molecules.

Phase-separated lipid mixtures have been modulated by *in-situ* generation of oxidized lipid species during fluorescent imaging. Once in an excited state, the oxygen remains excited for a given period during which it can diffuse an average of 100nm (Bacellar, I. O., Tsubone, T. M., Pavani, C., and Baptista, M. S., 2015) and interact with biomolecules. Lipid studies using unsaturated lipids take precautions to prevent lipid oxidation, which can confound interpretations of lipid membrane-based electrophysiology and fluorescent studies (Morales-Penningston, N. F., Wu, J., Farkas, E. R., Goh, S. L., Konyakhina, T. M., Zheng, J. Y., ... and Feigenson, G. W., 2010). Systematic titration of oxidized lipids disrupts membrane structure, revealing new self-organized structures leading to phase separation and permeability, including pore formation, demonstrated in optical experiments and electrophysiological experiments. Optical experiments used GUVs composed of the POPC-modified lipid ALDO-POPC, containing a truncated fatty-acyl chain capped with an aldehyde group at the ninth carbon of the unsaturated chain (Mertins, O., Bacellar, I. O., Thalmann, F., Marques, C. M., Baptista, M. S., and Itri, R., 2014). Electrophysiological experiments used black lipid membranes (BLMs) composed of the POPC-modified lipid POPC-OOH, containing a peroxide group at the ninth position of the unsaturated chain (Corvalán, N. A., Caviglia, A. F., Felsztyna, I., Itri, R., and Lascano, R., 2020). In both cases a threshold was reached which permeability became strongly nonlinear, suggesting self-organization.

Here, we investigated ROS as a heterosynaptic modulator by demonstrating how ROS enhanced membrane permeability to gene expression reagents, leading to enhanced gene expression across a population of vesicles (Figure 4.1). We identified ROS as the source of permeability by adding a known photosensitizer, methylene blue (MB), and sodium azide as a singlet oxygen quencher. Finally, an argument for pursuing electrophysiological studies using the droplet interface bilayer on lipid membranes composed of oxidized lipids will be presented. The findings presented here demonstrate the potential for heterosynaptic plasticity occurring in the absence of voltage-dependent alamethicin, in other words, in the absence of conventional homosynaptic plasticity.

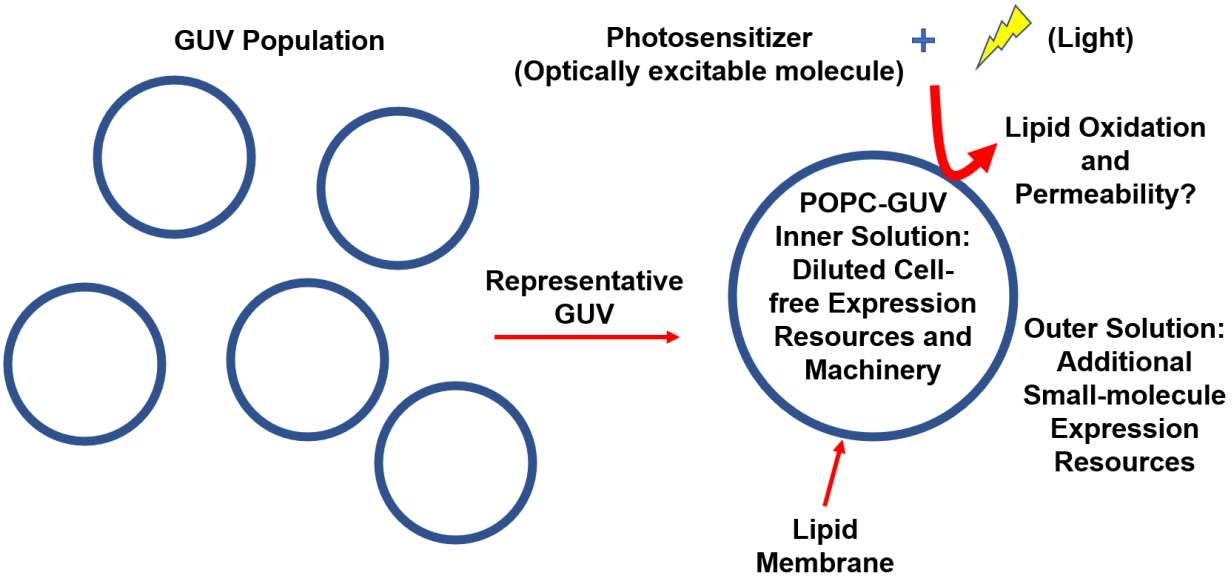


**Figure 4.1 Can GUV permeability to expression resources be enhanced using photosensitizers and lipid causing lipid oxidation?** GUVs encapsulated a diluted PURExpress In Vitro Protein Synthesis solution that resulted in diminished gene expression. This is the inner solution. The outer solution contains the small molecule expression resources, such as amino acids, salts, and energy molecules. Photosensitizers, photo-excitable molecules such as fluorophores and methylene blue, have the potential to interact with the GUV lipids, POPC, after becoming excited from light. POPC has an unsaturated bond that is reactive to excited state molecules including singlet oxygen and photosensitizers. Gene expression indicates enhanced permeability of the GUV membrane to gene expression resources in the outer solution.

Synthetic models such as this will provide the potential to reverse engineer the molecular-based operating principles of the brain, and systematically study the biophysics behind observed function.

## 4.3 Methods

### *4.3.1 Cell-free Gene Expression Preparation*

The PURExpress In Vitro Protein Synthesis Kit (New England Biolabs) was encapsulated in GUVs as demonstrated previously (Caveney, P. M., Dabbs, R. M., McClintic, W. T., Norred, S. E., Collier, C. P., and Simpson, M. L., 2019). GUVs are made using the oil-in-water emulsion transfer method. Aqueous inner (vesicle) solution is vortexed with paraffin oil combined with 30 mg of 1-palmitoyl-2-oleoyl-glycero-3-phosphocholine (POPC) lipid. The solution is transferred to another vial containing the outer (vesicle) solution and a thin layer of paraffin oil containing POPC lipid. With the inner solution emulsion on top of the thin layer of paraffin oil, the vial is centrifuged at 13,000 g for 20 minutes at room temperature. Inner solution contained 10 $\mu$L Solution A and 7.5 $\mu$L Solution B from PURExpress kit, 5 $\mu$L of sucrose solution (1 M), 0.25 $\mu$L Transferrin-AlexaFluor 647, 0.125 $\mu$L RNAsin (40 U/$\mu$L), 0.418 $\mu$L (1.67 nM) YFP encoding pEToppYB plasmid (200 ng, 478.2ng/$\mu$L stock), and nuclease-free water to bring the total inner solution volume to 30 $\mu$L. Outer solution contained 1.5 $\mu$L Amino acid solution, 11.3 $\mu$L ATP (100 mM), 0.75 $\mu$L CTP (500 mM), 0.75 $\mu$L UTP (500 mM), 1.8 $\mu$L Folinic Acid (0.5 M), 24 $\mu$L potassium glutamate (3.5 M), 11.3 $\mu$L magnesium acetate (0.5 M), 30 $\mu$L of HEPES (1 M), 60 $\mu$L glucose (1 M), and 141.8 $\mu$L autoclaved type 1 pure water for total outer solution volume of 300 $\mu$L. Solutions were diluted by 1/3 their standard concentrations by diluting Solution A and Solution B with nuclease-free water. Inner and outer vesicle solutions were osmotically balanced. MB trials contained MB at 10 μM. Sodium azide trials contained sodium azide at 20 mM.

### *4.3.2 GUV Imaging*

Vesicle imaging was performed on Zeiss LSM710 confocal scanning microscope with heating chamber to maintain 37°C. GUV solution was pipetted on a no. 1.5 glass-

bottom petri dish, covered with a lid, and mounted in the heating chamber. A 20x air objective was used to acquire images every 3 minutes in a z-stack; z-stacks contained 20 slices at 1 $\mu$m spacing, and the aperture for each slice was 1.00 Airy Units (open enough to allow ~1.5 $\mu$m depth of light). GUVs were imaged using three lasers: included as an investigational component of the protocol was 405 nm, 6.5 mW; YFP was excited with a 488 nm, 6.1 mW laser; and AF647 was excited with a 633 nm, 1.67 mW laser. YFP fluorescent emission was collected from 515 – 584 nm and AF647 fluorescent emission was collected from 638 – 756 nm. Less than 15 minutes elapsed from initial vesicle solution mounting and imaging.

### *4.3.3 Cell-free Expression Fluorescence Acquisition and Analysis*

Data was extracted from the acquired fluorescent images using the FIJI TrackMate (v3.8.0) plugin to select vesicles with a diameter of 10 $\mu$m using the Laplacian of Gaussian detector. The plugin extracted the average fluorescent intensity and diameter of selected vesicles. Vesicles were removed according to the following constraints: diameter <5 $\mu$m, diameter >19 $\mu$m, or contrast <0. The Linear Assignment Problem (LAP) tracker was used to link spots across z-stack slices in time to create steady-state expression fluorescence traces. Traces that had missing frames, traveled >5 $\mu$m between frames, or tracked for <45 of the 60 frames were removed from the data set.

## 4.4 Results and Discussion

Reactive oxygen species (ROS) are ubiquitous in biological systems. Constrained ROS leads to healthy cell signaling whereas unconstrained ROS leads to unhealthy cell signaling. This is because ROS interact with molecular constituents according to oxidation chemistry, leaving molecules profoundly modified after oxidation reactions occur. During cell free expression experiments, a method for normalizing the expression among a population of giant unilamellar vesicles (GUVs) was discovered (Caveney, P. M., Dabbs, R. M., McClintic, W. T., Norred, S. E., Collier, C. P., and Simpson, M. L., 2019). The method targets unsaturated bonds of POPC lipids via excited-state photosensitive fluorescent molecules present in the gene expression experiments. The

interaction between unsaturated acyl chains and excited-state fluorophores modified the lipid acyl, chains leading to enhanced transient pore formation, as shown in Figure 4.2.

### *4.4.1 Contact Dependent and Contact Independent Pathways for ROS Generation*

Enhanced lipid membrane permeability due to oxidative stress was shown to occur through two reaction pathways (Bacellar, I. O., Oliveira, M. C., Dantas, L. S., Costa, E. B., Junqueira, H. C., Martins, W. K., ... and Miotto, R., 2018). One pathway consisted of direct interaction between unsaturated acyl chains and photo-sensitive molecules that have entered an excited state via light absorption. Contact dependent oxidation reactions have been demonstrated between a photosensitizer in an excited state and unsaturated bonds of POPC acyl chains in liposomes (extruded through a 50 nm polycarbonate membrane; Bacellar, I. O., Oliveira, M. C., Dantas, L. S., Costa, E. B., Junqueira, H. C., Martins, W. K., ... and Miotto, R., 2018) and GUVs (Mertins, O., Bacellar, I. O., Thalmann, F., Marques, C. M., Baptista, M. S., and Itri, R., 2014). In liposomes, two photosensitizers were chosen: one was aqueous MB and the other was hydrophobic DO15, a dye that was confined to the acyl chain region of the lipid membrane. Contact dependent oxidative stress dominated in the hydrophobic photosensitizer trials due to sequestration to the hydrophobic region of the membrane, which encouraged contact between photosensitizer and unsaturated, carbon-carbon double bonds on the lipid.

A second pathway for oxidation reactions with the unsaturated bonds of the acyl chains also emerged, involving indirect interaction between unsaturated acyl chains and photo-sensitive molecules that have transferred their energy to diatomic oxygen in solution, shifting the energetic state from ground state triplet oxygen to singlet oxygen, the lowest excited state of molecular oxygen. This form of oxygen has an excited state lifetime correlated with a characteristic diffusion distance (~0.3$\mu$m) (Baier, J., Maier, M., Engl, R., Landthaler, M., and Bäumler, W., 2005). Within this diffusion distance singlet oxygen can react with suitable substrates. Substrates in the membrane include unsaturated acyl chains which lead to autocatalytic lipid peroxidation cycles.

### *4.4.2 Transient Pore Formation*

Transient pore formation occurred only in the presence of truncated aldehyde, modified POPC lipids. This was demonstrated with two experiments: a carboxyfluorescein (CF) autofluorescence assay of liposome-entrapped CF and testing light exposed liposome samples with mass spectrometry (MS) as a function of irradiation time. Leakage of liposome entrapped CF revealed liposome permeability as evidenced by the increase in CF fluorescence inside the liposome. MS assays for oxidized lipids at defined time intervals during irradiation allowed tracking of the oxidation progression in time. Analyzing the MS assay for lipid oxidation products against the time course of CF fluorescence suggested that only when lipid aldehydes were generated was there enhanced liposome permeability.

### *4.4.3 Prevent ROS-lipid Oxidation*

Interestingly, two scenarios inhibit lipid oxidation in the presence of excited state photosensitizer: model membranes composed of lipids with fully saturated acyl chains, and the presence of molecular species capable of quenching the excited state molecules. The same study discussed previously demonstrated the lack of oxidation in DPPC liposomes after DPPC liposomes were irradiated in the presence of the hydrophobic photosensitizer DO15 (Bacellar, I. O., Oliveira, M. C., Dantas, L. S., Costa, E. B., Junqueira, H. C., Martins, W. K., ... and Miotto, R., 2018). Separate studies demonstrated the utility of singlet oxygen quencher, sodium azide, to reduce lipid oxidation (Sankhagowit, S., Wu, S. H., Biswas, R., Riche, C. T., Povinelli, M. L., and Malmstadt, N., 2014; Maisch, T., Baier, J., Franz, B., Maier, M., Landthaler, M., Szeimies, R. M., and Bäumler, W., 2007).

### *4.4.4 Extending Gene Expression with Molecular Transport Through Oxidized Lipid Pores*

Here, under the “normal expression” conditions, the light protocol excites a fluorescent species in solution leading to some combination of contact dependent and contact independent oxidation reactions at the membrane (Figure 4.2). First consider that MB is

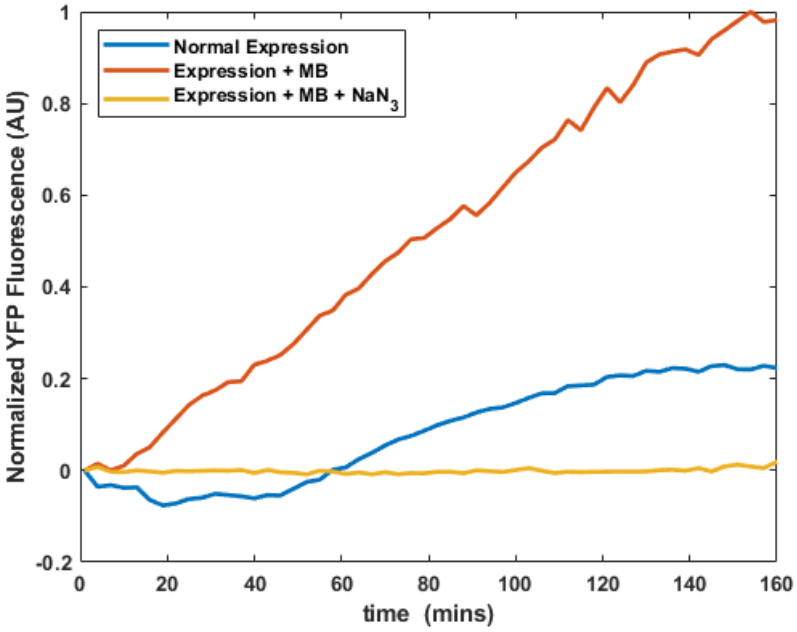


**Figure 4.1 Gene expression under ROS generating conditions and in the presence of ROS quencher.** Gene expression is tracked measuring the fluorescence of fluorescent reporter protein, YFP, in time. Experiments were setup so that gene expression did not occur unless the lipid membranes became permeable to gene expression reagents. The blue trace is considered "normal" gene expression under the light treatment protocol and contained the minimum molecular components needed for gene expression to occur. The red trace contained a known photosensitizer methylene blue (10 $\mu M$). Adding methylene blue enhanced gene expression. The yellow trace contained methylene blue and sodium azide (20 mM), a known singlet oxygen quencher. Incorporating sodium azide decreased gene expression.

excited under the 633nm laser illumination and this explains the drastic increase in expression fluorescence in the MB trace. This is consistent with the physical properties of the molecule coinciding with the experimental design as well as consistent with previous literature already discussed. Second, MB was added at 10 μM, compared to the fluorophore concentration two-orders of magnitude lower. In the absence of known photosensitizer MB, “normal expression” occurs as a decline in fluorescence followed by an increase and saturation. The dip could be related to the time delay between capturing the first image and the onset of gene expression. Notice the nearly sixty-minute delay. During this time, as images are being capturing, photobleaching is occurring. Once the inflection point is crossed fluorescence is produced at a faster rate than photobleaching, due to the light triggered membrane permeability and the associated delay in gene expression reagents needed for gene expression. The most interesting results occurred in the case with sodium azide (20 mM) present in solution. Sodium azide is a known reactive oxygen species scavenger, particularly singlet oxygen (Harbour, J. R., and Issler, S. L., 1982). Performing as a singlet oxygen quencher suggests that the lack in fluorescence occurred due to the lack of ROS triggered lipid membrane permeability to gene expression products needed for the reaction to gene expression to proceed. The results indicate contact independent oxidation reactions via singlet oxygen interaction with the unsaturated acyl chains of the lipid membrane.

### 4.5 Conclusion

It is still unclear which molecular species is generating ROS in the normal expression conditions. Intuition reasons a fluorophore present in the solution is responsible for ROS. Two fluorophores are excited in the vicinity of MB, namely AlexaFluora633 and Transferrin647. Designing experiments with a single fluorophore present allows for a systematic investigation into which fluorophore is responsible for generating ROS. Fluorophore concentrations can be increased to the level of MB (10 μM) to compare the rate of gene expression fluorescence of the fluorophore with the rate in the presence of MB. A control experiment for the gene expression machinery and reagents generating the ROS can be designed such that the vesicles are made without gene expression system and replaced with sucrose. With sucrose in the inner vesicle solution, glucose

can be incorporated in the outer solution, creating a contrast mismatch between the inner vesicle solution and the outer solution, enabling transport due to photooxidation of the lipid membrane to be observed (Mertins, O., Bacellar, I. O., Thalmann, F., Marques, C. M., Baptista, M. S., and Itri, R., 2014). While the evidence presented suggests singlet oxygen is present and interacts with the membrane leading to permeability, a final piece of evidence would be to conduct the same experiments presented here with lipids composed of fully saturated acyl chains. Typically, 1,2-dipalmitoyl-sn-glycero-3-phosphocholine (DPPC) is chosen as the saturated lipid in photodynamic studies (Bacellar, I. O., Oliveira, M. C., Dantas, L. S., Costa, E. B., Junqueira, H. C., Martins, W. K., ... and Miotto, R., 2018), however, 1,2-diphytanoyl-sn-glycero-3-phosphocholine (DPhPC) is a suitable choice for a saturated lipid in photodynamic studies, due to similar fluidity as unsaturated lipids but lack of unsaturated bonds in the acyl chain (Sankhagowit, S., Wu, S. H., Biswas, R., Riche, C. T., Povinelli, M. L., and Malmstadt, N., 2014).

One very exciting component of the work displayed here is the potential to combine cell-free gene expression with synthetic plasticity systems. Heterosynaptic plasticity *in vivo* has been demonstrated in vertebrates and invertebrates to require gene transcription and protein synthesis to store stable long-term memories. Here, we report oxidative stress related permeability via gene expression reporter protein fluorescence. Even so, these basic steps triggered the idea to incorporate gene expression in synthetic synaptic plasticity systems to emulate the real process of synaptic plasticity *in vivo*. The basic fruition of this idea is to use gene-expression “modulatory” chemicals to promote or inhibit gene expression of a key component of the synthetic synaptic plasticity system, for example a molecule that alters the number of ion channels in the membrane. Cell-free expression reagents can be incorporated on either side of the membrane, each side representing presynaptic and postsynaptic neurons, and gene promotors can flow from one side of the membrane to the other during short-term plasticity events such as paired-pulse facilitation.

Another very exciting impact of this work is the potential to use ROS to alter membrane permeability and, specifically, conductance, in combination with or without alamethicin,

a voltage-dependent ion channel. ROS induced changes in membrane permeability have the potential to be permanent, producing a purely heterosynaptic synthetic model. As the synthetic homosynaptic plasticity model with alamethicin revealed short-term plasticity dynamics (Najem, J. S., Taylor, G. J., Weiss, R. J., Hasan, M. S., Rose, G., Schuman, C. D., ... and Sarles, S. A., 2018), ROS triggered heterosynaptic plasticity can model long-term plasticity dynamics. Long-term plasticity *in vivo* implies more stable neuronal changes often lasting more than twenty-four hours. In synthetic systems, long-term changes would extend the PPF from the homosynaptic biomemristor during learning. In fact, a recent study showed POPC hydroperoxide (POPC-OOH) forms black lipid membranes (BLMs) and provided basic electrical characterization in I-V dynamics (Corvalán, N. A., Caviglia, A. F., Felsztyna, I., Itri, R., and Lascano, R., 2020). Including POPC-OOH provides two operating regimes: a linear regime and a nonlinear regime. The nonlinear current response to voltage occurs at a voltage threshold, very similar to alamethicin. The novelty of POPC-OOH as a memristive system is using a purely lipid system that still has the potential to be modified via photooxidation in the presence of a photo-excitable molecule. Experiments designed to emulate long-term plasticity need to demonstrate that POPC-OOH can perform PPF and PPD. Following, PPF can be used to achieve some learning state, given by the change in current or voltage response. Once the learning state is achieved, the light exposure protocol can lock-in the learning state by modifying the POPC-OOH lipids to become, in part, 1-palmitoyl-2-(9'-oxo-nonanoyl)-sn-glycero-3-phosphocholine (ALDOPC), a modified POPC lipid with an aldehyde cap on the acyl chain that had the unsaturated bond. ALDOPC is responsible for non-electric field dependent pore formation leaving the conductance state constant, as well as the learning state. Additionally, the same system is composed of lipids only potentially expressing memcapacitive dynamics below the voltage threshold.

Experiments investigating these ideas can be conducted in the droplet interface bilayer (DIB) composed of lipids with the potential to undergo oxidative modifications or oxidized lipids. Such experiments should investigate the memristive behavior of lipid membranes under systematic variation of oxidized lipid type and corresponding concentration in the DIB. While POPC-OOH has been thoroughly investigated using voltage scans, it serves as the lipid candidate of choice to study the neuromorphic

properties of lipid-only membranes. However, ALDOPC should also be investigated using electrophysiology in synthetic synaptic plasticity. Alternatively, as presented in this chapter, *in situ* generation of ROS, via irradiation of photo-sensitive molecules, and subsequent lipid membrane oxidation represents the more biologically natural scenario and the more complex scenario. Here, a sea of oxidized and non-oxidized lipids will be produced in the membrane and interesting phase behavior (Tsubone, T. M., Junqueira, H. C., Baptista, M. S., and Itri, R., 2019), along with non-electric field generated (Mertins, O., Bacellar, I. O., Thalmann, F., Marques, C. M., Baptista, M. S., and Itri, R., 2014) and electric field generated pore formation (Corvalán, N. A., Caviglia, A. F., Felsztyna, I., Itri, R., and Lascano, R., 2020) are likely to occur coincidentally. The latter experimental design can serve as a proof-of-concept light-triggered membrane conductance, and memristive dynamics, modulator.

Each choice of lipid membrane composition and route of membrane permeability should be thoroughly investigated for memristive dynamics, starting with the study of pinched hysteresis, PPF and PPD. Pinched hysteresis refers to the shape of the current-voltage (I-V) curve. In a memristive system in response to voltage (current), the forward current (voltage) path will differ from the reverse current (voltage) path. PPF and PPD make use of voltage (current) pulses, first individually to characterize rates of current (voltage) increase and decrease in response to a given pulse duration and amplitude, and secondly in a train pattern, or one after another, varying pulse width and spacing between pulses. These steps lead into more realistic synthetic systems, gradually increasing complexity, and create the library for neuronal circuit elements in next generation electronics that rely on heterosynaptic modulation.

# Chapter 5
# Conclusions

## 5.1 Research Summary

Heterosynaptic plasticity modulates homosynaptic plasticity by generating neuromodulators such as dopamine and serotonin, among other neuromodulatory chemicals, *in vivo*. While heterosynaptic plasticity *in vivo* involves an effective third neuron, termed an interneuron, that modulates the homosynaptic connections in its vicinity, synthetic heterosynaptic plasticity emulates natural heterosynaptic plasticity via generating global effects, some of which were discussed here, including aqueous-based macromolecular crowding, secondary peptide crowding on the membrane, and oxidative stress.

The overarching thesis of this dissertation was to learn how heterosynaptic processes for learning and memory can be emulated using synthetic systems. Specifically, the work presented here expands the potential to build new technology that can reach new levels of performance in power consumption, computational power, and adaptability, not yet seen. The natural prerequisite for achieving synaptic emulation included using similar biomolecules and molecular architecture found in brain synapses, termed bioarchitectures. A second prerequisite for achieving synaptic emulation was to increase the complexity of state-of-the-art synthetic systems. This dissertation incorporated molecular-based and global variables to modulate plasticity of the system. The following sections present the conclusions from the dissertation and future work.

### *5.1.1 Macromolecular Crowding as a Synthetic Heterosynaptic Modulator*

Chapter 2 demonstrated how macromolecular crowding is a potent synthetic heterosynaptic modulator. Crowding with nonelectrolyte, macromolecular crowders mimicking cytosolic macromolecules enhanced binding of membrane species which modulated the power requirements for ion channel formation. Specifically, the presence of crowder molecules introduced effective depletion forces between alamethicin decorated vesicles and the macroscopic membrane of the DIB, pushing the alamethicin decorated vesicles towards the membrane. The effect was to locally increase the concentration of alamethicin and lowered the voltage threshold for pore formation. Secondly, our system revealed that a crowding driven solvent gradient modulated the

power requirements for voltage driven ion channel formation. For solvent gradients aligned with the voltage-generated ionic gradients, required power was less. For solvent gradients against the voltage-generated ionic gradients, more power was required. These results demonstrate how colligative properties of the aqueous environment act as a global scale, heterosynaptic modulator.

### *5.1.2 Secondary Peptide Crowding and pH as a Synthetic Heterosynaptic Modulator*

Chapter 3 demonstrated how including a secondary membrane species to alamethicin in the membrane, namely, a pH responsive peptide termed “ATRAM2”, generated potent heterosynaptic modulation in synthetic systems by decreasing the voltage threshold required to form conducting pores in the membrane. While pH-dependent structural transitions in ATRAM2 were not directly detected from electrophysiological measurements carried out on alamethicin housed in DPhPC lipid membranes, it was clear that adsorption of secondary membrane bound species such as ATRAM2 enhanced alamethicin ion currents, primarily by blocking the rate of pore dissolution due to exiting reactions of peptide monomers from the pore, modulated by pH. Also, pH-induced increases in helical content in ATRAM2-DPhPC LUVs was measured using circular dichroism. Interestingly, the change in lipid from POPC to DPhPC resulted in less overall helical content. This likely results from the increased steric nature of DPhPC due to the additional eight methyl groups on each acyl chain compared to POPC, which offers less volume for ATRAM2 insertion and steric hindrance towards acyl chain separation by the ATRAM2 peptide. These results add to the understanding of how to use the environment to elicit modulation of synaptic plasticity of alamethicin ion channels on a global scale.

### *5.1.3 Lipid Oxidation Leads as Heterosynaptic Plasticity*

Chapter 4 demonstrated how oxidative stress can be a potent synthetic heterosynaptic modulator. This chapter presented light-triggered permeability in GUVs which led to enhanced gene expression. A light irradiation protocol was used to normalize gene expression across a population of GUVs containing the minimal concentrations of gene

expression machinery, requiring GUV permeability and transport of gene expression products to reach measurable fluorescence from the fluorescent reporter protein. Methylene blue was added to test similarity between the oxidative stress generation in the normal gene expression conditions under the light irradiation protocol and the trials with methylene blue added. Cases with methylene blue added saw enhanced rate of gene expression fluorescence. To test contact dependent or contact independent oxidative stress, sodium azide, a known singlet oxygen quencher, was added. The trials with sodium azide added produced no fluorescence from gene expression, indicating the method of oxidation stress was contact independent, singlet oxygen generation GUV permeability. It is still which fluorescent agent is responsible for the oxidative stress triggered membrane permeability in normal expression. While the chapter reported gene expression as the measure of synaptic plasticity, this chapter leads to ideas of combining gene expression with synthetic models of synaptic plasticity with bioarchitectures.

### 5.2 Practical Recommendations

Immediate, practical implications of the research presented in this dissertation affect two areas: neuromorphic, memristive computing and new bioarchitecture hardware based on lipid oxidation. First, evolutionary optimization for neuromorphic systems (EONS) are genetic algorithms that train neural networks within the characteristics and constraints of the hardware composing the network (Schuman, C. D., Plank, J. S., Disney, A., and Reynolds, J., 2016, July). EONS has been used for the training of neural networks composed of DIB memristors as synapses communicating with solid-state equivalent neurons (Hasan, M. S., Schuman, C. D., Najem, J. S., Weiss, R., Skuda, N. D., Belianinov, A., ... and Rose, G. S., 2018, November). Such a system of neurons wired to include heterosynaptic plasticity would enable modulation from a single synaptic terminal, to modulating subsections of the network, to modulating the entire network for practical long-term learning and memory consolidation. Also, heterosynaptic modulation can tune the plasticity of a single synaptic terminal to subsections and the entire network, such that plasticity thresholds are reduced. Effectively this enhances the networks ability for learning and memory consolidation.

The second immediate practical implication is memristive dynamics of lipid membranes composed of oxidized lipids. The feasibility of forming synthetic membranes using oxidized lipids and the potential to form pores via incorporation of oxidized lipids has been demonstrated in black lipid membranes Corvalán, N. A., Caviglia, A. F., Felsztyna, I., Itri, R., and Lascano, R., 2020). Pore formation in POPC/POPC-OOH membranes showed two regimes of pore formation dependent on voltage and oxidized lipid concentration: ohmic (linear) and nonlinear. Structural changes in the membrane are elicited from the generation of hydrophilic groups introduced upon oxidation, including hydroperoxides, aldehydes, carboxylic acids, alcohols, and ketones. The mechanism for pore formation in membranes containing oxidized lipids relies on structural changes to the membrane, such as decreased membrane thickness and increased area per lipid, parameters that can modulate not only the memristive but also the memcapacitive properties of the membrane and potentially move the current bioarchitecture away from oil. While the oil helps modulate the number of alamethicin ion channels via changes in membrane area due to electrostriction, *in situ* lipid oxidation has been demonstrated in GUV preparations without residual oil to increase lipid membrane area due to the addition of a polar oxygen moiety to the acyl chain of lipids with unsaturated bonds (Mertins, O., Bacellar, I. O., Thalmann, F., Marques, C. M., Baptista, M. S., and Itri, R., 2014). However, *in situ* lipid oxidation would result in a permanent change due to covalent modifications of the acyl chains of the membrane, potentially moving the synaptic model from short-term plasticity to long-term plasticity. However, while POPC GUVs in the presence of methylene blue were irradiated at the absorbance wavelength of methylene blue showed changes in area under electric potential, it is not clear whether DIB model membranes composed of oxidized lipids, such as POPC hydroperoxide (POPC-OOH), have reversible changes in membrane area under applied electric potential.

### 5.3 Future Work

Future work includes building on proof-of-concept and initial investigations to explore how computational and neuronal circuit elements can be built around the synthetic heterosynaptic platform, implementation of network heterosynaptic modulation and how

to mitigate against potential breakdowns of the computing elements. While the wet chemical components are performing the memristive feature, solid state components communicate with the system (Weiss, R., Najem, J. S., Hasan, M. S., Schuman, C. D., Belianinov, A., Collier, C. P., ... & Rose, G. S., 2018, October), thus the wet bioarchitecture, inherently prone to evaporation (Boreyko, J. B., Mruetusatorn, P., Sarles, S. A., Retterer, S. T., and Collier, C. P., 2013), will need a solution for preventing evaporation, perhaps using ionic liquids or completely closed systems. Others have demonstrated portability (Kawano, R., Tsuji, Y., Kamiya, K., Kodama, T., Osaki, T., Miki, N., & Takeuchi, S., 2014; Venkatesan, G. A., & Sarles, S. A., 2016) and durability (Challita, E. J., Najem, J. S., Monroe, R., Leo, D. J., & Freeman, E. C., 2018); Sarles, S. A., & Leo, D. J., 2010) of synthetic membrane systems, however, future work establishing portability and durability equivalent to the level of the solid-state counterpart is critical for offering a viable computing product. Running multiple droplet bilayers simultaneously has been showcased using microfluidics (Taylor, G., Nguyen, M. A., Koner, S., Freeman, E., Collier, C. P., & Sarles, S. A., 2019; Nguyen, M. A., Srijanto, B., Collier, C. P., Retterer, S. T., & Sarles, S. A., 2016), critical for scaling the number of droplet bilayer synapses needed for a processing or memory chip. Systems built from biomolecules have the potential to suffer from ambient environmental effects, such as ROS generation from ambient light exposure, microbial infection, or ambient temperature, reminding system designers to actively consider quality control in this novel computing hardware, such as closed systems to ambient conditions. Combining each of these ideas advances the technology from the basic science stage to the commercialization stage.

Another fruitful area of investigation is experimenting with droplets containing unique chemical composition. The models of synthetic heterosynaptic plasticity described in this thesis are limited to experiments conducted with identical conditions in both aqueous droplets apart from Chapter 2 which investigated the effect of non-identical crowder type in each droplet and led to interesting results due to gradients in the number of crowders in each droplet. Therefore, studying systems with unique chemistry in each droplet allows for more complexity and more customized mimics of specific biological structures, for example heterosynaptic modulators can be added to a single

droplet representing the presynaptic or postsynaptic terminal, identical to plasticity studies performed on neuron cultures (Martin, K. C., Casadio, A., Zhu, H., Yaping, E., Rose, J. C., Chen, M., ... and Kandel, E. R., 1997; Bailey, C. H., Giustetto, M., Zhu, H., Chen, M., and Kandel, E. R., 2000). This arena represents the foundation of biophysical experiments exploring synthetic membranes using electrophysiology and the BLM platform (Mueller, P., Rudin, D. O., Tien, H. T., & Wescott, W. C., 1962), including peptide transport across lipid membranes (Boheim, G., Hanke, W., & Jung, G., 1983), lipid flip-flop (Hall, J. E., 1981), insertion mechanisms of peptides (Hall, J. E., Vodyanoy, I. G. O. R., Balasubramanian, T. M., & Marshall, G. R., 1984), lipid membrane oscillator (Mueller, P., & Rudin, D. O., 1968), negative differential resistance, and action potentials (Mueller, P., & Rudin, D. O., 1968). Including unique chemical composition in DIB droplets increases the versatility of functions obtained and systems mimicked using a synthetic membrane platform.

The end goal is to reproduce brain synapses from the bottom-up. Such a goal entails step-like gains in complexity. Demonstrated in this dissertation were many steps using the environment as a heterosynaptic modulator. Increasing complexity using cell free gene expression will increase functionality, enhance adaptability, and introduce the potential of self-repair. A key feature governing synaptic strength or weight *in vivo* is gene expression and protein synthesis. This enables the synaptic terminals to grow and elicit stronger responses to stimulation. Post-translational modifications and synaptic vesicle exocytosis also influence synaptic plasticity, through delayed onset of long-term plasticity and transmission of key neurochemicals involved in synaptic plasticity, respectively. The steps to making more realistic models of neural synapses using synthetic systems have been laid out in this dissertation, now is the time to build the synthetic brain with brain-like architecture and function.

# Bibliography

Bacellar, I. O., Oliveira, M. C., Dantas, L. S., Costa, E. B., Junqueira, H. C., Martins, W. K., ... & Miotto, R. (2018). Photosensitized membrane permeabilization requires contact-dependent reactions between photosensitizer and lipids. Journal of the American Chemical Society, 140(30), 9606-9615.

Bacellar, I. O., Tsubone, T. M., Pavani, C., & Baptista, M. S. (2015). Photodynamic efficiency: from molecular photochemistry to cell death. International journal of molecular sciences, 16(9), 20523-20559.

Baier, J., Maier, M., Engl, R., Landthaler, M., & Bäumler, W. (2005). Time-resolved investigations of singlet oxygen luminescence in water, in phosphatidylcholine, and in aqueous suspensions of phosphatidylcholine or HT29 cells. The Journal of Physical Chemistry B, 109(7), 3041-3046.

Bailey, C. H., Giustetto, M., Huang, Y. Y., Hawkins, R. D., & Kandel, E. R. (2000). Is heterosynaptic modulation essential for stabilizing hebbian plasiticity and memory. Nature Reviews Neuroscience, 1(1), 11-20.

Bashford, C. L., Alder, G. M., Fulford, L. G., Korchev, Y. E., Kovacs, E., MacKinnon, A., ... &

Pasternak, C. A. (1996). Pore formation by S. aureus α-toxin in liposomes and planar lipid bilayers: effects of nonelectrolytes. The Journal of membrane biology, 150(1), 37-45.

Baumann, G., & Mueller, P. (1974). A molecular model of membrane excitability. Journal of supramolecular structure, 2(5-6), 538-557.

Bayley, H., Cronin, B., Heron, A., Holden, M. A., Hwang, W. L., Syeda, R., ... & Wallace, M. (2008). Droplet interface bilayers. Molecular BioSystems, 4(12), 1191-1208

Bezrukov, S. M., & Vodyanoy, I. (1993). Probing alamethicin channels with water-soluble polymers. Effect on conductance of channel states. Biophysical journal, 64(1), 16-25.

Bezrukov, S. M., Vodyanoy, I., & Parsegian, V. A. (1994). Counting polymers moving through a single ion channel. Nature, 370(6487), 279-281.

Bezrukov, S. M., Vodyanoy, I., Brutyan, R. A., & Kasianowicz, J. J. (1996). Dynamics and free energy of polymers partitioning into a nanoscale pore. Macromolecules, 29(26), 8517-8522.

Blinks, L. R. (1936). The effects of current flow on bioelectric porential: I. Valonia. The Journal of general physiology, 19(4), 633-672.

Boheim, G., & Hall, J. E. (1975). Oscillation phenomena in black lipid membranes induced by a single alamethicin pore. Biochimica et Biophysica Acta (BBA)-Biomembranes, 389(3), 436-443.

Boheim, G., Hanke, W., & Jung, G. (1983). Alamethicin pore formation: voltage-dependent flip-flop of α-helix dipoles. *Biophysics of structure and mechanism*, *9*(3), 181-191.

Boni, L. T., & Hui, S. W. (1987). The mechanism of polyethylene glycol-induced fusion in model membranes. In Cell fusion (pp. 301-330). Springer, Boston, MA.

Boreyko, J. B., Polizos, G., Datskos, P. G., Sarles, S. A., & Collier, C. P. (2014). Air-stable droplet interface bilayers on oil-infused surfaces. Proceedings of the National Academy of Sciences, 111(21), 7588-7593.

Bradley-Whitman, M. A., & Lovell, M. A. (2015). Biomarkers of lipid peroxidation in Alzheimer disease (AD): an update. Archives of toxicology, 89(7), 1035-1044.

Caveney, P. M., Dabbs, R. M., McClintic, W. T., Norred, S. E., Collier, C. P., & Simpson, M. L. (2019). Controlling Cell-Free Gene Expression Behavior by Tuning Membrane Transport Properties. bioRxiv, 604454.

Challita, E. J., Najem, J. S., Monroe, R., Leo, D. J., & Freeman, E. C. (2018). Encapsulating networks of droplet interface bilayers in a thermoreversible organogel. *Scientific reports*, *8*(1), 1-11.

Chang, Y. C., & Wang, Y. H. (2014). Resistive switching behavior in gelatin thin films for nonvolatile memory application. *ACS applied materials & interfaces*, *6*(8), 5413-5421.

Chen, F. Y., Lee, M. T., & Huang, H. W. (2002). Sigmoidal concentration dependence of antimicrobial peptide activities: a case study on alamethicin. Biophysical journal, 82(2), 908-914.

Chen, Y. C., Yu, H. C., Huang, C. Y., Chung, W. L., Wu, S. L., & Su, Y. K. (2015). Nonvolatile bio-memristor fabricated with egg albumen film. *Scientific reports*, *5*, 10022.

Cherry, R. J., Chapman, D., & Graham, D. E. (1972). Studies of the conductance changes induced in bimolecular lipid membranes by alamethicin. The Journal of Membrane Biology, 7(1), 325-344.

Chew, H., Solomon, V. A., & Fonteh, A. N. (2020). Involvement of Lipids in Alzheimer's Disease Pathology and Potential Therapies. Frontiers in Physiology, 11, 598.

Chiu, Y. C., Sun, H. S., Lee, W. Y., Halila, S., Borsali, R., & Chen, W. C. (2015). Oligosaccharide Carbohydrate Dielectrics toward High-Performance Non-volatile Transistor Memory Devices. *Advanced Materials*, *27*(40), 6257-6264.

Chua, L. (2014). If it's pinched it'sa memristor. Semiconductor Science and Technology, 29(10), 104001.

Corvalán, N. A., Caviglia, A. F., Felsztyna, I., Itri, R., & Lascano, R. (2020). Lipid Hydroperoxidation Effect on the Dynamical Evolution of the Conductance Process in Bilayer Lipid Membranes: A Condition Toward Criticality. Langmuir, 36(30), 8883-8893.

De Rosa, R., Spinozzi, F., & Itri, R. (2018). Hydroperoxide and carboxyl groups preferential location in oxidized biomembranes experimentally determined by small angle X-ray scattering: Implications in membrane structure. Biochimica et Biophysica Acta (BBA)-Biomembranes, 1860(11), 2299-2307.

Dinsmore, A. D., Wong, D. T., Nelson, P., & Yodh, A. G. (1998). Hard spheres in vesicles: curvature-induced forces and particle-induced curvature. Physical Review Letters, 80(2), 409.

Duclohier, H., & Wroblewski, H. (2001). Voltage-dependent pore formation and antimicrobial activity by alamethicin and analogues. The Journal of membrane biology, 184(1), 1-12.

Eisenberg, M., Hall, J. E., & Mead, C. A. (1973). The nature of the voltage-dependent conductance induced by alamethicin in black lipid membranes. The Journal of membrane biology, 14(1), 143-176.

Ferreira, L. A., Uversky, V. N., & Zaslavsky, B. Y. (2017). Role of solvent properties of water in crowding effects induced by macromolecular agents and osmolytes. Molecular BioSystems, 13(12), 2551-2563.

Gordon, L. G. M., & Haydon, D. A. (1975). Potential-dependent conductances in lipid membranes containing alamethicin. Philosophical Transactions of the Royal Society of London. B, Biological Sciences, 270(908), 433-447.

Granath, K. A., & Kvist, B. E. (1967). Molecular weight distribution analysis by gel chromatography on Sephadex. Journal of Chromatography A, 28, 69-81.

Hall, J. E. (1981). Voltage-dependent lipid flip-flop induced by alamethicin. *Biophysical journal*, *33*(3), 373-381.

Hall, J. E., Vodyanoy, I. G. O. R., Balasubramanian, T. M., & Marshall, G. R. (1984). Alamethicin. A rich model for channel behavior. Biophysical Journal, 45(1), 233-247.

Harriss, L. M., Cronin, B., Thompson, J. R., & Wallace, M. I. (2011). Imaging multiple conductance states in an alamethicin pore. Journal of the American Chemical Society, 133(37), 14507-14509.

Hasan, M. S., Najem, J. S., Weiss, R., Schuman, C. D., Belianinov, A., Collier, C. P., ... & Rose, G. S. (2018, October). Response of a memristive biomembrane and

demonstration of potential use in online learning. In 2018 IEEE 13th Nanotechnology Materials and Devices Conference (NMDC) (pp. 1-4). IEEE.

Haynes, C. A., Beynon, R. A., King, R. S., Blanch, H. W., & Prausnitz, J. M. (1989). Thermodynamic properties of aqueous polymer solutions: poly (ethylene glycol)/dextran. The Journal of Physical Chemistry, 93(14), 5612-5617.

He, K., Ludtke, S. J., Worcester, D. L., & Huang, H. W. (1996). Neutron scattering in the plane of membranes: structure of alamethicin pores. *Biophysical journal*, *70*(6), 2659-2666.

Helfrich, M. R., Mangeney-Slavin, L. K., Long, M. S., Djoko, K. Y., & Keating, C. D. (2002). Aqueous phase separation in giant vesicles. Journal of the American Chemical Society, 124(45), 13374-13375.

Huang, H. W. (2006). Molecular mechanism of antimicrobial peptides: the origin of cooperativity. Biochimica et Biophysica Acta (BBA)-Biomembranes, 1758(9), 1292-1302.

Huang, H. W., & Wu, Y. (1991). Lipid-alamethicin interactions influence alamethicin orientation. Biophysical journal, 60(5), 1079-1087.

Hunt, J. F., Rath, P., Rothschild, K. J., & Engelman, D. M. (1997). Spontaneous, pH-dependent membrane insertion of a transbilayer α-helix. Biochemistry, 36(49), 15177-15192.

Israelachvili, J. N. (2015). Intermolecular and surface forces. Academic press.

Kawano, R., Tsuji, Y., Kamiya, K., Kodama, T., Osaki, T., Miki, N., & Takeuchi, S. (2014). A portable lipid bilayer system for environmental sensing with a transmembrane protein. *PLoS One*, *9*(7), e102427.

Khandelia, H., & Mouritsen, O. G. (2009). Lipid gymnastics: evidence of complete acyl chain reversal in oxidized phospholipids from molecular simulations. Biophysical journal, 96(7), 2734-2743.

Kim, M. K., & Lee, J. S. (2018). Short-term plasticity and long-term potentiation in artificial biosynapses with diffusive dynamics. ACS nano, 12(2), 1680-1687.

Koner, S., Najem, J. S., Hasan, M. S., & Sarles, S. A. (2019). Memristive plasticity in artificial electrical synapses via geometrically reconfigurable, gramicidin-doped biomembranes. Nanoscale, 11(40), 18640-18652.

Korchev, Y. E., Bashford, C. L., Alder, G. M., Kasianowicz, J. J., & Pasternak, C. A. (1995). Low conductance states of a single ion channel are not 'closed'. The Journal of membrane biology, 147(3), 233-239.

Larimi, M. G., Mayse, L. A., & Movileanu, L. (2019). Interactions of a Polypeptide with a Protein Nanopore Under Crowding Conditions. ACS nano, 13(4), 4469-4477.

Lee, T., Yagati, A. K., Pi, F., Sharma, A., Choi, J. W., & Guo, P. (2015). Construction of RNA–quantum dot chimera for Nanoscale resistive biomemory application. *ACS nano*, *9*(7), 6675-6682.

Leitgeb, B., Szekeres, A., Manczinger, L., Vágvölgyi, C., & Kredics, L. (2007). The history of alamethicin: a review of the most extensively studied peptaibol. Chemistry & biodiversity, 4(6), 1027-1051.

Levine, I. N. (1995). Physical chemistry. New York: McGraw-Hill.

Ling, K., Jiang, H., & Zhang, Q. (2013). A colorimetric method for the molecular weight determination of polyethylene glycol using gold nanoparticles. Nanoscale research letters, 8(1), 538.

Lowel, S., & Singer, W. (1992). Selection of intrinsic horizontal connections in the visual cortex by correlated neuronal activity. *Science*, *255*(5041), 209-212.

Lv, Z., Zhou, Y., Han, S. T., & Roy, V. A. L. (2018). From biomaterial-based data storage to bio-inspired artificial synapse. *Materials today*, *21*(5), 537-552.

Maisch, T., Baier, J., Franz, B., Maier, M., Landthaler, M., Szeimies, R. M., & Bäumler, W. (2007). The role of singlet oxygen and oxygen concentration in photodynamic inactivation of bacteria. Proceedings of the National Academy of Sciences, 104(17), 7223-7228.

McClintic, W. T., Taylor, G. J., Simpson, M. L., & Collier, C. P. (2020). Macromolecular Crowding Affects Voltage-Dependent Alamethicin Pore Formation in Lipid Bilayer Membranes. The Journal of Physical Chemistry B.

Meng, F., Jiang, L., Zheng, K., Goh, C. F., Lim, S., Hng, H. H., ... & Chen, X. (2011). Protein-Based Memristive Nanodevices. *Small*, *7*(21), 3016-3020.

Mertins, O., Bacellar, I. O., Thalmann, F., Marques, C. M., Baptista, M. S., & Itri, R. (2014). Physical damage on giant vesicles membrane as a result of methylene blue photoirradiation. Biophysical journal, 106(1), 162-171.

Montine, T. J., Neely, M. D., Quinn, J. F., Beal, M. F., Markesbery, W. R., Roberts II, L. J., & Morrow, J. D. (2002). Lipid peroxidation in aging brain and Alzheimer's disease. Free Radical Biology and Medicine, 33(5), 620-626.

Morales-Penningston, N. F., Wu, J., Farkas, E. R., Goh, S. L., Konyakhina, T. M., Zheng, J. Y., ... & Feigenson, G. W. (2010). GUV preparation and imaging: minimizing artifacts. Biochimica et Biophysica Acta (BBA)-Biomembranes, 1798(7), 1324-1332.

Mourão, M. A., Hakim, J. B., & Schnell, S. (2014). Connecting the dots: the effects of macromolecular crowding on cell physiology. Biophysical journal, 107(12), 2761-2766.

Mueller, P. (1958). Prolonged action potentials from single nodes of Ranvier. The Journal of general physiology, 42(1), 137-162.

Mueller, P., & Rudin, D. O. (1968). Action potentials induced in biomolecular lipid membranes. Nature, 217(5130), 713-719.

Mueller, P., & Rudin, D. O. (1968). Oscillation phenomena in black lipid membranes induced by a single alamethicin pore. *Biochimica et Biophysica Acta (BBA)-Biomembranes*, *389*(3), 436-443.

Mueller, P., Rudin, D. O., Tien, H. T., & Wescott, W. C. (1962). Reconstitution of cell membrane structure in vitro and its transformation into an excitable system. *Nature*, *194*(4832), 979-980.

Mueller, P., Rudin, D. O., Tien, H. T., & Wescott, W. C. (1962). Reconstitution of cell membrane structure in vitro and its transformation into an excitable system. Nature, 194(4832), 979-980.

Najem, J. S., Dunlap, M. D., Rowe, I. D., Freeman, E. C., Grant, J. W., Sukharev, S., & Leo, D. J. (2015). Activation of bacterial channel MscL in mechanically stimulated droplet interface bilayers. Scientific reports, 5, 13726.

Najem, J. S., Hasan, M. S., Williams, R. S., Weiss, R. J., Rose, G. S., Taylor, G. J., ... & Collier, C. P. (2019). Dynamical nonlinear memory capacitance in biomimetic membranes. Nature communications, 10(1), 1-11.

Najem, J. S., Taylor, G. J., Weiss, R. J., Hasan, M. S., Rose, G., Schuman, C. D., ... & Sarles, S. A. (2018). Memristive ion channel-doped biomembranes as synaptic mimics. ACS nano, 12(5), 4702-4711.

Nguyen, M. A., Srijanto, B., Collier, C. P., Retterer, S. T., & Sarles, S. A. (2016). Hydrodynamic trapping for rapid assembly and in situ electrical characterization of droplet interface bilayer arrays. *Lab on a Chip*, *16*(18), 3576-3588.

Nguyen, M. H., DiPasquale, M., Rickeard, B. W., Doktorova, M., Heberle, F. A., Scott, H. L., ... & Katsaras, J. (2019). Peptide-induced lipid flip-flop in asymmetric liposomes measured by small angle neutron scattering. *Langmuir*, *35*(36), 11735-11744.

Nguyen, V. P., Alves, D. S., Scott, H. L., Davis, F. L., & Barrera, F. N. (2015). A novel soluble peptide with pH-responsive membrane insertion. Biochemistry, 54(43), 6567-6575.

Nguyen, V. P., Dixson, A. C., & Barrera, F. N. (2019). The effect of phosphatidylserine on a ph-responsive peptide is defined by its noninserting end. Biophysical journal, 117(4), 659-667.

Nguyen, V. P., Palanikumar, L., Kennel, S. J., Alves, D. S., Ye, Y., Wall, J. S., ... & Barrera, F. N. (2019). Mechanistic insights into the pH-dependent membrane peptide ATRAM. Journal of Controlled Release, 298, 142-153.

Norred, S. E., Caveney, P. M., Chauhan, G., Collier, L. K., Collier, C. P., Abel, S. M., & Simpson, M. L. (2018). Macromolecular crowding induces spatial correlations that control gene expression bursting patterns. ACS Synthetic Biology, 7(5), 1251-1258.

Okuda, K., Højgaard, K., Privitera, L., Bayraktar, G., & Takeuchi, T. (2020). Initial memory consolidation and the synaptic tagging and capture hypothesis. European Journal of Neuroscience.

Pan, J., Tristram-Nagle, S., & Nagle, J. F. (2009). Alamethicin aggregation in lipid membranes. *Journal of Membrane Biology*, *231*(1), 11.

Parsegian, V. A., Fuller, N., & Rand, R. P. (1979). Measured work of deformation and repulsion of lecithin bilayers. Proceedings of the National Academy of Sciences, 76(6), 2750-2754.

Parsegian, V. A., Rand, R. P., & Rau, D. C. (2000). Osmotic stress, crowding, preferential hydration, and binding: A comparison of perspectives. Proceedings of the National Academy of Sciences, 97(8), 3987-3992.

Peña-Bautista, C., Baquero, M., Vento, M., & Cháfer-Pericás, C. (2019). Free radicals in Alzheimer's disease: Lipid peroxidation biomarkers. Clinica Chimica Acta, 491, 85-90.

Pena-Bautista, C., Vento, M., Baquero, M., & Chafer-Pericas, C. (2019). Lipid peroxidation in neurodegeneration. Clinica Chimica Acta, 497, 178-188.

Prickett, R. C., Elliott, J. A., & McGann, L. E. (2011). Application of the multisolute osmotic virial equation to solutions containing electrolytes. The Journal of Physical Chemistry B, 115(49), 14531-14543.

Qin, S., Dong, R., Yan, X., & Du, Q. (2015). A reproducible write–(read) n–erase and multilevel bio-memristor based on DNA molecule. *Organic Electronics*, *22*, 147-153.

Reshetnyak, Y. K., Andreev, O. A., Lehnert, U., & Engelman, D. M. (2006). Translocation of molecules into cells by pH-dependent insertion of a transmembrane helix. Proceedings of the National Academy of Sciences, 103(17), 6460-6465.

Riske, K. A., Sudbrack, T. P., Archilha, N. L., Uchoa, A. F., Schroder, A. P., Marques, C. M., ... & Itri, R. (2009). Giant vesicles under oxidative stress induced by a membrane-anchored photosensitizer. *Biophysical journal*, *97*(5), 1362-1370.

Rivas, G., & Minton, A. P. (2016). Macromolecular crowding in vitro, in vivo, and in between. Trends in biochemical sciences, 41(11), 970-981.

Sankhagowit, S., Wu, S. H., Biswas, R., Riche, C. T., Povinelli, M. L., & Malmstadt, N. (2014). The dynamics of giant unilamellar vesicle oxidation probed by morphological transitions. Biochimica et Biophysica Acta (BBA)-Biomembranes, 1838(10), 2615-2624.

Sansom, M. S. (1991). The biophysics of peptide models of ion channels. Progress in biophysics and molecular biology, 55(3), 139-235.

Sarles, S. A., & Leo, D. J. (2010). Physical encapsulation of droplet interface bilayers for durable, portable biomolecular networks. *Lab on a Chip*, *10*(6), 710-717.

Sarles, S. A., & Leo, D. J. (2011). Membrane-based biomolecular smart materials. Smart materials and structures, 20(9), 094018.

Sarles, S. A., Stiltner, L. J., Williams, C. B., & Leo, D. J. (2010). Bilayer formation between lipid-encased hydrogels contained in solid substrates. ACS applied materials & interfaces, 2(12), 3654-3663.

Schwarz, G., & Savko, P. (1982). Structural and dipolar properties of the voltage-dependent pore former alamethicin in octanol/dioxane. Biophysical Journal, 39(2), 211-219.

Stankowski, S., Schwarz, U. D., & Schwarz, G. (1988). Voltage-dependent pore activity of the peptide alamethicin correlated with incorporation in the membrane: salt and cholesterol effects. Biochimica et Biophysica Acta (BBA)-Biomembranes, 941(1), 11-18.

Strukov, D. B., Snider, G. S., Stewart, D. R., & Williams, R. S. (2008). The missing memristor found. nature, 453(7191), 80-83.

Sultana, R., Perluigi, M., & Butterfield, D. A. (2013). Lipid peroxidation triggers neurodegeneration: a redox proteomics view into the Alzheimer disease brain. Free Radical Biology and Medicine, 62, 157-169.

Sun, B., Zhou, G., Guo, T., Zhou, Y. N., & Wu, Y. A. (2020). Biomemristors as the next generation bioelectronics. *Nano Energy*, 104938.

Taylor, G. J., & Sarles, S. A. (2015). Heating-enabled formation of droplet interface bilayers using Escherichia coli total lipid extract. Langmuir, 31(1), 325-337.

Taylor, G. J., Heberle, F. A., Seinfeld, J. S., Katsaras, J., Collier, C. P., & Sarles, S. A. (2017). Capacitive detection of low-enthalpy, higher-order phase transitions in synthetic and natural composition lipid membranes. Langmuir, 33(38), 10016-10026.

Taylor, G. J., Venkatesan, G. A., Collier, C. P., & Sarles, S. A. (2015). Direct in situ measurement of specific capacitance, monolayer tension, and bilayer tension in a droplet interface bilayer. Soft matter, 11(38), 7592-7605.

Taylor, G., Nguyen, M. A., Koner, S., Freeman, E., Collier, C. P., & Sarles, S. A. (2019). Electrophysiological interrogation of asymmetric droplet interface bilayers reveals surface-bound alamethicin induces lipid flip-flop. Biochimica et Biophysica Acta (BBA)-Biomembranes, 1861(1), 335-343.

Tsubone, T. M., Baptista, M. S., & Itri, R. (2019). Understanding membrane remodelling initiated by photosensitized lipid oxidation. Biophysical Chemistry, 254, 106263.

Tsubone, T. M., Junqueira, H. C., Baptista, M. S., & Itri, R. (2019). Contrasting roles of oxidized lipids in modulating membrane microdomains. Biochimica et Biophysica Acta (BBA)-Biomembranes, 1861(3), 660-669.

Venkatesan, G. A., & Sarles, S. A. (2016). Droplet immobilization within a polymeric organogel improves lipid bilayer durability and portability. *Lab on a Chip*, *16*(11), 2116-2125.

Vera-Tasama, A., Gomez-Cano, M., & Marin-Hurtado, J. I. (2019, February). Memristors: A perspective and impact on the electronics industry. In 2019 Latin American Electron Devices Conference (LAEDC) (Vol. 1, pp. 1-4). IEEE.

Vodyanoy, I., & Bezrukov, S. M. (1992). Sizing of an ion pore by access resistance measurements. Biophysical journal, 62(1), 10.

Vodyanoy, I., Bezrukov, S. M., & Parsegian, V. A. (1993). Probing alamethicin channels with water-soluble polymers. Size-modulated osmotic action. Biophysical journal, 65(5), 2097-2105.

Vodyanoy, I., Hall, J. E., & Balasubramanian, T. M. (1983). Alamethicin-induced current-voltage curve asymmetry in lipid bilayers. Biophysical journal, 42(1), 71-82.

Vodyanoy, I., Hall, J. E., & Vodyanoy, V. I. T. A. L. Y. (1988). Alamethicin adsorption to a planar lipid bilayer. Biophysical journal, 53(5), 649-658.

Wang, H., Du, Y., Li, Y., Zhu, B., Leow, W. R., Li, Y., ... & Chen, X. (2015). Configurable Resistive Switching between Memory and Threshold Characteristics for Protein-Based Devices. *Advanced Functional Materials*, *25*(25), 3825-3831.

Wang, H., Meng, F., Cai, Y., Zheng, L., Li, Y., Liu, Y., ... & Chen, X. (2013). Sericin for resistance switching device with multilevel nonvolatile memory. *Advanced Materials*, *25*(38), 5498-5503.

Weiss, R., Najem, J. S., Hasan, M. S., Schuman, C. D., Belianinov, A., Collier, C. P., ... & Rose, G. S. (2018, October). A soft-matter biomolecular memristor synapse for neuromorphic systems. In 2018 IEEE Biomedical Circuits and Systems Conference (BioCAS) (pp. 1-4). IEEE.

Wilson, W. W., & DeLucas, L. J. (2014). Applications of the second virial coefficient: protein crystallization and solubility. Acta Crystallographica Section F: Structural Biology Communications, 70(5), 543-554.

Yang, Y., Chen, B., & Lu, W. D. (2015). Memristive physically evolving networks enabling the emulation of heterosynaptic plasticity. Advanced Materials, 27(47), 7720-7727.

Yantorno, R., Takashima, S., & Mueller, P. A. U. L. (1982). Dipole moment of alamethicin as related to voltage-dependent conductance in lipid bilayers. Biophysical journal, 38(2), 105-110.

Ye, C., Chai, Q., Zhong, M., & Wei, Y. (2013). Effect of crowding by Ficolls on OmpA and OmpT refolding and membrane insertion. Protein Science, 22(2), 239-245.

Ye, S., Li, H., Wei, F., Jasensky, J., Boughton, A. P., Yang, P., & Chen, Z. (2012). Observing a model ion channel gating action in model cell membranes in real time in situ: membrane potential change induced alamethicin orientation change. Journal of the American Chemical Society, 134(14), 6237-6243.

Zaslavsky, B. Y., & Uversky, V. N. (2018). In aqua veritas: The indispensable yet mostly ignored role of water in phase separation and membrane-less organelles. Biochemistry, 57(17), 2437-2451.

Zhu, J., Zhang, T., Yang, Y., & Huang, R. (2020). A comprehensive review on emerging artificial neuromorphic devices. Applied Physics Reviews, 7(1), 011312.

Zimmerberg, J., & Parsegian, V. A. (1986). Polymer inaccessible volume changes during opening and closing of a voltage-dependent ionic channel. Nature, 323(6083), 36-39.

Zimmerberg, J., Bezanilla, F., & Parsegian, V. A. (1990). Solute inaccessible aqueous volume changes during opening of the potassium channel of the squid giant axon. Biophysical journal, 57(5), 1049-1064.

# Vita

Home of Nascar’s fastest half-mile and twin-city to Bristol, Virginia, Bill McClintic comes from Bristol, Tennessee. He attended Tennessee High School and afterwards attended the University of Tennessee, receiving a Bachelor of Science degree of Biomedical Engineering. Following undergraduate training, he accepted a Bredesen Center fellowship at the University of Tennessee to pursue a doctoral degree in Energy Science and Engineering. His research interests include disrupting technology innovation with biotechnology that mimics molecular principles of the brain and nervous system to perform function. After graduation, he will pursue postdoctoral opportunities in neurophysiology and entrepreneurship in new computing platforms. Bill is incredibly grateful to his wife, children, and family for their support.